AD-A265 728

MENTATION PAGE

Form Approved
OMB No. 0704-0188

REPORT DATE	3. REPORT TYPE AND DATES COVERED
	Final Report 15 Dec 89 0 14 Jan. 93

4. TITLE AND SUBTITLE
Nonlinear Laser Spectroscopy studies of Semiconductor Heterostructures

5. FUNDING NUMBERS
AFOSR-90-0100

6. AUTHOR(S)
Professor Duncan Steel

AFOSR-TR 93 0397

7. PERFORMING ORGANIZATION NAME(S) AND ADDRESS(ES)
Department of Electrical Engineering and Computer Science
Department of Physics
Harrison M Randall Laboratory of Physics
Univ of Michigan
Ann Arbor, MI 48109

8. PERFORMING ORGANIZATION REPORT NUMBER

9. SPONSORING / MONITORING AGENCY NAME(S) AND ADDRESS(ES)
AFOSR/NE
110 Duncan Avenue Suite B115
Bolling AFB DC 20332-0001
Howard Schlossberg

10. SPONSORING / MONITORING AGENCY REPORT NUMBER
2301/A1

11. SUPPLEMENTARY NOTES

12a. DISTRIBUTION / AVAILABILITY STATEMENT
UNLIMITED

DISTRIBUTION STATEMENT A
Approved for public release;
Distribution Unlimited

12b. DISTRIBUTION CODE

13. ABSTRACT *(Maximum 200 words)*

SEE ATTACH PAGE

93-13141

93 6 11 034

14. SUBJECT TERMS	15. NUMBER OF PAGES
	16. PRICE CODE

17. SECURITY CLASSIFICATION OF REPORT	18. SECURITY CLASSIFICATION OF THIS PAGE	19. SECURITY CLASSIFICATION OF ABSTRACT	20. LIMITATION OF ABSTRACT
UNCLASSIFIED	UNCLASSIFIED	UNCLASSIFIED	UNLIMITED

FINAL REPORT
to
THE AIR FORCE OFFICE OF SCIENTIFIC RESEARCH

Program Title: Nonlinear Laser Spectroscopy studies of Semiconductor Heterostructures

Research Supplement Title: Studies of the Application of Amplitude Squeezed Light

GRANT NO. AFOSR-90-0100
GRANT PERIOD 12/15/89-1/14/93

Principal Investigator: Duncan G. Steel
Department of Electrical Engineering and Computer Science
Department of Physics
Harrison M. Randall Laboratory of Physics
The University of Michigan
Ann Arbor, MI 48109
Phone: 313-764-4469

INTRODUCTION

Research progress in quantum optoelectronics has dominated much of the recent literature in semiconductors because of the new physical phenomena which can be observed and because of the potential for new smaller and higher speed devices of importance to communications, computing, and other high information density applications. Much of the work has focused on III-V compounds because it is believed these materials may provide improved performance over silicon. In addition since they are a direct band gap semiconductor, there are also potential optical applications.

Under this AFOSR grant, our laboratory has been involved in the general area of the study of the optical physics of semiconductors. These studies have provided new insight into the nature of optical properties as well as material properties. The work has emphasized the application of coherent nonlinear laser spectroscopy methods in the study of bulk GaAs and GaAs/AlGaAs quantum wells. This work is based on frequency and time domain four-wave mixing techniques, many of which were developed by our group under earlier AFOSR support. These experiments are enabling us to measure many properties of these systems as well as showing that in heterostructures, the effects of disorder must be included in order to provide a complete understanding. We have also made considerable progress in understanding the nonlinear optical response, due in part to our collaboration with the theoretical group at the University of Arizona under the direction of Stephan Koch, and have shown that dynamical effects actually dominate the nonlinear response at low to moderate exciton densities.

Toward the end of this program, we received a supplement to initiate experiments to study the quantum optical properties of semiconductor lasers, emphasizing the production of amplitude squeezed light with noise below the so-called standard quantum limit. Results in this area have been very encouraging including the demonstration of room temperature squeezing and squeezing by injection locking.

In the balance of this Final Report, we include a publication and education summary. This is followed by a very brief summary of progress during this period. The last section contains a complete set of reprints and preprints of journal articles where the details of the results can be found.

PUBLICATION AND EDUCATION SUMMARY

JOURNAL PUBLICATIONS

Hailin Wang, J.T. Remillard, M.D. Webb, and D.G. Steel, "High Resolution Laser Spectroscopy of Relaxation and the Excitation Line Shape of Excitons in GaAs Quantum Well Structures," Surf. Sci. **228** pp69-73 (1990).

J.T. Remillard, H. Wang, M.D.Webb, D.G. Steel, ""Frequency domain four-wave mixing spectroscopy of temperature and optical intensity dependent relaxation in CdSSe microcrystallite doped glass," J. Opt. Soc. Am. B. **7**, pp897-901 (1990)

George W. Ford and Duncan G. Steel, "Comment on 'Nonlinear Magneto-Optics in Vacuum: Second Harmonic Generation,'" Phys. Rev. Lett. **21**, p2734 (1990).

H. Wang, M. Jiang, D.G. Steel, "Measurement of Phonon-Assisted Migration of Localized Excitons in GaAs/AlGaAs Multiple-Quantum-Well Structures," Phys. Rev. Lett. **65**, 1255 (1990).

D.G. Steel, H. Wang, J.T. Remillard, M. Jiang, "Application of Frequency Domain High Resolution Nonlinear Laser Spectroscopy to the Study of Excitons in GaAs/AlGaAs Quantum Well Structures," invited paper, in *Laser Optics of Condensed Matter*, pp265-272, Elsa Garmire, Alexei A. Maradudin, Karl K. Rebane, eds, Plenum Press, New York (1991).

H. Wang and D. G. Steel, "Effects of spectral diffusion on frequency domain four wave mixing spectroscopy." Phys. Rev. A **43**, pp3823-3831 (1991).

Hailin Wang and Duncan G. Steel, "High resolution laser spectroscopy of exciton relaxation in GaAs quantum wells," invited paper, Applied Physics A, Solids and Surfaces **53**, pp 514-544 (1991).

D.G. Steel and J. Shah, "Coherent transient optical phenomena in semiconductors," Opt. Phot. **2**, pp 25-26 (1991).

H. Wang, M. Jiang, R. Merlin, D.G. Steel, "Spin Flip Induced Hole Burning in Quantum Wells," Phys. Rev. Lett. **69**, 804-807 (1992).

D.G. Steel, H. Wang, S.T. Cundiff "Four-wave mixing in quantum well systems," invited chapter in *Optics of Semiconductor Nanostructures*, Fritz Henneberger, Stefan Schmitt-Rink, and Ernst Göbel, eds (VCH-Germany, 1993).

Min Jiang, Hailin Wang, Duncan G. Steel, "Nonlinear Optical Absorption and Dynamics in Quantum Wells", Appl. Phys. Lett. **61**, 1301-1303 (1992).

D.G. Steel, S.T. Cundiff, H. Wang, "Coherent Nonlinear Laser Spectroscopy of Excitons in Quantum Wells," to be published in the Proceedings of the NATO ARW on *Frontiers of Optical Phenomena in Semiconductor Structures of Reduced Dimensions*, 1992.

M. Freeman, H. Wang, D.G. Steel, D. Scifers, R. Craig, "Amplitude Squeezed Light from Quantum Well Lasers," Opt. Lett. **18**, 379-381 (1993).

Hailin Wang, Kyle Ferrio, Duncan G. Steel, Y. Hu, Rolf Binder, Stephan Koch "Excitation Induced Dephasing Optical Nonlinearity in GaAs," submitted to Phys. Rev. Lett. (1993).

Min Jiang, Hailin Wang, R. Merlin, M. Cardona[¶] D.G. Steel[†], "Nonlinear Magneto-Optics and Field Induced Reduction in Mobility in GaAs," submitted to Physical Review Letters (1993).

INVITED CONFERENCE PROCEEDINGS

H. Wang, J. T. Remillard, M. Jiang, M. D. Webb, D. G. Steel, "Frequency Domain Nonlinear Optical Studies of Multiple Quantum Well Structures," Proceedings of SPIE Symposium on Opto Electronics, Conference 1216 (1990) (see above citation).

D. G. Steel, H. Wang, J. T. Remillard, M. Jiang, "Application of Frequency Domain High Resolution Nonlinear Laser Spectroscopy to the Study of Excitons in GaAs/AlGaAs Quantum Well Structures," presented at the Fourth US-USSR Binational Symposium, Irvine, CA, 1990 (see above citation).

D.G. Steel, H. Wang, S.T. Cundiff, M. Jiang, "Coherent Nonlinear Spectroscopy of Excitons in GaAs/AlGaAs Mulitple Quantum Wells", Conference on Lasers and Electro-Optics, CLEO '91, Technical Digest Series **10**, pp308-309 (1991).

D.G. Steel, "High Resolution Spectroscopy and Photon Echoes in GaAs Quantum Wells," invited paper at the APS March Meeting, Bull. Am. Phys. Soc. **36**, p338 (1991).

D.G. Steel, H. Wang, S.T. Cundiff, M. Jiang, "Nonlinear Optics and Spectroscopy in Systems with Reduced Dimensionality," Nonlinear Optics Gordon Conference, 1991.

D.G. Steel, H. Wang, S.T. Cundiff, M. Jiang, "Nonlinear Spectroscopy of Excitons: A Probe of Disorder," to be presented the symposium "Frontier in Laser-Condensed Matter Interactions", ILS'92, organized by M.V. Klein.

Duncan G. Steel, "Coherences and Dynamics of Resonances in Semiconductor Heterostructures," Workshop on Optical Properties of Mesoscopic Semiconductor Structures, Snowbird, 1993.

CONTRIBUTED CONFERENCE PROCEEDINGS

H. Wang, J.T. Remillard, M Jiang, and D.G. Steel, "Precision Nonlinear Laser Spectroscopy of Exciton Dynamics in GaAs/AlGaAs Multiple Quantum Well Structures," Nonlinear Optics, NLO'90, IEEE, p121 (1990).

H. Wang, J.T. Remillard, M. Jiang, M.D. Webb, D.G. Steel, "Frequency Domain Nonlinear Optical Studies of Multiple Quantum Well Structures," invited paper, Proceedings of SPIE Symposium on Nonlinear Optical Materials and Devices for Photonic Switching **1216**, pp206-214 (1990) (see above citation).

H. Wang, M. Jiang, D.G. Steel, J.E. Cunningham, "Studies of Exciton Recombination and Transport in High Purity GaAs Using High Resolution Nonlinear Spectroscopy," International Quantum Electronics Conference (IQEC '90), Technical Digest **8**, pp310-311 (1990).

H. Wang, M. Jiang, and D.G. Steel, "High Resolution nonlinear spectroscopy studies of the dynamics of localized excitons in GaAs/AlGaAs quantum wells," International Quantum Electronics Conference (IQEC '90), Technical Digest **8**, pp60-61 (1990).

Ming Jiang, Hailin Wang, D.G. Steel, "Anomalous Nonlinear Optical Processes in GaAs/AlGaAs Quantum Wells," Quantum Electronics and Laser Science (QELS'91), Technical Digest Series **11**, pp252-253 (1991).

D.G. Steel, S.T. Cundiff, M. Jiang, Hailin Wang, M.D. Webb, "Coherent Nonlinear Laser Spectroscopy Studies of Exciton Relaxation, Dephasing and Energy Transport in GaAs Quantum Wells", Quantum Optoelectronics, OSA Technical Digest, **7** (1991).

H. Wang, M. Jiang, R. Merlin, D.G. Steel, "Spin-flip induced spectral hole burning of magnetoexcitons in GaAs/AlGaAs quantum wells", QELS'92, OSA Technical Digest **13**, 34-35 (1992)

M. Jiang, H. Wang, R. Merlin, D.G. Steel, "High resolution spectroscopic measurements of magneto-exciton in thin film GaAs," QELS'92, OSA Technical Digest **13**, 214-215 (1992).

Hailin Wang, Kyle Ferrio, and Duncan Steel, "Polarization dependent transient nonlinear optical response of heavy and light hole excitons in GaAs," Conference on Quantum Electronics and Laser Science (QELS'93).

M. Freeman, Hailin Wang, Duncan G. Steel, D. Scifers, H. Craig, "Amplitude Squeezing in a Semiconductor Quantum Well Laser," Conference on Quantum Electronics and Laser Science (QELS'93).

Min Jiang, Hailin Wang, Roberto Merlin, D.G. Steel, "Nonlinear optical response of magneto-excitons in GaAs," Conference on Quantum Electronics and Laser Science (QELS'93).

Hailin Wang, M. Freeman, Duncan G. Steel, D. Scifers, H. Craig, "Amplitude-Squeezed Light by Injection-Locking of Quantum Well Lasers" Conference on Quantum Electronics and Laser Science (QELS'93).

H. Wang, M. Jiang, R. Merlin, D.G. Steel, "Spin-flip induced spectral hole burning of magnetoexcitons in GaAs/AlGaAs quantum wells," APS March Meeting, APS Bull. **37**,p 708 (1992).

Education Summary

The AFOSR program has provided a very active education environment for both graduate students and undergraduate students.

Hailin Wang, Ph.D., Research Investigator, The University of Michigan.
Jeff Remillard, Ph.D., Staff Engineering, Ford Research Labs.
Mike Freeman (Ph.D. expected in 1994)
Laura Grego (B. S., beginning post graduate work at Cornell or Cal Tech)

RESEARCH PROGRESS SUMMARY

Nonlinear Laser Spectroscopy Studies in Quantum Wells

In this Section we review recent results obtained in the study of excitons in GaAs/AlGaAs quantum well (QW) structures based on frequency domain and time domain coherent nonlinear spectroscopy. The discussion emphasizes the study of the dynamical behavior of excitons at low temperature, where the excitons are stable against ionization by LO phonons. At sufficiently low excitation densities the coherent emission arises from the third order optical susceptibility. In this regime the excitonic susceptibility is significantly affected by the effects of disorder induced localization of the excitons. This approach is in contrast to other work which has emphasized studies at higher excitation density to examine the many body nature of the interaction. At these high densities the effects of disorder are reduced due to saturation of that part of the response. By working at low excitation density, it has been the objective of our group and others to learn more about the nature of the material as well as those factors which could ultimately determine device performance. In the following section, we will demonstrate how the nonlinear optical interactions may be more complex than previously identified in the absence of disorder.

Frequency Domain FWM Spectroscopy

High resolution frequency domain spectroscopy based on cw FWM is a powerful coherent spectroscopy method that can provide information on various relaxation phenomena and energy level structure. In addition, this method can eliminate the inhomogeneous broadening due to interface roughness or random crystal fields . This latter feature enables measurement of the homogeneous line shape. Since these measurements are performed in energy space, they are particularly sensitive to relaxation processes involving energy shifts of the excitation (i.e., spectral diffusion) such as the migration of excitons between different energy sites discussed above. The narrow excitation bandwidth also permits improved spectral resolution over the usual time domain measurements. This feature is important since many of the relaxation parameters vary spectrally across the exciton absorption feature. However, the frequency domain measurements lose relative sensitivity with increasing polarization excitation decay rates. In this case, time domain measurements remain especially helpful.

For frequency domain measurements in this section, we use the experimental configuration shown in Fig. 1 for backward four wave mixing. Tuning Ω_1 or Ω_2 provides a line shape determined by energy relaxation processes (so-called T_1 type times) including spatial diffusion rates and other inelastic type scatter processes while tuning Ω_3 provides a line shape determined

by the homogeneous broadening (T_2) and spectral diffusion (the scattering of an exciton from energy E to energy E'.) This latter line shape is free of inhomogeneous broadening.

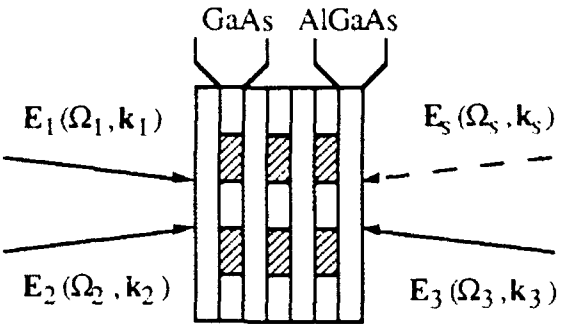

Figure 1. Geometry for backward four-wave mixing spectroscopy. The cross-hatched regions schematically represent the excitation grating created by fields 1 and 2.

There are many measurements which we have made on these heterostructures including determination of the mechanism of relaxation of localized excitons, the details of exciton mobilities, etc. and these are presented in the attached reprints. However, two classes of measurements have been particularly significant. We will focus on these measurements in this review.

The first measurement demonstrates spectral hole burning and enables the first direct confirmation of spectral diffusion of excitons between localization sites. In these experiments, a grating formed by $\mathbf{E}_1 \cdot \mathbf{E}_2^*$ creates a spatial modulation of the exciton population and a corresponding spectral hole. The four wave mixing line shape obtained by tuning Ω_3 then probes the resulting spectral hole as well as the effects of spectral diffusion. Figure 2 shows a FWM line shape where excitons are optically excited by $\mathbf{E}_1 \cdot \mathbf{E}_2^*$ 1.5 meV below the absorption line center. The narrow resonance in the response corresponds to exciton spectral hole burning, and the width of the hole gives an exciton homogeneous line width of $2\gamma_{ph} \sim 0.04$ meV, assuming no contribution due to spectral diffusion. (Recall that in the absence of spectral diffusion, the observed width is $4\gamma_{ph}$.)

The broad Stokes shifted feature in Fig. 2 is due to the quasi-equilibrium distribution of the exciton population, and the response is a function of the steady state exciton population assuming all excitons in the spectral region concerned give rise to the same cw nonlinear response. The FWM line shape in Fig. 2 can be fit to a simple model which neglects migration to states above the excitation energy. The calculation is based on the nonlinear optical response of a simple two level system and assumes a Gaussian distribution for the quasi-equilibrium population of excitons that have migrated to states below the excitation energy. The spectral profile of the hole-burning resonance is assumed to be Lorentzian. The result is plotted as the solid line in Fig. 2.

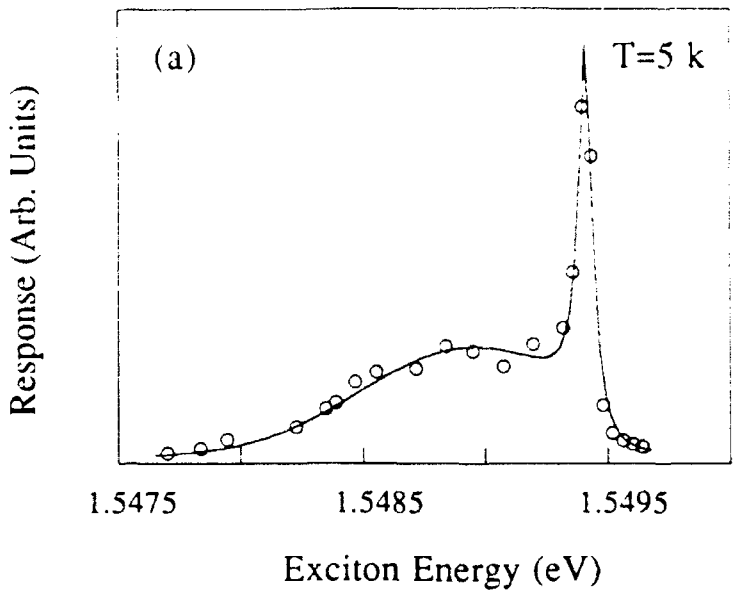

Figure 2. The nondegenerate four-wave mixing response obtained by tuning Ω_3. The line shape is determined by homogeneous broadening as well as contributions from spectral diffusion in the limit that $|\omega_2-\omega_1|<<\Gamma$, the spectral diffusion rate. The narrow feature is the spectral hole produced by $\mathbf{E}_1 \cdot \mathbf{E}_2^*$ 1.5 meV below absorption line center. The broad feature represents the quasi-equilibrium distribution of excitons produced by spectral diffusion.

Further insight into the mechanism of exciton migration is had by returning to the data in Fig. 2 and measuring the spectral diffusion rate as a function of temperature since the migration process is likely to involve absorption or emission of acoustic phonons. The theoretical model for phonon assisted exciton migration was developed recently by Takagahara. In the model, excitons resonantly excited are in a non-equilibrium state and can migrate to other sites by emitting or absorbing acoustic phonons. Migration is possible due to the overlap of the exciton wave function in different sites when the inter-site distance is small. When the inter-site distance is much greater than the localization length the process occurs by inter-site dipole-dipole coupling. The typical magnitude of participating phonon wave vectors is within a few times of the inverse of the localization length corresponding to phonon energies of order 0.01 to 0.1 meV. The theory predicts a distinctive temperature dependence for the migration rate. At low temperatures, the dependence is described by $\exp(\beta T^{\alpha})$. In this expression, β is positive and independent of temperature but is expected to increase with the exciton energy and depends on details of interface roughness; α is estimated to be between 1.6 and 1.7. The predicted temperature dependence is quite different from that of variable range hopping used by Mott to interpret electronic conduction in the localized regime. The difference has been attributed to the long-range nature of the inter-site interaction and the phonon emission process involved in the

migration of the localized exciton. The temperature dependence has been observed in transient hole burning experiments in an InGaAs/InP QW where all excitons are localized by alloy disorder. Our measurements discussed in the reprints show that this behavior also characterizes GaAs quantum wells. However, in this case, the disorder is more likely due to interface roughness. As we show in an attached reprint, the measurements show that the temperature dependence is well fit by Takagahara's model.

The great precision afforded in frequency domain FWM measurements and the ability to eliminate inhomogeneous broadening is also useful to obtain new information on energy level structure. This is especially powerful in cases where linear spectroscopic methods fail due to the large inhomogeneous broadening compared to the relevant energy scale. The capability has been critical in our studies of spin flip induced hole burning and measurements of the exciton Zeeman splitting in modest magnetic fields.

To understand these experiments, we note that the electronic energy spectrum of quantum well structures is fully quantized under a magnetic field parallel to the growth axis. Optical absorption reveals a ladder of magnetoexcitons corresponding to transitions between electron and hole Landau levels. The accompanying Zeeman splitting lifts the Kramers degeneracy and is characterized by an effective g-factor which depends sensitively on the details of the band structure. In addition, the energy separation between the different spin leads to an increase in the spin relaxation time since now spin relaxation can only take place via inelastic processes.

There have been numerous studies of the electron g-factor, however, determination of the Zeeman splitting has been more difficult because of the large inhomogeneous broadening due to disorder and the fact that the exciton Zeeman splitting in a quantum well is much smaller than in bulk. Earlier magneto-reflectance measurements were able to resolve Zeeman splittings for the light-hole but not the heavy-hole exciton. However, using the methods described above, we have been able to obtain the first direct measurements of the exciton Zeeman splitting in a GaAs quantum wells. The measurements reveal a heavy-hole splitting much smaller than that reported for bulk GaAs at low magnetic field, and show a nonlinear dependence of the splitting on magnetic field strength. The results reflect the effects of the complex band structure of a quantum well.

In these experiments, a nearly monochromatic optical beam with σ_- circular polarization is used to excite a narrow spectral-hole at the lowest heavy-hole (HH1) exciton associated with the 3/2 to 1/2 transition (see Fig. 3 for the 2-D exciton energy level diagram in a magnetic field). The width of the spectral-hole is determined by the homogeneous line width. Spin relaxation of these excitons generate a spectral-hole of excitons associated with the -3/2 to -1/2 transition. The induced spectral hole burning is probed using an optical beam with σ_+ circular polarization.

Zeeman splitting can then be obtained by measuring the energy spacing between the spin-flip-induced spectral hole and the original spectral hole resonance.

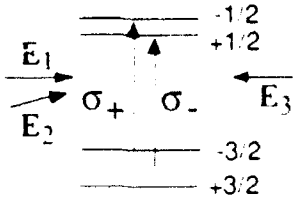

Figure 3. Energy level diagram and experimental configuration for FWM studies of magnetoexcitons in a quantum well.

In practice, the measurements proposed above are complicated by strong spectral diffusion of the localized excitons, as seen in Fig. 2. In the limit where the spin-flip time is long compared with the spectral diffusion time, nearly all spin-flipped excitons have diffused in energy. Hence, the spin-flip-induced spectral hole burning resonance will be completely smeared out by the spectral diffusion process. To avoid the above complications, we exploit the power of FWM spectroscopy which enables us to eliminate the spectral diffusion contribution to the lineshape. As before, nearly (frequency) degenerate beams $\mathbf{E}_1$ and $\mathbf{E}_2$ interfere in the sample to excite a traveling wave grating which oscillates at a frequency equal to the detuning between the two beams $\delta = |\Omega_2 - \Omega_1|$. The amplitude of the grating is proportional to $\left(\delta + i\Gamma_{pop}\right)^{-1}$. Measuring the FWM signal as a function of ω_3 probes the spectral profile of the grating. In the presence of spectral diffusion, the spectral-hole excited by $\mathbf{E}_1 \cdot \mathbf{E}_2^*$ diffuses in energy and the FWM response arises from both the spectral-hole and the quasi-equilibrium distribution of the exciton population as discussed above. The decay of the spectral hole is determined by the sum of the exciton spectral diffusion and recombination rates. However, the life time of the quasi-equilibrium distribution is determined solely by the recombination time of the exciton as we discussed earlier . In the limit where the spectral diffusion rate is much larger than the exciton recombination rate, detuning $\mathbf{E}_1$ and $\mathbf{E}_2$ by an amount large compared with the recombination rate (but still smaller than or comparable with the spectral diffusion rate) significantly decreases the amplitude of the grating associated with the quasi-equilibrium distribution. As a result, the FWM nonlinear optical response will be dominated by the spectral hole burning resonance.

For these measurements, experiments were carried out at 2.5 K using a split-coil superconducting magnet. The effects of spectral diffusion were reduced on the spectral hole burning resonance by using two acousto-optic modulators to set the detuning between $\mathbf{E}_1$ and $\mathbf{E}_2$ to 140 MHz. In the first set of measurements, we used three circularly polarized optical beams rotating in the same direction in the lab frame. The nonlinear optical response, shown as squares in Fig. 4, involves only the σ_- excitons associated with the 3/2 to 1/2 transition. As expected, the contribution from spectral diffusion is nearly nonexistent.

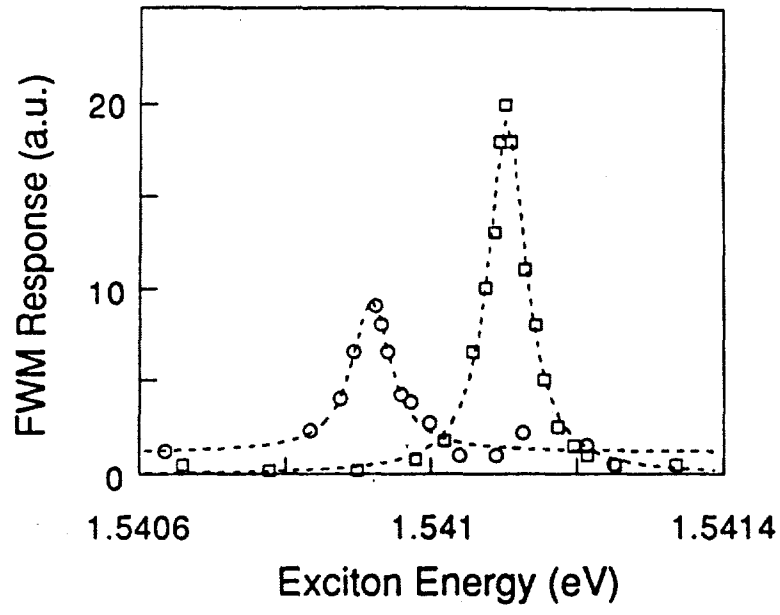

Figure 4. The FWM response of magnetoexcitons in a quantum well obtained by tuning ω_3. The grating is written using σ_- polarized E_1 and E_2 The high frequency resonance is the original spectral hole observed when E_3 is σ_- polarized while the lower frequency resonance is the result of spin flip induced hole burning, observed when E_3 is σ_+ polarized.

When the electron or hole associated with a σ_- exciton created with $\mathbf{E}_1 \cdot \mathbf{E}_2^*$ flip their spin, the nonlinear response probed by reversing the polarization direction of the third beam will exhibit a resonance associated with a spectral hole located at the energy of the σ_+ exciton. The nonlinear response at the σ_+ exciton arises due to phase space filling caused by the presence of electrons (holes) with -1/2 (+3/2) angular momentum. The resulting resonance, shown as circles in Fig. 4, clearly shows narrow spectral hole burning at a lower energy. The energy difference is the exciton Zeeman splitting, which is 0.19 meV at 4T. The nearly constant background signal in Fig. 6 is due to excitons that have spectrally diffused. Note that spin-flips of σ_+ excitons require absorption of acoustic phonons, and are slower compared with spin-flips of σ_- excitons. The observed spin-flip-induced spectral hole burning resonance is considerably weaker at 4T when $\mathbf{E}_1 \cdot \mathbf{E}_2^*$ excites σ_+ excitons.

Recent measurements have shown that at low and intermediate magnetic field, the electron g-factor at the lowest Landau level in GaAs quantum wells is close to the value for bulk GaAs. In contrast, the Zeeman splitting of the HH1 exciton obtained above is very small in comparison with that reported for bulk GaAs. Our results seem to be in agreement with the earlier magneto-reflectance measurements where the heavy hole Zeeman doublet was not resolved. Small Zeeman splittings attributed to the strong valence band mixing in quantum well structures have been recently predicted by numerical calculations of magnetoexcitons using the Luttinger

Hamiltonian. In particular, the mixing of σ_- excitons with excitons at higher energy pushes the σ_- exciton to lower energy. The theory also predicts an eventual sign change of the Zeeman splitting at higher magnetic fields where the band mixing effects overcome those of the Zeeman interaction. However, theoretical determination of the magnetic field at which the zero crossing occurs is difficult since the cancellation of the two competing contributions depends strongly on parameters of the model. The sign change of the splitting has not been observed in our measurements up to 6 T.

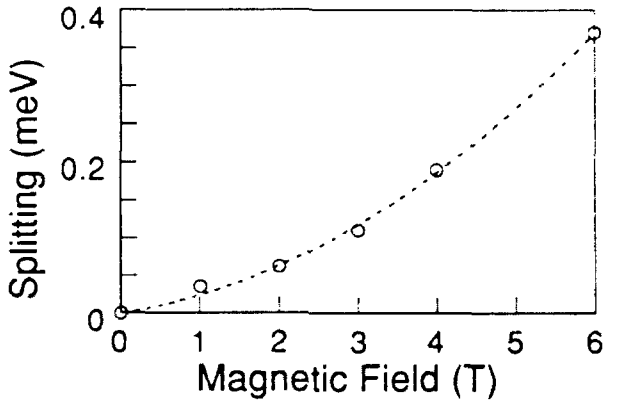

Figure 5. Magnetic field dependence of the magnetoexciton Zeeman splitting.

Figure 5 displays the magnetic field dependence of the Zeeman splitting for the HH1 exciton. The validity of the quadratic dependence indicated in the figure (dashed line) is clearly questionable since our data covers only a relatively small field range. Nevertheless, the observed field dependence is somewhat surprising since the calculations predict a field dependence slower than linear. The observed dependence may be due in part to the nonparabolicity of the conduction band which was not included in the calculations.

Picosecond Transient FWM Spectroscopy

In this section, we summarize our experimental results based on using coherent transient techniques, specifically stimulated photon echoes and free polarization decay based on the backward FWM geometry shown in Fig. 6. Compared to cw FWM spectroscopy, these methods are more sensitive to phenomena characterized by a range of dephasing times since the amplitude of the signal is independent of the dephasing time when the pulse widths are short compared to these times. As in the case of cw FWM, coherent nonlinear transient effects can also eliminate the effects of inhomogeneous broadening, although these methods are not as sensitive to energy dependent decay phenomena such as spectral diffusion. In the presence of inhomogeneous broadening, the emission in a transient FWM experiment is delayed with respect to the last pulse

and is called a photon echo, whereas in a homogeneously broadened system, the signal is prompt and called a free polarization decay.

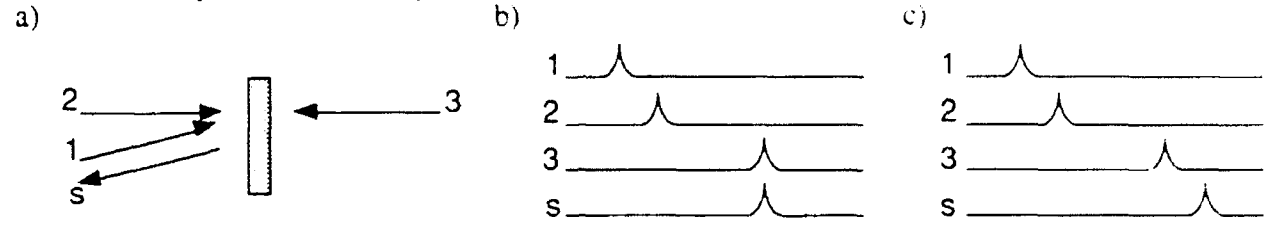

Figure 6. Experimental geometry and timing sequence for three pulse TFWM. In (b), the system is homogeneously broadened and the signal field is a free polarization decay emitted coincidently with the third field. In (c), the system is inhomogeneously broadened, and the signal is a stimulated photon echo emitted at a time after the third pulse equal to the time difference between the first and second pulses.

Coherent optical transient effects arising from atomic transitions are now well understood and have provided extensive information on decay processes of isolated atoms as well as atoms undergoing collisions with neutral ground state perturbers. However, there has been recent progress in developing the theoretical formalism for understanding coherent interactions in semiconductors as discussed elsewhere. As discussed above, because the carriers are Fermions, this problem is considerably more complex than simple atomic systems.

Work in this program has included the use of transient FWM studies of the response where we have time resolved the emission. As discussed in the attached reprints, we have observed highly complex temporal behavior at low to moderate excitation density. These results which could not be satisfactorily explained by either the modified optical Bloch equations o the more accurate semiconductor Bloch equations have motivated our most recent series of experiments, discussed in detail in the attached preprint and summarized here.

To understand the results, we first note that for these experiments it is easy to show based on the existing semiconductor Bloch equations that self diffracted FWM experiments using linearly polarized light should give a signal amplitude which is independent of the relative orientation of the two polarizations of the two input fields. However, as indicated above in our own experiments and in other labs (in quantum wells) this is not the case. Hence, if biexciton effects were excluded, it was clear that the nonlinear response had to arise from a spin independent coupling. Based on numerical estimates, we believed that the most likely explanation was that the nonlinear response was due to classical Coulomb scattering.

For these experiments, we worked in high quality GaAs to avoid problems associated with disorder in quantum wells. Figure 7 shows the simple differential transmission spectrum. The heavy hole shows the classical second derivative type response of collisional broadening. Indeed, the area under the curve is only 5% of the positive area, i.e., it is nearly zero as expected for a nonlinear response arising due to collisional broadening.

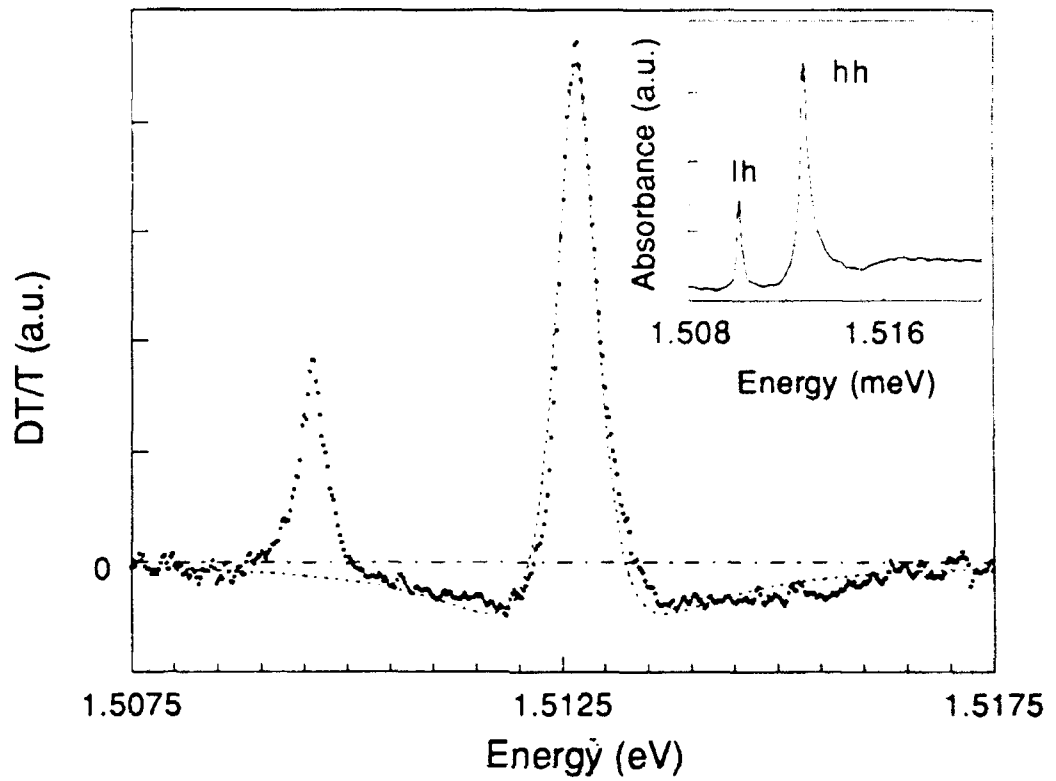

Figure 7. DT spectrum at an exciton density of $3x10^{15}/cm^3$. The dashed line is a fit to the assumed subtracted-Lorentzian corresponding to the simple model of the nonlinear response for the heavy hole due to pressure broadening. Inset : Linear absorption of the sample. The sample is strained to remove the heavy-hole-light-hole degeneracy. The heavy hole is higher energy in this case compared to the light hole.

To further confirm the internal consistency of this result, we showed that the |+1> hh1 exciton - |+1> hh1 exciton scattering cross section is the same as the |-1> hh exciton |+1> hh exciton. (|+1> and |-1> correspond to exciton excited from the m=-3/2 to m=-1/2 state and m=+3/2 to m=+1/2 state, respectively.) Figure 8a shows the result of the FWM response measured with σ_+ polarized light. The response is determined with and with out a prepulse which either created |+1> or |-1> exciton. As shown the FWM response is reduced identically, independent of which exciton is created by the prepulse. The reduction of the FWM amplitude with increased dephasing is another unique signature of the collision induced nonlinear response.

Since the co-polarized scattering is due to both Coulomb scattering as well as manybody spin dependent effects such as exchange, we would expect the co-polarized response to be larger. In addition, as the excitation density increases resulting in an increase in the scattering rate, the ratio should decrease, asymptotically approaching 1 as the scattering rate approaches a constant. This behavior is shown in Fig. 8b.

The theoretical predictions (S. W. Koch et al., The University of Arizona) based on the semiconductor Bloch equations are shown in Fig. 9. These predictions are in excellent agreement with the experimental results and are the result of the addition of dynamical terms in the equations of motion. These terms enter as an imaginary part of the exciton self-energy.

Work to demonstrate this behavior in quantum wells is currently underway, however, we have previously demonstrated that at low excitation densities, electromagnetic scattering is spin independent while at higher excitation densities, the scattering is spin dependent, as shown in Fig. 10. In this figure, we plot the polarization of the signal as a function field intensity. The grating is written with circupolarized fields and read with a linealry polarized field. The results show that low intensity, the scattering is independent of the polarization of E_3 while at high intensity, the interaction is becoming polarization dependent. The picture is totally consistent with the understanding developed in bulk material.

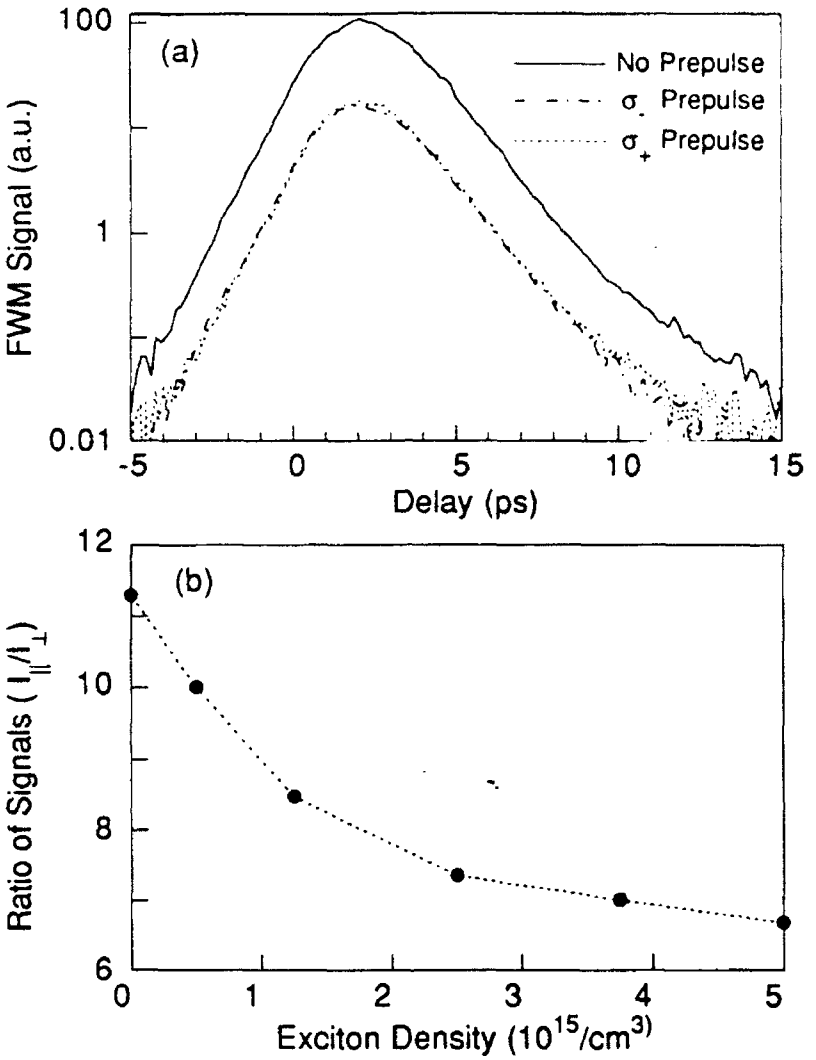

Figure 8. (a) Effect of σ+ and σ- prepulses on the hh FWM responses. Measurements as a function of delay between E_2 and E_1. (b) Ratio of co- and cross- linearly polarized FWM signals at the hh resonance as a function of the exciton density generated by the prepulse. Dashed lines are guide to eyes.

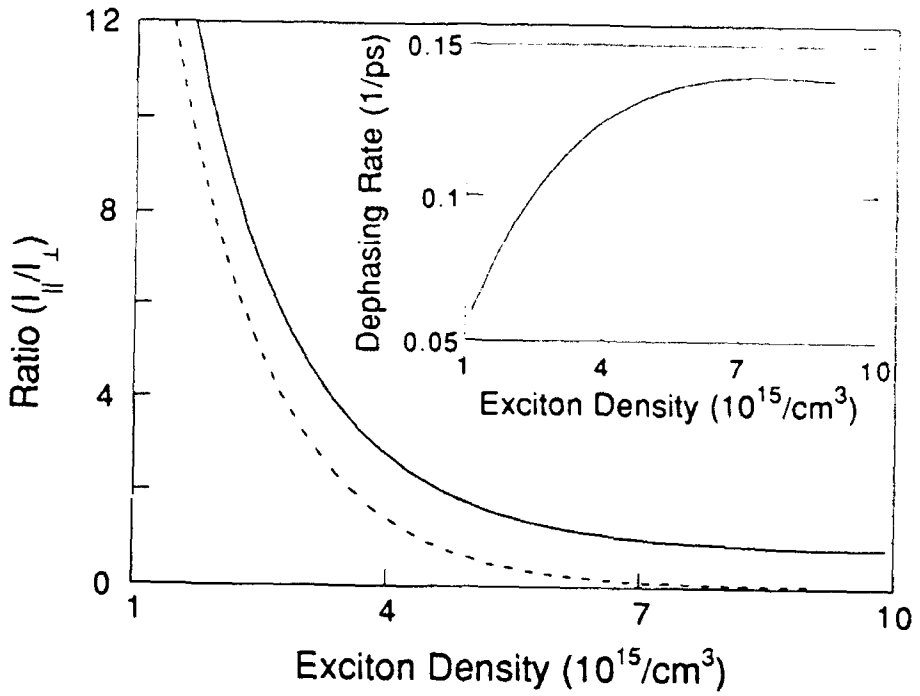

Figure 9. Theoretical results of the ratio of co- and cross- linearly polarized hh FWM signals as a function of the exciton density generated by the prepulse. Dashed lines are results (divided by 10) without including exchange interactions. Inset shows density dependence of the exciton dephasing.

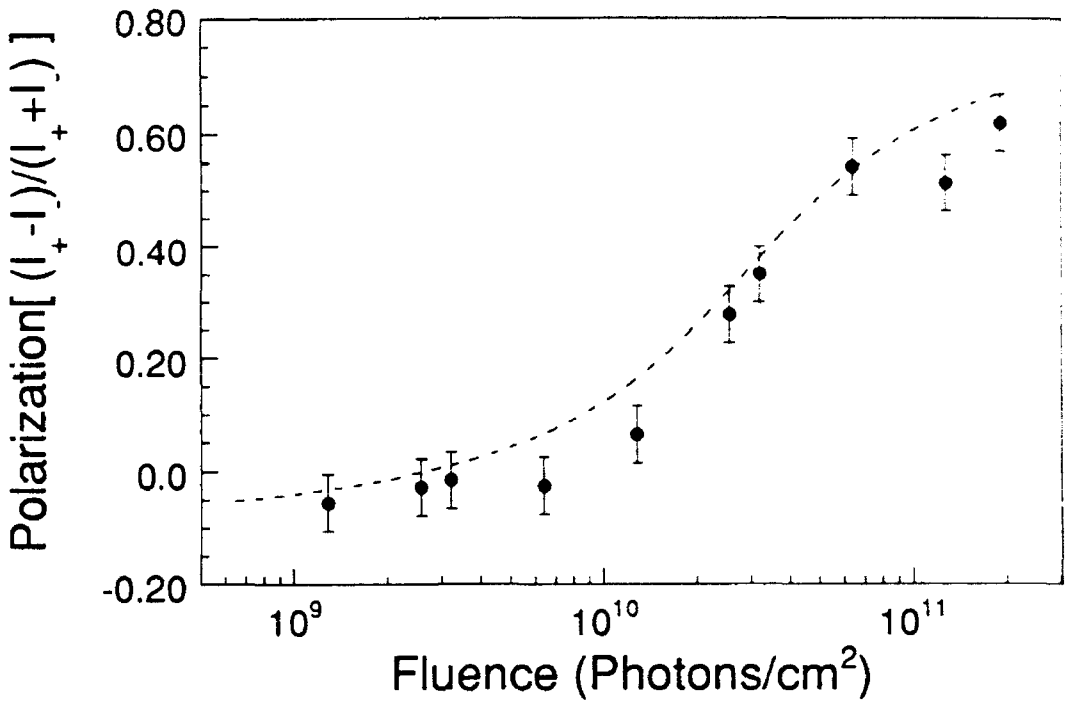

Figure 10. The signal depolarization as a function of incident flux when E_1 and E_2 are co-circularly-polarized and E_3 is linearly polarized. For the vertical axis I_+ is the intensity for the signal component co-polarized with E_1 and E_2 and I_- is the component cross-polarized, hence a polarization of zero indicates linear polarization and a value of 1 indicates circular polarization of the same sense as the first two fields. At low intensity, the scattering of E_3 is nearly independent of the E_3 polarization.

(NOTE: The work presented in this report on the collisional nonlinearity was initiated under this program, but was completed on a new AFOSR program after this program was terminated. For completeness and because of the importance of this work and because this program was critical in making these measurements a reality, this work was included in this report.)

Quantum Optical Effects in Semiconductors and Photon Number Squeezing

Amplitude squeezed light, which is characterized by photon number noise below the shot noise limit (SNL), is of fundamental interest in optical physics and is potentially useful for precision measurements and optical communication. In this work, we initiated a collaboration with Spectra Diode to demonstrate that high impedance pump noise suppression could be used to generate amplitude squeezing in an index guided quantum well laser. The work was motivated in part by the first demonstration of this effect (using a TJS laser) by Yamamoto at NTT. Light exhibiting photon number noise 1.4 dB below the shot noise limit was observed and the corresponding polarization properties were studied. This work also demonstrated that close coupling of the laser-detector combination made with an *unsaturated* detector revealed 2.9 dB of squeezing.

A typical run exhibiting 1.4 dB of squeezing is shown in Fig. 11 (trace c) for a current bias level of $I/I_{th}=19$, where I_{th} is the threshold current for lasing. For these experiments, the laser and a collimating lens are placed inside a cryostat. (The periodic structure is due to a delay line which enables a simultaneous observation of the sum and difference from the balanced detectors. The sum corresponds to the amplitude noise and the difference establishes the shot noise level.) The observed (I_1-I_2) noise level agrees well with the shot noise level established independently with a red filtered white light source (trace b) and with a LED. The thermal background noise level (trace d) was subtracted from both curves. This data was taken with the laser at 15K, where the emission wavelength was 810 nm, the threshold current was 0.9 mA, and the differential quantum efficiency was 78%. The laser current to detector current transfer ratio was 0.51 mA/mA above threshold, and thus the overall detection quantum efficiency was 65%. Correcting for this detection efficiency, the 1.4 dB of observed squeezing corresponds to 2.4 dB of squeezing at the laser output facet.

A significant increase in the difference current noise level appeared when a polarizer (extinction ratio $>10^4$:1) located between the laser and the detection setup was removed (trace a of Fig. 11). Previous amplitude squeezing experiments using similar balanced detection schemes were not sensitive to this type of noise because an optical isolator was used. The extra noise results from the use of a polarization beam splitter (PBS) and initially appears surprising since the polarization extinction ratio of the laser was better than 400. However, the PBS mixes the initially orthogonally polarized fields generated by the laser, leading to the increased noise. The theoretical justification for this is provided in an attached reprint.

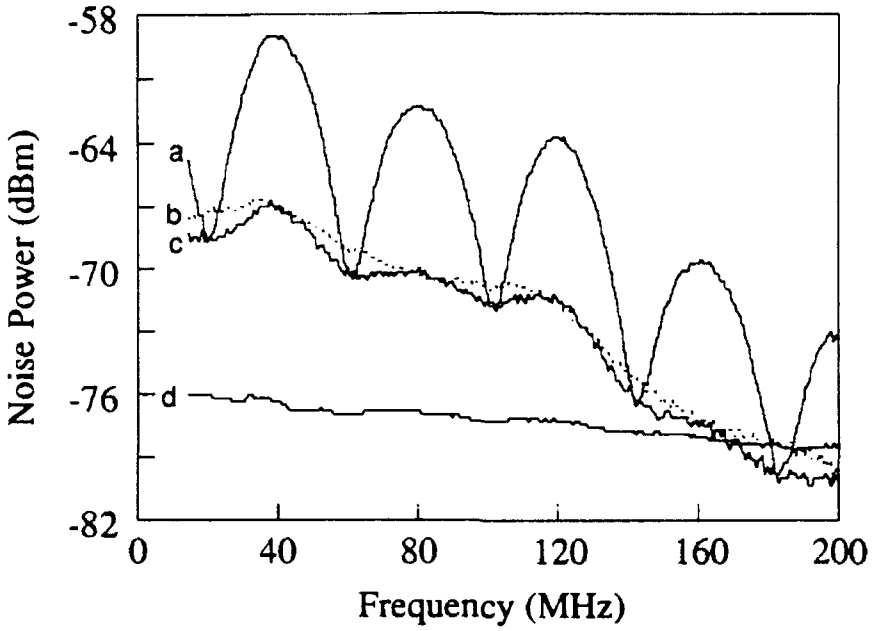

Figure 11. Balanced mixer amplitude fluctuation spectra for the laser (traces a and c) and for a red filtered white light source (trace b). All three were taken with a total dc photo detector current of 8.00 mA. The amplifier thermal noise (trace d) was subtracted in traces a, b, and c and is given for reference.

Given the differential quantum efficiency of our laser, at least 6.6 dB of squeezing at the laser output facet is theoretically expected far above threshold. The discrepancy between this value and the largest observed squeezing (2.4 dB at the output facet) is likely due to a combination of multimode operation and weak optical feedback into the laser. Measurements of the laser output spectrum indicate that there is a strong correlation between power in modes other than the primary lasing mode and increased photon number noise, eventually leading to a loss of squeezing at high pump levels ($I/I_{th}>35$). Optical feedback may also play a role, though replacing the polarizer with an optical isolator (isolation >40 dB) did not increase the observed squeezing.

To characterize the squeezing in a high detection efficiency and low optical feedback regime, a second set of experiments was performed. These experiments consisted of close-coupling the laser to a single detector and directly monitoring the photocurrent noise spectrum. Since this configuration relies on direct detection instead of a balanced mixer, the shot noise level must be calibrated independently and then compared to the noise level generated by the laser. This raises a concern because differing conditions between calibration and laser noise measurement, such as spot size, could alter detector saturation, making interpretation of the experimental results

difficult. For example, increased saturation due to a laser spot size much smaller than that of the calibration source would lead to a lower displayed noise power and thus could be mistaken for amplitude squeezing. The details of the exhaustive studies made to avoid these problems are described in the reprint. The saturation effects, however, are demonstrated in Fig. 12a

For these experiments, the shot noise level was again calibrated using a red filtered white light source and verified with a LED. To minimize possible errors, the detector and its associated amplifiers were kept at room temperature while the laser was cooled to 10K. Here the threshold current was 0.78 mA, and the differential laser current to detector current transfer ratio above threshold was 0.67 mA/mA. The results of one experiment for a bias level of $I/I_{th}=16$ (detector current 8.00 mA) are shown in Fig. 12b. The amount of squeezing obtained in the limit of low frequencies (where the effects of saturation are smallest) fell between 2.4 and 2.9 dB as the distance between the laser and detector was varied from 1.5 mm (0.17 mm^2 spot size) to 3.5 mm (.92 mm^2 spot size), and did not increase at higher bias levels. Due to a lack of direct correlation with distance, this slight variation in squeezing is believed to have been due to weak optical feedback from the detector to the laser which was dependent on the exact orientation of the two devices. When corrected for the detection quantum efficiency of 85%, 2.9 dB of squeezing corresponds to 3.7 dB at the output facet of the laser.

While the observed squeezing level increased in the close coupled geometry, the value was still below the theoretically expected value of 6.6 dB. Other lasers of the same type gave similar levels of squeezing, although the temperature at which the maximum squeezing was observed varied from laser to laser. Simultaneous monitoring of the laser mode (by collecting light from the back facet and analyzing it with a monochromater) and amplitude fluctuations revealed that longitudinal mode characteristics were responsible for this temperature dependence. The best squeezing was obtained with a dominant primary mode, indicating that cross gain saturation did not result in complete negative cross correlation between the modes. As the side mode power (relative to the main mode) and the number of side modes increased, so did the amplitude noise. Unfortunately at high pump levels, this always occurred (typically $I/I_{th}>25$) and is the likely reason the full theoretical level of squeezing could not be attained in this system. This raises the possibility that mode stabilization may enhance the observed squeezing.

We note in closing of this section that these conclusions regarding the impact of side modes have now been confirmed in the new AFOSR program and a dramatic improvement has been obtained. These results were described at QELS'93 in a post deadline paper and will be described in the annual report for the new program.

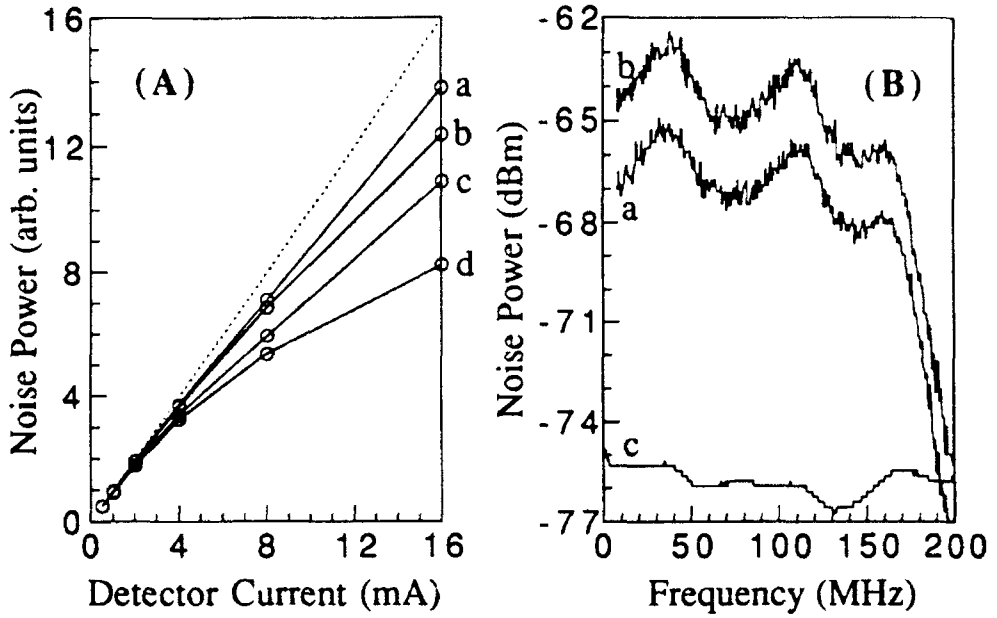

Figure 12. (A) A red filtered white light source was used to study the frequency dependent saturation characteristic of the detector. The frequencies shown are: (a) 10 MHz, (b) 50 MHz, (c) 100 MHz, and (d) 150 MHz. The broken line represents the response of an ideal detector. (B) Demonstration of the amplitude squeezing obtained upon close coupling the diode laser and detector. Trace (a) shows the laser noise spectra, trace (b) shows the shot noise level corresponding to trace (a), and trace (c) shows the amplifier thermal noise level which was subtracted from traces (a) and (b).

SUMMARY

In summary, this program has enabled us to make considerable progress both in the area of understanding the nonlinear optical response and complex dynamics in semiconductors but also in allowing us to develop a new area of research in the area of quantum optics of semiconductors. In addition to the new intellectual efforts and progress, we have also established strong collaborations with industry as well as another University which has allowed us to demonstrate sub-shot noise operation of quantum well lasers as well as significant new features in the nonlinear optical response of semiconductors. The current program is already building on this progress with the demonstration of improved squeezing by mode suppression and studies on semiconductor quantum dots.

Nonlinear optical absorption and dynamics in quantum wells

Min Jiang, Hailin Wang, and Duncan G. Steel
Harrison M. Randall Laboratory of Physics, The University of Michigan, Ann Arbor, Michigan 48109-1120

(Received 24 April 1992; accepted for publication 6 July 1992)

We present measurements of differential transmission and four-wave mixing in GaAs quantum well structures at 1.8 K near the inhomogeneously broadened lowest heavy-hole (*hh*1) exciton resonance using narrow band cw excitation. The data show an *increase* in absorption and an excitation lifetime of order 1–10 μs outside the spectral hole produced by the pump. The long lifetime and the experimentally determined absence of excitation spatial diffusion in this region suggests that optical absorption produces electron-hole pairs that are correlated but separately localized due to disorder. A phenomenological model is proposed to explain the nonlinear response based on two-photon absorption.

The optical properties immediately below the band edge of direct band-gap semiconductors are dominated by excitonic effects. In a quantum well (QW), the strong transient nonlinear optical response associated with the exciton resonance has been shown by numerous theoretical and experimental studies to be due to many-body effects including phase space filling, exchange effects and to a lesser degree, screening.[1] However, the nonlinear response and exciton dynamics are greatly complicated and qualitatively changed by the presence of interface disorder in QW structures.[2] Early measurements suggested large atomically flat areas at the interface.[3] More recent measurements show the presence of monolayer flat island formation on a scale of 50 Å,[4] leading to the proposal that there is a bimodal distribution for island size.[5] At low temperature, excitons can be localized by the interface disorder which leads to strong inhomogeneous broadening of the optical absorption spectrum. Localized excitons, however, can migrate between localization sites by emitting and absorbing acoustic phonons.[6,7]

To improve the understanding of the intrinsic nonlinear optical response and the effects of disorder in GaAs quantum well structures, we present what we believe are the first measurements of the *cw nonlinear response* near the lowest heavy-hole (*hh*1) exciton at low temperature (1.8–5 K) where the effects of disorder is a dominating factor. The experiments are based on *nondegenerate* differential transmission (DT) and four-wave mixing (FWM). Nondegenerate DT measures the sign and magnitude of the imaginary part of the third-order susceptibility while nondegenerate FWM measures the magnitude (squared) of the third-order susceptibility and is useful for determining various relaxation rates.[8,9] While the results of many-body theory[1] have been highly successful in accounting for the nonlinear response observed using short pulse excitation at high excitation density ($>10^9$ *excitons/cm*^{2}/layer),[10] we show in this letter that the present understanding cannot account for the experimental results observed at low excitation density under cw excitation. We believe the discrepancy is due to the presence of disorder and propose a possible phenomenological model to explain the data.

The data reported in this letter are obtained in QW structures consisting of 65 periods of 96 Å GaAs wells and 98 Å $Al_{0.3}Ga_{0.7}As$ barriers, grown at 630 °C by molecular beam epitaxy on semi-insulating (100) GaAs substrates with interrupted growth. The *hh*1 exciton absorption linewidth is 2.3 meV [Fig. 1(a)] with a Stokes shift of 1 meV between the *hh*1 exciton absorption and emission. Similar experiment results have also been obtained on several $GaAs/Al_{0.3}Ga_{0.7}As$ samples differing in the number of layers and where the absorption line widths varied from 1.0 to 2.5 meV with a corresponding Stokes shift varying from <0.2 to 1.5 meV. Samples are mounted on a sapphire disk (c-axis normal) with the substrate removed and placed in a liquid helium immersion cryostat.

Measurements are performed using two frequency stabilized cw dye layers. For DT measurements, one laser supplies a pump beam at a fixed frequency Ω_1 while the second laser supplies a probe beam at Ω_2. Both beams are linearly and orthogonally polarized to avoid coherent effects. The nonlinear spectral response proportional to $\mathrm{Im}\chi^{(3)}$ is obtained by measuring the probe transmission as a function of Ω_2 where $\chi^{(3)}$ is the third-order susceptibility. For nondegenerate backward FWM, two nearly degenerate co-polarized beams $\mathbf{E}_1(\mathbf{k}_1,\Omega_1)$ and $\mathbf{E}_1'(\mathbf{k}_1',\Omega_1+\delta)$ with $\delta \ll \Omega_1$ intersect in the sample with a small angle θ between the beams producing a traveling-wave modulation of the absorption and dispersion with a period $\Lambda=\lambda/(2\sin\theta/2)$. The grating is probed by an orthogonally polarized beam $E_2(\mathbf{k}_2,\Omega_2)$ where $\mathbf{k}_2=-\mathbf{k}_1$ producing a coherent signal, proportional to $|\chi^{(3)}|^2$, propagating in the direction $-\mathbf{k}_1'$. Tuning Ω_2 again measures the spectral response.[9] Tuning δ provides information on the excitation decay dynamics probed at Ω_2.[7] This decay rate depends on γ, Γ_{sd}, and Γ_d where γ is the recombination rate, Γ_{sd} is the spectral diffusion rate and $\Gamma_d=4\pi^2D/\Lambda^2$ is the rate due to spatial diffusion where D is the diffusion coefficient.

Figure 1 shows a comparison between the FWM spectrum [Fig. 1(b)] and the DT spectrum [Fig. 1(c)] obtained by tuning Ω_2 [Fig. 1(b) is similar to that reported earlier[7,11]]. Ω_1 is given by the arrow in the *hh*1 linear absorption feature shown in Fig. 1(a). The sharp resonance at $\Omega_2=\Omega_1$ in Fig. 1(b) is the result of spectral hole burning of the inhomogeneously broadened localized excitons. The width of the hole is twice the homogeneous width.[8,9] The comparable DT spectrum [Fig. 1(c)], obtained at the same

 0003-6951/92/361301-03$03.00

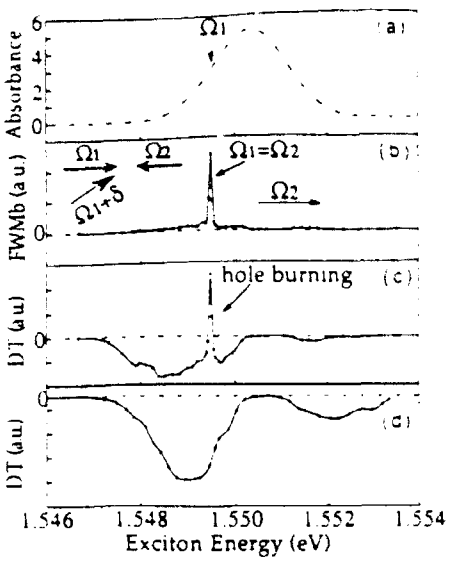

FIG. 1. A comparison of the cw four-wave mixing and differential transmission spectra. (a) The *hh*1 linear absorption spectrum. The arrow shows the location of Ω_1 for (b) and (c). (b) The four-wave mixing spectrum obtained by tuning Ω_2. (c) The corresponding differential transmission spectrum. (d) The differential transmission spectrum obtained when Ω_1 is set to 1.2 eV above the *hh*1 absorption peak.

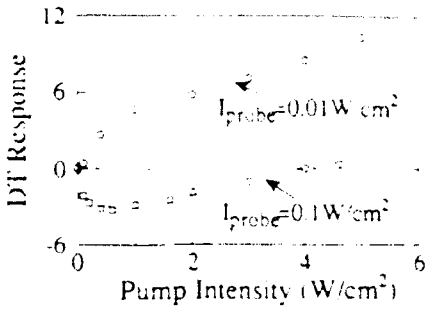

FIG. 2. The intensity dependence of DT spectra as a function of pump intensity for two different probe intensities. Measurements are made for the case of Fig. 1(c) where Ω_2 is set 1.1 meV below Ω_1. The dotted curves show the fitting based on a two component model: an incoherent two photon stepwise excitation dominates at high probe intensity (square) and a single saturation type nonlinear response dominates at low probe intensity (circle) characterized by a smaller saturation intensity than that of a two photon-type nonlinear response.

excitation intensity ($\sim$0.5 W/cm^2), shows the sharp resonance again corresponding to the spectral hole seen in Fig. 1(b). As expected from phase space filling effects, a decrease in absorption is observed in the spectral hole (a positive signal corresponds to a *decrease* in absorption). However, away from the spectral hole, the DT measurement shows an unexpected *increase in absorption*. It is easy to see that the DT response ($\propto \mathrm{Im}\chi^{(3)}$) away from the spectral hole is much larger than expected based on FWM ($\propto \chi^{(3)2}$). Figure 1(d) shows the DT spectrum obtained when the pump frequency Ω_1 is tuned to 1.2 meV above the *hh*1 absorption line center where no spectral hole is expected or observed.[12] This spectrum [Fig. 1(d)] demonstrates that the increase in absorption around *hh*1 is *not related to the spectral hole*. A similar DT spectrum is observed when Ω_1 is tuned above the band edge where free carriers are directly excited. In contrast no signal is obtained when Ω_1 is tuned well below the *hh*1 resonance.

Measurements of the intensity dependence of the FWM signal show that the spectral hole amplitude depends linearly on each of the intensities of the three input beams, indicating that there is minimal contribution from higher order terms in the susceptibility. In the usual approach of estimating the exciton density based on a radiative lifetime of order 1 ns and the input intensity, the exciton density is of order 10^7–10^8 excitons/cm^2/layer. However, even at this low excitation level, the DT signal in Fig. 1(d) is not linear in the pump intensity. In fact, the response also *depends on the probe intensity*. Figure 2 shows the unusual intensity dependence of the DT response as a function of pump intensity for two different probe intensities. Measurements are made for the case of Fig. 1(c) where Ω_2 is set 1.1 meV below Ω_1.

We further characterize the nonlinear response by measuring the relaxation time in the region showing increased absorption. Independent measurements using amplitude modulation DT spectroscopy[13] and FWM by tuning δ[7] show a decay time of order 1–10 μs in contrast to the 0.5–1 ns excitonic recombination rate obtained in this sample by time-resolved luminescence and FWM at the hole burning resonance. While the slow time scale suggests that the nonlinear response could arise due to photorefractive or thermal effects, the first possibility is eliminated since we have determined that there is no energy transfer between beams as would be expected in the presence of two beam coupling. Thermal effects are also eliminated for two reasons: (1) The DT signal strength does not decrease when the sample is immersed in liquid helium as would be expected since in liquid helium, the induced temperature gradient is dramatically reduced; (2) more importantly, the absence of any dependence of the grating decay on the grating spacing sets the upper limit of the diffusion coefficient at 3×10^{-4} cm^2/s. If the nonlinear response were due to thermal effects, then this measurement would correspond to a thermal conductivity at least 4 orders of magnitude below that of GaAs. Hence, we conclude the excitation is electronic in nature and note that the long lifetime results in an estimated excitation density four orders of magnitude higher than that expected based on a 0.5–1.0 ns exciton lifetime.

In discussing these results we first note that many-body effects such as exciton-exciton interactions, band-gap renormalization, and screening can produce a shift or a broadening of the resonance, leading to regions of increased absorption. However, these features resemble the first or second derivative of the resonance, clearly not in agreement with the measurement. Hence, while the current theory has been highly successful in interpreting experimental results obtained on short time scales at high excitation density,[1,10] the results show that the theory does not describe the leading terms in the low intensity cw nonlinear response measured by differential transmission. We would like to stress that identical behavior has been observed in the three different samples we investigated. Earlier experimental evidence for this effect was reported in transient

DT measurements using picosecond lasers.[2] At zero time delay, the low-temperature excitonic response showed a decrease in absorption due to bleaching, yet on longer time scales ($\sim$100 ps), the DT signal changed sign, showing an increase in absorption.

The nonlinear response outside the spectral hole can be qualitatively explained by a phenomenological model involving an incoherent two photon stepwise excitation along with an ordinary saturating type nonlinear response (not associated with the spectral hole). In a rate equation description for this system [i.e., a simple two level system (2LS) and an independent three level system (3LS)], a probe dependent DT response similar to the data is obtained as shown by the dotted lines in Fig. 2. In this model, the transition rates for both transitions in the 3LS are comparable. When the pump beam is resonant with the transition from level 1 to level 2 and the probe beam is resonant with the transition from level 2 to level 3, the DT signal due to the 3LS would show an increase in absorption if the beam intensities are reasonably low. However, if the 2LS saturation intensity is smaller than saturation intensities for the 3LS, at very low intensities, the DT signal is dominated by the 2LS. Hence, decreased absorption is observed as shown in Fig. 2. As the probe intensity increases, the relative importance of the 3LS will increase due to the small saturation intensity for the 2LS, resulting in increased absorption in the DT response. Finally, when the pump beam intensity is very high such that both transitions in the 3LS are saturated, the stepwise two-photon transition will be overwhelmed by the saturation effect and an overall decrease in absorption will be observed as shown in Fig. 2.

The relaxation measurements also provide some additional insight into the microscopic origin of the observed nonlinear response in the QW. In particular, even though the nonlinear response is clearly associated with the *hh*1 exciton, the long lifetime of the excitation is not consistent with the presence of ordinary excitons, nor is the negligibly small diffusion coefficient. To explain these effects, we propose that in the presence of disorder, optical excitation produces electron-hole pairs which are localized in separate but closely correlated positions. If we assume that the electron and hole wave functions are localized on a scale length of order 100 Å and then also assume the lifetime is simply related to the wave function overlap, we can estimate that the separation distance is of order 200 Å. Furthermore, using the excitation intensity at the minimum value of the lower DT curve (saturation point of the DT spectrum), we can estimate the resulting *e-h* density to be of order 6×10^{11} *e-h*/cm^2/layer (using 0.5 W/cm^2, taking 50% of the energy distributed over the first 10 layers, and an effective excitation lifetime of 5 μs. This would correspond to an average distance between *e-h* pairs on the order of 140 Å, the same order of magnitude as the *e-h* separation estimated based on the *e-h* pair lifetime. This number could be interpreted as the average distance between *localization* sites. While it is difficult to relate this to interface morphology, it is comparable to that reported by chemical mapping.[4] The stepwise two photon transition discussed in the above 3LS model may correspond to excitations of two closely correlated *e-h* pairs. The unexpected low saturation intensities for the 3LS and 2LS are due to the long lifetime of these systems and the finite number of localization sites (recall that the saturation intensity is $\simeq\hbar\omega N_T/\alpha_0\tau$ where α_0 is the absorption coefficient and N_T is the density of the localization sites).

Our model also provides an explanation for the discrepancy between the FWM and the DT spectra. As is well known, the FWM signal strength is proportional to the contrast ratio of the excitation grating produced by $\mathbf{E}_1^*\cdot\mathbf{E}_1'$. The contrast ratio is reduced if the input beams saturate the system. At the beam intensities used in the measurement ($I_1, I_1' \sim 0.5$ W/cm^2, $I_2 \sim 0.1$ W/cm^2), the density of excitation (associated with spectral hole) is well below the saturation level, however the excitation in the increased absorption region is partially saturated, causing a grating flattening and resulting in a reduced FWM response.

In summary, we have shown that the low intensity nonlinear optical response in GaAs multiple QW is greatly affected by the presence of disorder. The measurements show that the existing theoretical work is inadequate to explain the low intensity nonlinear response in these systems. Finally, the long life time may need to be taken into account in potential device applications.

This work was supported by the Air Force Office of Scientific Research. The authors wish to acknowledge their appreciation to Professor P. K. Bhattacharya for supplying samples.

[1] See, for example, S. Schmitt-Rink, D. S. Chemla, and D. A. B. Miller, Adv. Phys. 38, 89 (1989).
[2] J. Hegarty and M. D. Sturge, J. Opt. Soc. Am. B 2, 1143 (1985).
[3] C. Weisbuch, R. Dingle, A. A. Gossard, and W. Wiegmann, Solid State Commun. 38, 709 (1981).
[4] See, for example, A. Ourmazd, D. W. Taylor, J. Cunningham, and C. W. Tu, Phys. Rev. Lett. 62, 933 (1989).
[5] C. A. Warwick, W. Y. Jan, A. Ourmazd, and T. D. Harris, Appl. Phys. Lett. 56, 2666 (1990); D. Gammon, B. V. Shanabrook, and D. S. Katzer, Phys. Rev. Lett. 67, 1547 (1991).
[6] T. Takagahara, J. Lumin. 44, 347 (1989).
[7] H. Wang, M. Jiang, and D. G. Steel, Phys. Rev. Lett. 65, 1255 (1990).
[8] D. G. Steel and J. T. Remillard, Phys. Rev. A 36, 4330 (1987).
[9] H. Wang and D. G. Steel, Phys. Rev. A 43, 3823 (1991).
[10] D. A. B. Miller, D. S. Chemla, D. J. Eilenberger, P. W. Smith, A. C. Gossard, and W. T. Tsang, Appl. Phys. Lett. 41, 679 (1982); W. H. Knox, R. L. Fork, M. C. Downer, D. A. B. Miller, D. S. Chemla, C. V. Shank, A. C. Gossard, and W. Wiegmann, Phys. Rev. Lett. 54, 1306 (1985); N. Peyghambarian, H. M. Gibbs, J. L. Jewell, A. Antonetti, A. Migus, D. Hulin, and A. Mysyrowicz, Phys. Rev. Lett. 53, 2433 (1984). See also papers cited in Ref. 1.
[11] The scan in Fig. 1(b) covers a larger spectral region than the data in Ref. 7. However, additional structure is seen at energies away from the spectral hole in Fig. 1(b) compared to Ref. 7 because the value of δ was set to in these data to enable the detection of slower components. In Ref. 7, δ was set to 100 kHz to ensure that only the simple excitonic component was detected.
[12] H. Wang and D. G. Steel, Appl. Phys. A 53, 514 (1991).
[13] In these measurements, the amplitude or phase shift on the lock-in amplifier is measured as a function of the modulation frequency and can then be easily related to the relaxation time.

Amplitude-squeezed light from quantum-well lasers

M. J. Freeman, H. Wang, and D. G. Steel

Randall Laboratory of Physics, The University of Michigan, Ann Arbor, Michigan 48109

R. Craig and D. R. Scifres

Spectra Diode Laboratories, San Jose, California 95134

Received October 7, 1992

High-impedance pump noise suppression was used to generate amplitude squeezing in an index-guided quantum-well laser. Light exhibiting photon-number noise 1.4 dB below the shot-noise limit was observed, and the corresponding polarization properties were examined. Close-coupled laser-detector measurements made with an unsaturated detector revealed 2.9 dB of squeezing.

Amplitude-squeezed light, which is characterized by photon-number noise below the shot-noise limit (SNL), is of fundamental interest in optical physics and is potentially useful for precision measurements[1] and optical communication.[2] Although it has been known that the photon-number fluctuations of an ideal laser operating far above threshold stem from pump noise and vacuum field fluctuations,[3] it has been appreciated only recently that the laser does not necessarily feature the full shot noise.[4-6] By eliminating pump noise, the output of the laser can, in principle, have an arbitrary amount of amplitude squeezing within the cavity bandwidth.[4,5] Several methods for suppressing pump noise, and thus attaining this type of amplitude squeezing, have been proposed.[4-6] Of these, constant-current operation of a semiconductor diode laser is of particular interest because electrical current pump noise can be easily suppressed to >15 dB below the SNL[7] and because the high quantum efficiency of the diode laser allows the sub-Poissonian electron pump statistics to be transferred to photon statistics.[5] To date, the largest level of amplitude squeezing has been achieved in transverse junction stripe semiconductor lasers. Measurements that close coupled a transverse junction stripe laser to a detector demonstrated a photocurrent fluctuation 8.3 dB below the SNL.[8] With balanced detection, photocurrent fluctuations 1.3 dB below the SNL were obtained.[9]

We report measurements of photon-number fluctuations in an index-guided quantum-well laser. The laser (Spectra Diode Laboratories SDL-5410-C) differs considerably from the transverse junction design used nearly exclusively in earlier research.[7-9] In a collimated geometry, it exhibited photon-number fluctuations 1.4 dB below the SNL when driven by a constant current. The balanced detection scheme used in these measurements also allowed the polarization fluctuations of the laser to be investigated, whereas close coupling the laser to a detector improved the amplitude squeezing to 2.9 dB.

For the first set of experiments, the laser and a collimating lens are placed inside a cryostat, along with a drive circuit consisting of a series resistor ($R = 680\ \Omega$) and a bypass capacitor ($C = 0.1\ \mu$F). The noise properties of the output are measured by balanced detection with a delay line.[9] Equal division of the laser power is obtained with a half-wave plate and a polarization beam splitter (PBS). The resulting two beams are then focused onto Hamamatsu (Model S1722-01) p-i-n photodiodes (quantum efficiency 85%). The ac photocurrents are amplified, one is delayed, and then their difference is obtained with a 180° hybrid junction. This setup yields a common mode suppression >25 dB from 10 to 200 MHz. The delay line allows the sum ($I_1 + I_2$) current, which reflects the laser noise level, and difference ($I_1 - I_2$) current, which gives the shot-noise level, to be simultaneously monitored on a spectrum analyzer.[9,10] The signal alternates between the two as a function of frequency owing to the frequency-dependent phase shift introduced by the delay line.

A typical run exhibiting 1.4 dB of squeezing is shown in Fig. 1 (trace c) for a bias level $I/I_{th} = 19$. The observed ($I_1 - I_2$) noise level agrees well with the shot-noise level established independently with a red-filtered white-light source (trace b) and with a light-emitting diode. These data were taken with the laser at 15 K, where the emission wavelength was 810 nm, the threshold current was 0.9 mA, and the differential quantum efficiency was 78%. The differential laser current-to-detector current transfer ratio was 0.51 above threshold, and thus the overall detection efficiency was 65%. Correcting for this detection efficiency, the 1.4 dB of observed squeezing corresponds to 2.4 dB of squeezing at the laser output facet.

A significant increase in the difference current noise level appeared when a polarizer (extinction ratio $>10^4$:1) located between the laser and the detection setup was removed (trace a of Fig. 1). Previous amplitude-squeezing experiments with similar balanced detection schemes were not sensitive to this type of noise because an optical isolator was used.[7-9] The extra noise results from the use of a PBS and initially appears surprising because the polarization

0146-9592/93/050379-03$5.00/0

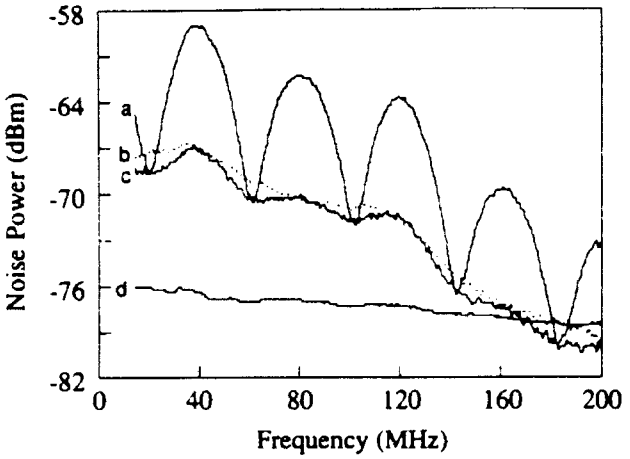

Fig. 1. Balanced mixer amplitude-fluctuation spectra for the laser (traces a and c) and for a red-filtered white-light source (trace b). All three were taken with a total dc photodetector current of 8.00 mA. The amplifier thermal noise (trace d) was subtracted in traces a, b, and c and is given for reference.

extinction ratio of the laser was >400. However, the PBS mixes the initially orthogonally polarized fields generated by the laser, leading to the increased noise.

The mixing can be described quantum mechanically by a unitary transformation relating the input and output photon annihilation operators[11]:

$$\begin{bmatrix} \hat{b}_\perp \\ \hat{b}_\parallel \end{bmatrix} = \begin{bmatrix} \cos(\theta) & \sin(\theta) \\ -\sin(\theta) & \cos(\theta) \end{bmatrix} \begin{bmatrix} \hat{a}_\perp \\ \hat{a}_\parallel \end{bmatrix},$$

$\hat{a}_\perp$ and $\hat{a}_\parallel$ are operators for the orthogonal polarization components of the lasing mode, $\hat{b}_\perp$ and $\hat{b}_\parallel$ are, respectively, operators for the orthogonally polarized transmitted and reflected modes of the PBS, and θ is the angle between the polarization directions of $\hat{a}_\perp$ and $\hat{b}_\perp$. Assigning $\hat{a}_\perp$ to the primary polarization direction of the laser leaves little power for the $\hat{a}_\parallel$ mode. However, this mode leads to the observed extra noise in trace a, as can be seen by calculating the variance of $(I_1 + I_2)$ and $(I_1 - I_2)$ for the case of balanced ($\theta = 45°$) detection:

$$[\Delta(\hat{M}_\perp + \hat{M}_\parallel)]^2 = (\Delta\hat{N}_\perp)^2 + (\Delta\hat{N}_\parallel)^2, \quad (1)$$

$$[\Delta(\hat{M}_\perp - \hat{M}_\parallel)]^2 = \langle\hat{N}_\perp\rangle + \langle\hat{N}_\parallel\rangle + 2\langle\hat{N}_\perp\rangle\langle\hat{N}_\parallel\rangle - 2|\langle\hat{a}_\perp^\dagger\hat{a}_\parallel\rangle|^2 + 2\,\mathrm{Re}[(\Delta\hat{a}_\perp^\dagger\hat{a}_\parallel)^2], \quad (2)$$

where $\hat{N} = \hat{a}^\dagger\hat{a}$ and $\hat{M} = \hat{b}^\dagger\hat{b}$. Equation (1) describes the data in Fig. 1 (trace a) at frequencies leading to $(I_1 + I_2)$. It indicates that the measured amplitude noise in this case corresponds to the simple sum of the noise power contributions of the independent input modes. The agreement between traces a and c at these sum frequencies (recalling that a polarizer was used to eliminate the contribution of the nonlasing polarization in trace c) indicates that the nonlasing mode did not make a detectable contribution to the sum-frequency amplitude noise found in trace a, as expected based on its low power level.

At frequencies where $(I_1 - I_2)$ is displayed, the situation is more complex. Each of the first two terms in Eq. (2) represents the average photon number of one of the two laser polarizations, and their sum gives the SNL. However, the remaining terms are not negligible. The third term is a cross term given by twice the product of each input mode's average photon number, and the last two terms depend on the coherence properties of the two modes.

If both laser modes ($\hat{a}_\perp$ and $\hat{a}_\parallel$) are in coherent states of the electric field, or if either mode has zero photons, the last three terms cancel, giving the shot-noise level. This is clearly not the case for the experiment described, because trace a displays 8 dB of extra noise at the subtracted frequencies, and the sum frequencies indicate a sub-Poissonian primary mode. Similar difference-frequency noise behavior has been observed in split photodetector balanced detection,[12] where it was attributed to stochastic position noise due to regeneratively amplified spontaneous emission into nonlasing modes. Regeneratively amplified spontaneous emission into the nonlasing polarization probably leads to the 8 dB of extra noise observed here also. The statistical properties of this mode become easily observable in this setup because of their interference with the lasing mode.

Given the differential quantum efficiency of our laser, at least 6.6 dB of squeezing at the laser output facet is theoretically expected far above threshold.[5,8,13] The discrepancy between this value and the largest observed squeezing (2.4 dB at the output facet) is probably due to a combination of multimode operation and weak optical feedback into the laser. Measurements of the laser output spectrum indicate a strong correlation between power in modes other than the primary lasing mode and increased photon-number noise, eventually leading to a loss of squeezing at high pump levels ($I/I_{th} > 35$). Optical feedback may also play a role, although replacing the polarizer with an optical isolator (isolation dB) did not increase the observed squeezing.

A second set of experiments was performed, which consisted of close coupling the laser to a single detector. Because this configuration relies on direct detection, the shot-noise level must be calibrated independently. This raises a concern because differing conditions between calibration and laser noise measurement, such as spot size, could alter detector saturation, making interpretation of the experimental results difficult. For example, increased saturation due to a laser spot size much smaller than that of the calibration source would lead to a lower displayed noise power and thus could be mistaken for amplitude squeezing.

Several steps were taken to avoid errors due to detector saturation. The detector (Hamamatsu Model S1722-01) was chosen for its large area (13.2 mm^2) and excellent saturation characteristics.[14] These saturation characteristics were determined experimentally under conditions similar to those for the close-coupled laser. One such experiment used a red-filtered white-light source, focused to a 1.0-mm^2 spot, to generate the shot-noise level at several dc detector current levels (dc detector current was linear with input power to within 0.2% up to 30 mA). The

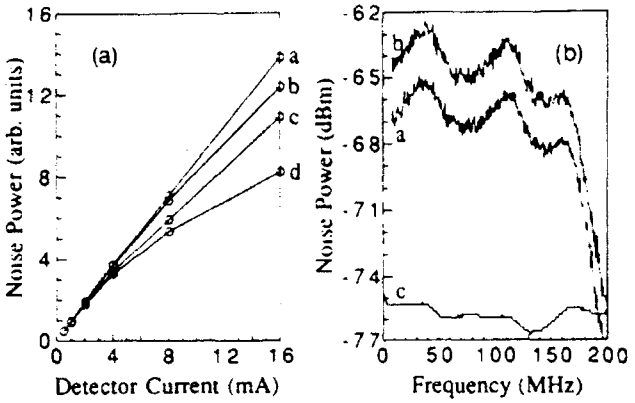

Fig. 2. (a) Red-filtered white-light source was used to study the frequency-dependent saturation characteristic of the detector. The frequencies shown are 10 MHz (trace a), 50 MHz (trace b), 100 MHz (trace c), and 150 MHz (trace d). The dotted line represents the response of an ideal detector. (b) Demonstration of the amplitude squeezing obtained on close coupling the diode laser and detector. Trace a shows the laser noise spectra, trace b shows the shot-noise level corresponding to trace a, and trace c shows the amplifier thermal noise level, which was subtracted from traces a and b.

results are shown in Fig. 2(a). The data indicate that detector saturation is minimal at low frequencies (<50 MHz) out to beyond 8.00 mA.

To ensure that differences between calibration source and laser-beam spot size did not affect the level of this saturation, several laser-to-detector distances (and corresponding spot sizes) were used in the experiments described below. The measured laser noise level remained constant ±6% over a factor of 5 change in spot size and was not directly correlated with spot size. This result, coupled with the fact that the largest laser spot size (0.9 mm^2) was comparable with the calibration spot size (1.0 mm^2), shows that intensity-dependent detector saturation had little effect on the results of these experiments.[14] The insensitivity of this detector to spot size also extended to larger areas (data taken with red light and light-emitting diode spot sizes of up to 10 mm^2 were nearly identical to the 1.0-mm^2 data).

To minimize possible errors, the detector and its associated amplifiers were kept at room temperature while the laser was cooled to 10 K. Here the threshold current was 0.78 mA, and the differential laser current-to-detector current transfer ratio above threshold was 0.67. The results of one experiment for a bias level of $I/I_{th} = 16$ (detector current 8.00 mA) are shown in Fig. 2(b). The amount of squeezing obtained low frequencies (where the effects of saturation are smallest) fell between 2.4 and 2.9 dB as the distance between the laser and detector was varied from 1.5 mm (0.17-mm^2 spot size) to 3.5 mm (0.92-mm^2 spot size) and did not increase at higher bias levels. Owing to a lack of direct correlation with distance, this slight variation in squeezing is believed to be due to weak optical feedback, which depended on the exact orientation of the laser and detector. When corrected for a detection efficiency of 85%, 2.9 dB of squeezing corresponds to 3.7 dB at the output facet of the laser, which is still less than the theoretically expected value of 6.6 dB.

Other lasers of the same type gave similar levels of squeezing, although the temperature at which maximum squeezing was observed varied from laser to laser. Simultaneous monitoring of the laser mode (by collecting light from the back facet and analyzing it with a monochromator) and amplitude fluctuations revealed that longitudinal-mode characteristics were responsible for this temperature dependence. The best squeezing was obtained with a dominant primary mode, indicating that cross-gain saturation did not result in complete negative correlation between the modes.[15] As the side-mode power (relative to the main mode) and the number of side modes increased, so did the amplitude noise. Unfortunately, at high pump levels (typically $I/I_{th} > 25$) this always occurred, which is probably why the full theoretical level of squeezing could not be attained and raises the possibility that mode stabilization may enhance the observed squeezing.

We acknowledge helpful discussions with H. J. Kimble. This research is supported by the U.S. Air Force Office of Scientific Research and is based on research supported under a National Science Foundation Graduate Fellowship.

References

1. H. P. Yuen, Phys. Rev. Lett. **56,** 2176 (1986).
2. Y. Yamamoto and H. A. Haus, Rev. Mod. Phys. **58,** 1001 (1986).
3. M. Sargent III, M. O. Scully, and W. E. Lamb, Jr., *Laser Physics* (Addison-Wesley, Reading, Mass., 1974).
4. Y. M. Golubev and I. V. Sokolov, Sov. Phys. JETP **60,** 234 (1984).
5. Y. Yamamoto, S. Machida, and O. Nilsson, Phys. Rev. A **34,** 4025 (1986); see also Y. Yamamoto and S. Machida, Phys. Rev. A **35,** 5114 (1987).
6. H. Ritsch, P. Zoller, C. W. Gardiner, and D. F. Walls, Phys. Rev. A **44,** 3361 (1991).
7. W. H. Richardson and R. M. Shelby, Phys. Rev. Lett. **64,** 400 (1990).
8. W. H. Richardson, S. Machida, and Y. Yamamoto, Phys. Rev. Lett. **66,** 2867 (1991).
9. S. Machida and Y. Yamamoto, Opt. Lett. **14,** 1045 (1989).
10. H. P. Yuen and V. W. S. Chan, Opt. Lett. **8,** 177 (1983).
11. S. Prasad, M. O. Scully, and W. Martienssen, Opt. Commun. **62,** 139 (1987).
12. M. D. Levenson, W. H. Richardson, and S. H. Perlmutter, Opt. Lett. **14,** 779 (1989).
13. Y. Yamamoto and H. A. Haus, Phys. Rev. A **45,** 6596 (1992).
14. The saturation characteristics of NDL-2208, EG&G C30957E, and Melles Griot 13DSI003 silicon photodiodes were also investigated and were found to be unsatisfactory at the intensity levels imposed by the close-coupled laser. The onset of saturation in these devices was much more abrupt, and the sensitivity to spot-size variations was greater than that of the Hamamatsu detectors.
15. S. Inoue, H. Ohzu, S. Machida, and Y. Yamamoto, Phys. Rev. A **46,** 2757 (1992).

Surface Science 228 (1990) 69–73
North-Holland

HIGH RESOLUTION LASER SPECTROSCOPY OF RELAXATION AND THE EXCITATION LINESHAPE OF EXCITONS IN GaAs QUANTUM WELL STRUCTURES

Hailin WANG, J.T. REMILLARD, M.D. WEBB, D.G. STEEL, J. PAMULAPATI, J. OH and P.K. BHATTACHARYA

Departments of Physics and Electrical Engineering, Harrison M. Randall Physics Laboratory, University of Michigan, Ann Arbor, MI 48109, USA

Received 2 June 1989; accepted for publication 18 August 1989

A new class of measurements on GaAs quantum well structures based on frequency domain nonlinear laser spectroscopy is described. Room temperature measurements of the excitation relaxation show an interference effect in the lineshape which is interpreted as a shift in exciton frequency. Low temperature measurements on the localized exciton provide an excitation lineshape which eliminates the effects of inhomogeneous broadening and shows the presence of spectral diffusion.

The room temperature nonlinear optical response near the band edge in GaAs quantum wells has resulted in considerable interest in these materials because of their potential importance to optoelectronic devices [1]. Studies of these materials have also resulted in new understanding of the fundamental physics of excitons [2–4]. In this paper, we describe a new class of measurements based on high resolution frequency domain nonlinear laser spectroscopy which are distinguished from earlier measurements because of the ability to report on excitation lineshapes as well as the ability to provide greater sensitivity in measurements of excitation relaxation. The measurements of the excitation lineshape are significant because this spectroscopy eliminates the contribution of inhomogeneous broadening which characterizes low temperature absorption measurements.

The basic experimental configuration for these experiments is based on backward four wave mixing (FWM) [5]. In these experiments, two optical beams intersect each other at a small angle. One beam is designated the probe beam with field amplitude $E_p(\omega_p, k_p)$ while the remaining beam is the forward pump beam with field amplitude $E_f(\omega_f, k_f)$. The beams are nearly normal to the growth direction of the quantum well and produce an interference pattern which results in a spatial and temporal modulation of excitation proportional to $E_f(\omega_f, k_f) \cdot E_p^*(\omega_p, k_p)$. A coherent signal, $E_s(\omega_s, k_s)$, is produced by the scattering of a back beam with field amplitude $E_b(\omega_b, k_b)$. Spectroscopic information is obtained by varying any one frequency with respect to the remaining two frequencies. In particular, the FWMp response is obtained by varying ω_p holding $\omega_f = \omega_b$ while the FWMb response is obtained by varying ω_b, holding $\omega_p - \omega_f =$ constant. The FWMp response provides a lineshape related to the excitation decay rate and contains contributions such as inelastic scattering and carrier or excitonic recombination in addition to the contribution of nonradiating states. The FWMb response provides a measure of the excitation lineshape without contributions from inhomogeneous broadening [5,6].

At room temperature, the exciton absorption lineshape is dominated by homogeneous broadening due to the rapid LO phonon ionization rate. Hence, a study of the FWMb response provides little additional information. However, the nonlinear response arises because the electron–hole plasma generated from the ionization of the exciton results in band filling and exchange effects which lead to a modification of the optical proper-

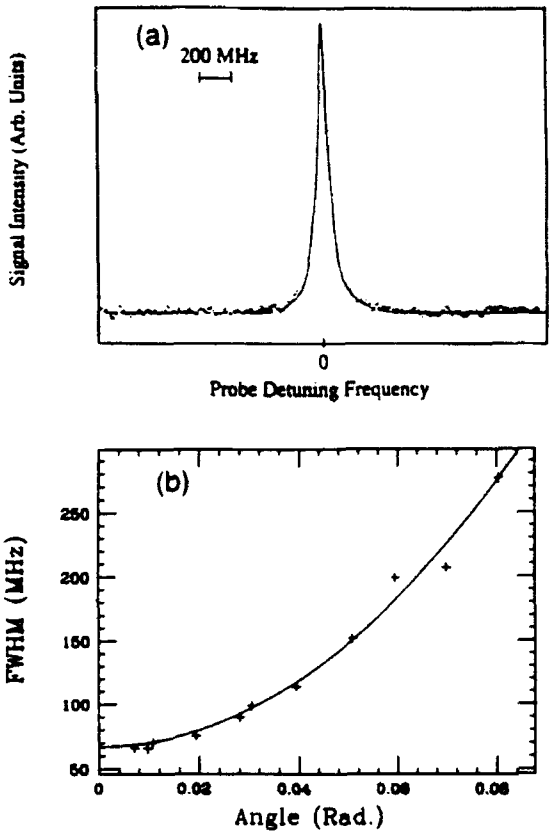

Fig. 1. (a) Room temperature FWMp lineshape. (b) Angle dependence of the FWMp line width.

ties of the exciton including the oscillator strength, dephasing rate, and resonance frequency. Hence, a grating produced by the interference of the forward pump and probe has a decay rate determined by the e–h recombination time and the time it takes carriers to spatially diffuse across the grating. Fig. 1a shows the FWMp response at room temperature along with a fit of a Lorentzian. The line width is given by $\gamma_{e-h} + D|\Delta k|^2$ where γ_{e-h} is the e–h recombination rate, D is the ambipolar diffusion coefficient, and $|\Delta k| = |k_f - k_p|$. Fig. 1b shows the angle dependence of the FWMp line width as a function of angle and the solid line is a fit of the above line width expression. From the shape of the curve, we can obtain the ambipolar diffusion coefficient (18 cm^2/s) and from the y-intercept, we can obtain the e–h recombination rate (5 ns)

Using the method of correlated optical fields [7] to eliminate interlaser jitter contributions to the lineshape, we examined the FWMp response near $\omega_p - \omega_f = 0$. Fig. 2 shows the lineshape. There are two important observations which can be drawn from fig. 2a. First, there exists a strong (dominant) contribution to the room temperature nonlinear response which is slow (10 μs). Secondly, the lineshape is characterized by a shape which is typical of interference effects [*1]. We believe this lineshape is due to a shift in the exciton resonance. Solutions to the optical Bloch-type equations which have been phenomenologically modified to account for band filling and exchange effects show that this interference profile results when the Bloch equations are further modified to account for a shift in the exciton resonance [9]. The curve in fig. 2b is the calculated FWMp response, showing the interference lineshape. It is important to stress that the solutions of the modified Bloch equations only show interference effects when the exciton resonance is allowed to shift due to the presence of the e–h plasma or some other laser induced mechanism. We also note that the shape of the FWMp response is dependent on the wavelength of the back pump. Fig. 2c shows the FWMp lineshape measured when the back pump is tuned red of the peak of the heavy hold exciton. (The forward pump and probe beams remained tuned on the peak of the heavy hold exciton.) Fig. 2d shows the lineshape calculated from the modified Bloch equations when the back pump is shifted red of the exciton resonance.

At low temperatures, the excitons are stable against phonon ionization. Hence, studies of relaxation provide information on the exciton dynamics. In addition, because the exciton is now stable, data obtained from the FWMb response provide information on the excitation lineshape. At 5 K, the absorption lineshape is inhomogeneously broadened due to fluctuations in the well thickness. The HH1 absorption line width in this sample is 3.7 meV. The sample was further characterized by performing luminescence measure-

[*1] Interference effects are common in nonlinear laser spectroscopy as discussed in ref. [8]. However, the origin of the interference effects in this paper is new and distinct.

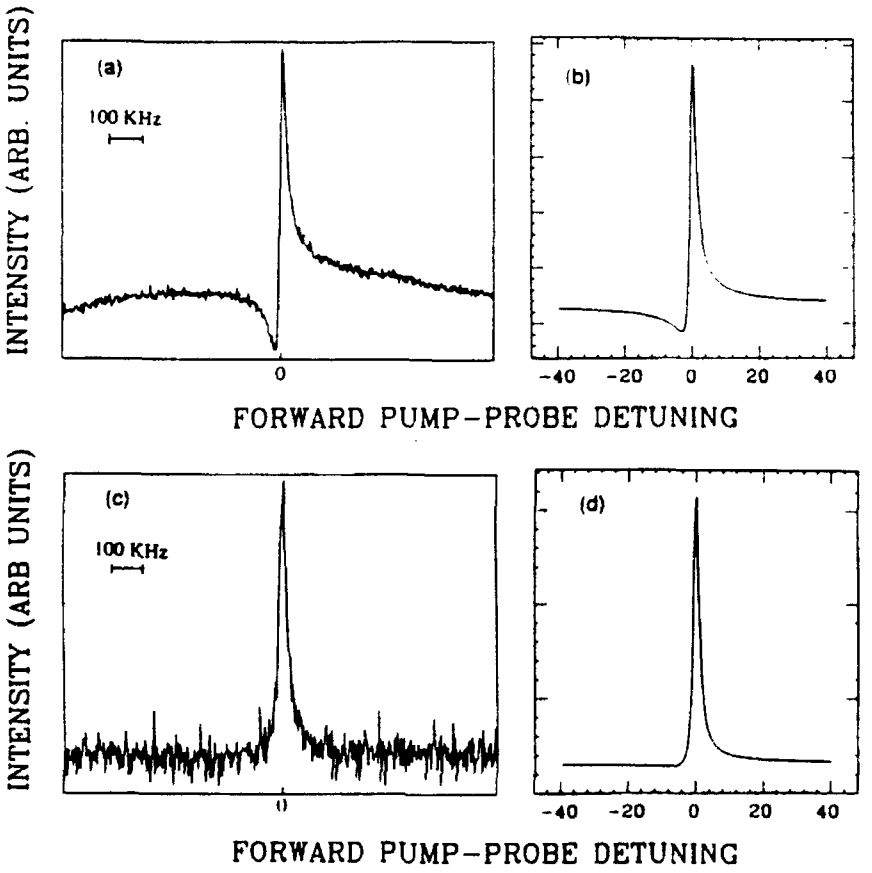

Fig. 2. The FWMp line shape using the technique of correlated fields. (a) Interference profile when the back beam wavelength is on the exciton peak. (c) The lineshape when the back beam is tuned red of the exciton peak. (b, d) Calculated lineshapes using modified Bloch equations.

ments as well as obtaining a degenerate four wave mixing (DFWM) spectrum. (A DFWM spectrum is obtained by using one laser for all beams in the nonlinear interaction and observing the change in intensity of the signal as the frequency of the laser is tuned across the exciton resonance.) The peak of the luminescence from the excitons is shifted 2.8 meV to the red of the HH1 absorption maximum. The red shifted luminescence is interpreted as being due to the recombination of excitons which have become localized due to fluctuations in well thickness. The DFWM measurements show a peak which coincides exactly with the luminescence peak, suggesting the nonlinear response is also due to localized excitons.

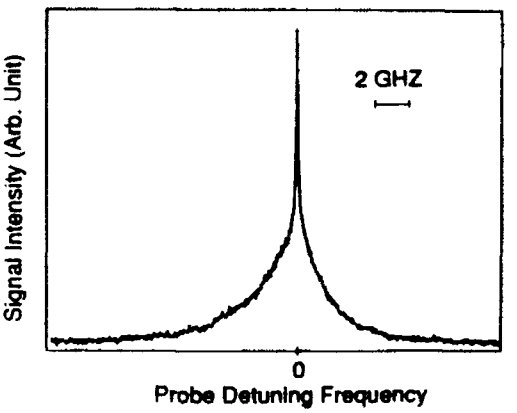

Fig. 3. The FWMp lineshape at 5 K showing the presence of multiple relaxation mechanisms.

In the first set of measurements, we examined the FWMp response to determine the excitation relaxation dynamics. In the simple picture of the exciton undergoing a single relaxation due to radiative decay, the lineshape would be a single Lorentzian. Fig. 3 shows the FWMp line width obtained at 5 K. The curve shows clear evidence of multiple decay processes rather than a single decay. In particular, three decay channels are observed in fig. 3. The fastest and slowest channels having relaxation times of 100 ps and 15 ns are clearly observed in this figure. However a third component to the lineshape corresponding to a relaxation time of 1.5 ns is observable upon expansion of the center portion of the figure. The 1.5 ns feature corresponds to the expected radiative decay time for a well of thickness of 98 Å [10]. The origin of the 100 ps feature is most likely due to decay of the excitation by spectral diffusion via phonon assisted tunneling. Similar behavior has been reported in transient pump–probe measurements [4]. Further evidence for this is given below. The origin of the 15 ns decay rate is due possibly to the presence of electric fields in the material which are known to extend the life time of the exciton.

FWMb experiments were then conducted to determine the lineshape of the excitation. Note that the energies at which the following FWMb lineshapes were recorded are referenced with respect to the position of the peak of the absorption. Fig. 4a shows the FWMb lineshape obtained 3.45 meV to the low energy side of the absorption maximum. The lineshape is slightly asymmetric on the high energy side. This asymmetry becomes much clearer in the FWMb spectra recorded at the absorption line center as seen in fig. 4b. The presence of asymmetry in the FWMb response is highly significant, since it can be shown [6] that if we are measuring just the homogeneous lineshape, the FWMb response should be symmetric about $\omega_b - \omega_f = 0$, even if the homogeneous lineshape is asymmetric. However, such asymmetric lineshapes can be observed in the FWMb response in the presence of spectral diffusion. Hence we believe these measurements show directly that excitons are spectrally diffusing, as suggested by earlier work [4]. Fig. 4c shows a comparison of the measured temperature dependence of the line width in fig. 4a to a theory based on phonon assisted tunnelling. The curve varies as $e^{\beta T^{1.6}}$ and is in general agreement with theoretical expectations [11].

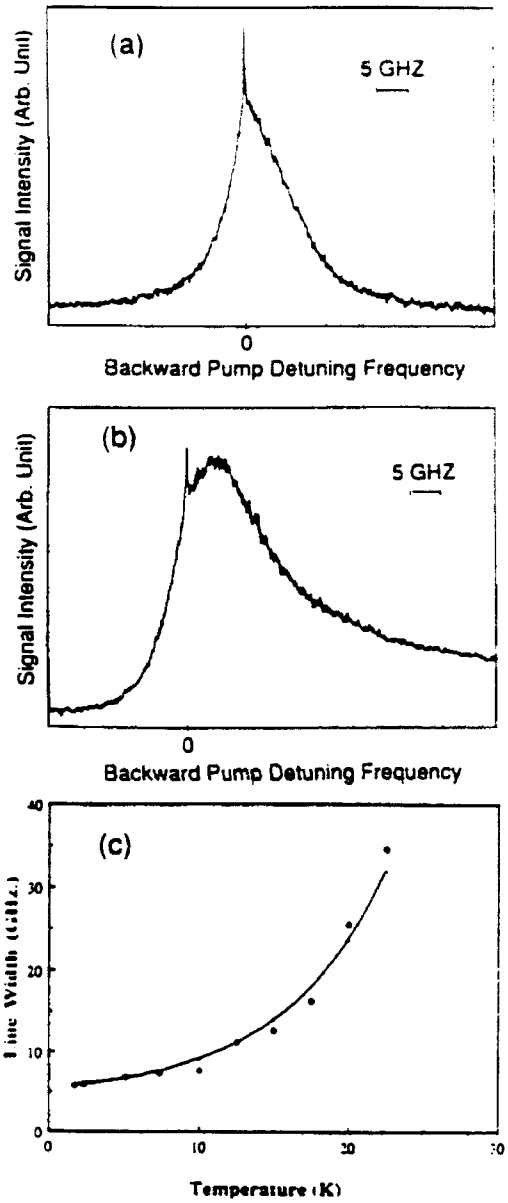

Fig. 4. The FWMb line shape at 5 K. (a) The lineshape red of the absorption maximum. (b) The lineshape measured at the peak of the exciton absorption. (c) The temperature dependence of the line width in (a).

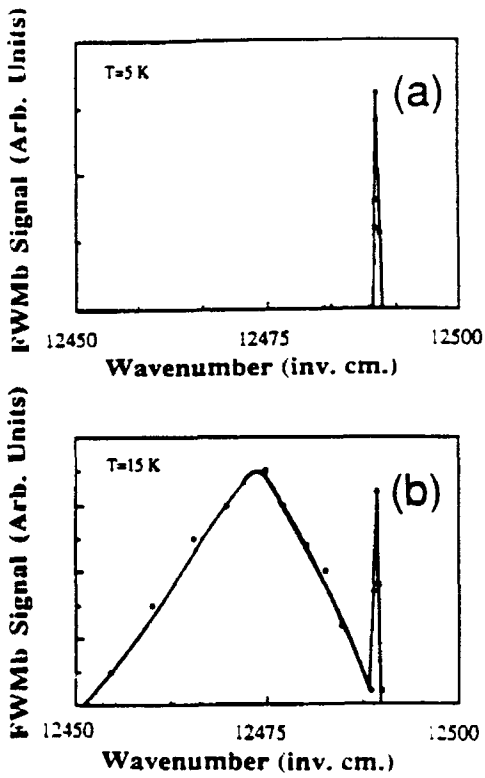

Fig. 5. FWMb response shown for 2 temperatures. (a) The response at 5 K. (b) The response at 15 K illustrating the spectral diffusion of the excitation to lower energies.

Further evidence for spectral diffusion is shown in fig. 5. Fig. 5a is an extended scan of the data shown in fig. 4b at 5 K. Fig. 5b shows the same data taken at 15 K illustrating the spectral diffusion of excitons to lower energies, the peak of the response occurring at the same energy as the peak of the luminescence. As in the case of the luminescence peak, the wide resonance in the FWMb spectra shown in fig. 5b represents the energy distribution of the localized excitons. Theoretical results of the FWMb line shape obtained from optical Bloch-type equations, modified to include spectral diffusion, show similar behavior. It is interesting to note that while we obtain clear evidence for energy diffusion, there is no evidence in the data to suggest that the excitons are spatially diffusing.

In summary, we have used high resolution frequency domain nonlinear spectroscopy to study relaxation and excitation lineshapes in GaAs multiple quantum wells. At room temperature, we have measured the ambipolar diffusion coefficient and the free carrier recombination time. In addition, we have observed an interference effect in the FWMp lineshape which we believe is due to a shift in the exciton resonance. At low temperature, we have identified contributions to the relaxation of the exciton population due to spectral diffusion and exciton recombination. Using FWMb spectroscopy, we have obtained measurements of the lineshape of the excitation. The observation of asymmetric FWMb lineshapes and the measured temperature dependence of the line width provide evidence that the excitons are spectrally diffusing via phonon assisted tunnelling.

This work is supported by the AFOSR, US ARO and the US ARO URI.

References

[1] D.S. Chemla, S. Schmitt-Rink and D.A.B. Miller, in: Nonlinear Effects and Instabilities in Semiconductors, Ed. H. Haug (Academic Press, New York, 1988).
[2] S. Schmitt-Rink, D.S. Chemla and D.A.B. Miller, Phys. Rev. B 32 (1985) 6601.
[3] D.S. Chemla and D.A.B. Miller, J. Opt. Soc. Am. B 2 (1985) 1155.
[4] J. Hegarty and M.D. Sturge, J. Opt. Soc. Am. B 2 (1985) 1143.
[5] D.G. Steel and J.T. Remillard, Phys. Rev. A 36 (1987) 4330.
[6] J.T. Remillard, H. Wang, D.G. Steel, J. Oh, J. Pamulapati and P.K. Bhattacharya, Phys. Rev. Lett. 62 (1989) 2861.
[7] D.G. Steel and S. Rand, Phys. Rev. Lett. 55 (1985) 2285.
[8] M.D. Levenson and S. Kano, in: Introduction to Nonlinear Laser Spectroscopy, revised ed. (Academic Press, New York, 1988) p. 156.
[9] J.T. Remillard, H. Wang, M.D. Webb, D.G. Steel, J. Oh, J. Pamulapati and P.K. Bhattacharya, High Resolution Nonlinear Laser Spectroscopy of Room Temperature GaAs Quantum Well Structures: Observation of Interference Effects, Opt. Lett. 14 (1989) 1131.
[10] J. Feldmann, G. Peter, E.O. Gobel, P. Dawson, K. Moore, C. Foxxon and R.J. Elliot, Phys. Rev. Lett. 59 (1987) 2337.
[11] T. Takagahara, Phys. Rev. B 32 (1985) 7013.

Reprinted from Journal of the Optical Society of America B

Frequency domain four-wave mixing spectroscopy of temperature and optical-intensity-dependent relaxation in CdSSe microcrystallite-doped glass

J. T. Remillard, H. Wang, M. D. Webb, and D. G. Steel

Departments of Physics and Electrical Engineering, Randall Laboratory of Physics, University of Michigan, Ann Arbor, Michigan 48109

Received May 25, 1989; accepted December 8, 1989

We describe cw frequency-domain nonlinear laser spectroscopy results obtained in the study of relaxation in glasses doped with microcrystallites of CdSSe. Measurements are made as a function of temperature and optical intensity, using low-intensity cw optical excitation. The results are interpreted based on the assumption that the dynamics of the nonlinear response in this material is controlled by traps.

Applications to nonlinear-optical problems and the possibility of learning about the physics of quantum-size effects have led to considerable recent interest in glasses doped with semiconductor microcrystallites. These glasses are doped with $CdS_{1-x}Se_x$ and are commercially available as sharp-cut colored glass filters.[1]

In the commercial material the microcrystallites typically have an average diameter of 100 Å with a full width at half-maximum distribution of 50 Å as determined by electron microscopy (obtained for the Corning material[2]), which results in a relatively featureless room-temperature absorption edge. At low temperature these materials have been reported to exhibit structure in the luminescence spectrum attributed to quantum confinement[3], and more recent results have shown the existence of structure in the modulated absorption spectrum.[4] More careful material processing methods have produced material with a uniform size distribution that shows clear structure in the room-temperature linear absorption spectrum; this has been attributed to quantum-size effects.[5] One group[6] has produced structures as small as 12 Å in CdS, CdSe, and CuCl. Another group[2] has made glasses doped with microcrystallites in which the size distribution is controlled by a heat treatment process, and microcrystallites as small as 25 Å have been observed.

Because of the relative ease of fabrication, the large, fast, nonlinear-optical response, and the fact that the host material is a glass, the applications of these materials to optical switches and integrated optics have been studied by numerous groups. In addition, there have been several studies discussing the physics of these materials. As early as 1964, the material was used to demonstrate a Q switch in a laser.[7] Optical bistability was demonstrated by McCall and Gibbs[8] and by Gibbs *et al.*[9]; however, the slow response suggested that the nonlinearity was thermal in origin.[10] Using a Q-switched laser and transient excitation, Jain and Lind[11] demonstrated optical phase conjugation and showed that a large nonlinear-optical susceptibility was observable ($\chi^{(3)} \approx 10^{-8}$ esu). They determined that the relaxation time was faster than 8 nsec (determined as an upper limit.) The model for the nonlinear response proposed by Jain and Lind was based on the production of a short-lived electron–hole plasma. This work was followed by numerous other experimental[12–22] and theoretical[23–25] reports of the nonlinear response; here pulsed excitation was used. Included in these observations have been several measurements of the dynamical behavior[26–29] that are of key importance to high-speed applications. These measurements show that carrier relaxation times are in the picosecond time domain. The range of fast relaxation times reported in the literature has been attributed to defects that decrease the relaxation time and that are induced by high-power optical irradiation (photodarkening).[21] More recently, measurements of transient absorption obtained by the methods of ultrafast laser spectroscopy have shown relaxation processes occurring on the time scale of a few hundred femtoseconds.[30,31] Measurements on CdSSe glasses in which quantum confinement effects dominate have demonstrated the importance of phonon broadening and have shown evidence for spectral hole burning at low temperatures.[32] Other measurements of hole burning in small (35–55-Å) microcrystallites of CdSe clusters suspended in a polystyrene film have resulted in measurements of the contributions of homogeneous and inhomogeneous broadening to the electronic absorption spectra.[33] The recent applications are discussed in Ref. 34.

In this paper we examine the physical behavior of a slower but much larger nonthermal contribution to the nonlinear optical response obtained under cw excitation. The first indication of the possibility of a large cw nonlinear response was provided by the observation of low-frequency dynamical behavior leading to subharmonic generation and near-chaotic behavior in semiconductor-doped glass observed at low temperature (140 K) by Zheludev *et al.*[35] This work was followed by measurements in our laboratory, using degenerate four-wave mixing, of the room-temperature cw nonlinear response, which showed a nonlinear response much larger but slower than than the response that was obtained based on pulsed excitation.[36] The results showed $\chi^{(3)} \approx 10^{-7}$ esu. Using four-wave mixing spectroscopy, we found a narrow resonance (4.4 kHz) in the nonlinear susceptibility corresponding to a 72-μsec excitation–relaxation time. In that

0740-3224/90/060897-05$02.00

publication, we attributed the origin of the nonlinear dynamics to contributions from traps, a result suggested by earlier measurements[3,13] and confirmed in more recent researches.[29,37]

This paper extends the earlier measurements to show the temperature and optical-intensity dependence of the nonlinear response. These results are discussed based on the assumption that the dynamics of the nonlinear response is controlled by traps. As a result of this research, we have demonstrated[34] that a large third-order susceptibility ($\chi^{(3)} \approx 2 \times 10^{-4}$ esu) can be obtained at 125 K. In addition, the current research provides a measure of an effective thermal activation energy, and a model is discussed that suggests that the saturation of the nonlinear response reported in our earlier publication is due to saturation of the available traps. The large nonlinear response has been used to demonstrate efficient optical phase conjugation, and the narrow bandwidth and near-angle-independent response have been used to demonstrate a tunable optical filter.[34]

The experimental configuration for these measurements is based on backward four-wave mixing, using a frequency stabilized tunable cw dye laser. Two counterpropagating pump beams with fields $\mathbf{E}_f(\omega)$ and $\mathbf{E}_b(\omega)$ interact with a probe beam $\mathbf{E}_p$ ($\omega_p = \omega + \delta$) in the sample, which is contained in a variable-temperature cryostat. The angle between the forward pump and probe beams is θ. The three beams interact through the nonlinear response to produce a signal field ($\mathbf{E}_s$) arising from a polarization proportional to $\chi^{(3)}(\mathbf{E}_f \cdot \mathbf{E}_p^*)\mathbf{E}_b$. For these measurements $\mathbf{E}_f \| \mathbf{E}_p \perp \mathbf{E}_b$ (no signal is obtained for $\mathbf{E}_f \| \mathbf{E}_b \perp \mathbf{E}_p$ for low-power cw excitation), and the signal arises from the coherent scattering of $\mathbf{E}_b$ from the traveling-wave grating of excitation produced by $\mathbf{E}_f \cdot \mathbf{E}_p$. In the limit where the dephasing rate is large compared with the excitation–relaxation rates, a measurement of $|\mathbf{E}_s|^2$ as a function of δ for fixed ω [the four-wave mixing–probe (FWMp) response] gives a line shape related to relaxation rates associated with the excitation grating produced by the forward pump and probe. (If the dephasing rate is not large, the FWMp response may include interference effects arising from the induced dipole.[38]) A simple physical understanding of the FWMp response can be obtained by considering the response in the limit of small and large δ. For a δ small compared with the excitation–relaxation rate, the spatial modulation of the excitation is in phase with the intensity pattern formed by $E_f E_p^*$, and a strong signal is produced by the scattering of the backward pump beam from the grating. However, for a δ large compared to the excitation–relaxation rates, the spatial modulation of the excitation is washed out, and there is no grating to produce a coherent signal.[39]

In this system we assume that the nonlinear response is due to phase-space filling effects that are caused by the free carriers produced by the forward pump and probe; these effects result in a modulation of the transition oscillator strength.[40] As indicated above, because of the slow response, it is believed that the dynamics of the nonlinear response are dominated by the presence of traps.[41] If an electron (or hole) decays to a long-lived trap, the remaining hole (or electron) can still contribute to the band filling. Thus a component of the band-filling relaxation rate will be determined by the effective decay time of the carriers from the traps. The linewidth of a FWMp measurement is thus related to the effective trap relaxation rate.

A detailed study of the FWMp linewidth was performed with the experimental setup described in Ref. 36. Since the linewidths were much smaller than the interlaser jitter that is associated with a measurement based on a system in which one stabilized dye laser provides the pump beams and a second dye laser provides the probe beam, we used the method of correlated optical fields, employing two acousto-optic modulators driven by two phase-locked frequency synthesizers. In this approach the first-order Bragg-scattered beam from the first modulator provided the pump beams, while the second acousto-optic cell provided the probe beam. The first acousto-optic modulator was operated at a fixed drive frequency of 40 MHz. The second driver could be varied about the 40-MHz drive frequency. In this way we could vary δ over the range needed for the measurement in order to obtain line shapes without contributions from laser jitter.

Figure 1 shows the FWMp linewidth obtained at 125 K in RG630. The data show that the profile is not a pure Lorentzian, suggesting that if trap dynamics is responsible for the behavior, then the response is most likely an average over a distribution of traps, a possibility supported by additional data below. The inset on the left shows the FWMp profile as a function of excitation wavelength near the filter absorption edge. There is a dependence on excitation wavelength, with the linewidth varying from 214 to 429 Hz at this temperature as the wavelength is varied from 600 to 614 nm. The inset on the right shows this dependence with a linear fit of the data. In addition, the strength of the nonlinear response also varies. On the blue side of the data the incident beams are strongly absorbed by the material, whereas on the red side there is a decrease in the optical coupling. For the remaining data below, all measurement were made at the peak of the response.

The FWMp response was studied as a function of temperature. Figure 2 shows the log of the FWMp linewidth as a function of $1/T$. All linewidths were observed to have a linear dependence on optical intensity. The data used for Fig. 2 correspond to the zero-intensity intercept. (Further discussion is given below regarding intensity-dependent effects.) The general form of the data in Fig. 2 suggests a functional form for the effective trap decay rate given by $\gamma(0) + \Gamma \exp(-\mathcal{E}_b/kT)$, where $\gamma(0)$ is the zero-temperature decay rate and $\Gamma \exp(-\mathcal{E}_b/kT)$ is the probability per unit time for the electron or hole to escape from a thermally activated trap ($\mathcal{E}_b$ is the activation energy). The solid curve shown in Fig. 2 is the best fit of the functional form for the effective trap decay rate given above. The asymptotic value of the curve gives the zero-temperature decay rate. The slope of the curve gives the activation energy, determined to be 137 meV. The decay parameters Γ is 0.7 MHz, and the zero-temperature decay rate $\gamma(0)$ is 43 Hz.

It is most likely that at these powers the excitation is in near equilibrium with the crystal lattice embedded in the glass material, and the actual details of decay are most likely far more complex than indicated by such a simple description. Experiments have been reported in colloidal suspensions of CdS clusters[42] in which luminescence decay is interpreted based on a theory for multiphonon-assisted excitation transfer.[43] For our measurements we are unable to distinguish between these different decay mechanisms.

We also observe that the FWMp linewidth is intensity

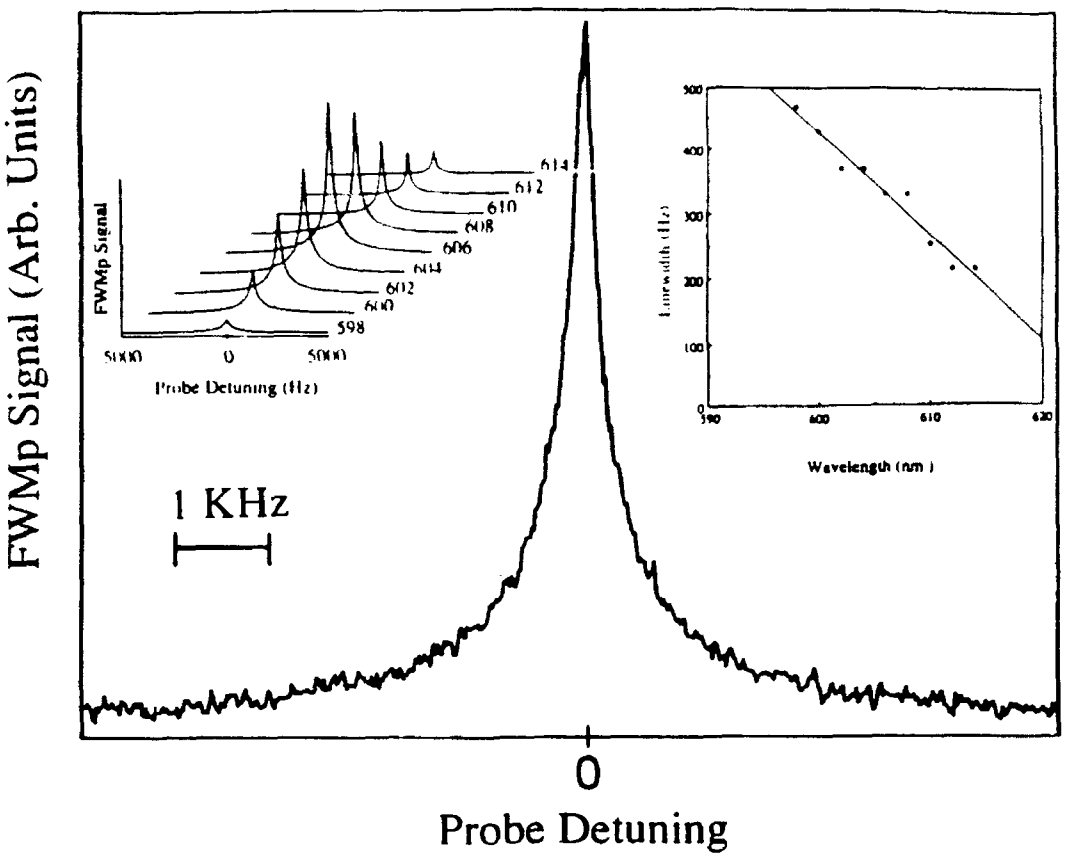

Fig. 1. FWMp spectrum obtained by the method of correlated optical fields. The inset on the left shows the FWMp line shape obtained for different excitation wavelengths at a constant temperature. The inset on the right shows the dependence of linewidth on wavelength.

dependent, as shown in Fig. 3, showing a linear dependence on intensity at low powers. Additionally, as reported in Ref. 34, we observed a rolloff in the nonlinear response at high pump intensities. (At 125 K, saturation of the nonlinear response occurred around 10 W/cm^2). A qualitative understanding of the saturation behavior reported in Ref. 34 and the results obtained in the FWMp measurements can be obtained by considering a simple model of the nonlinear response based on the energy-level diagram shown in Fig. 4. In this model optical radiation induces a transition from the valence band to the conduction band, producing an electron–hole pair. The electron in the conduction band can decay back to the valence band with decay rate γ_{cv} or to a trap with decay rate KN_t in the limit that the traps are unsaturated, where N_t is the total trap density. (For this discussion we consider only electron traps.) The trapped electron can then be thermally activated from the trap and return to the conduction band with rate γ_{tc} or recombine with a hole in the valence band with rate γ_{rec}.

In the absence of traps the FWMp line shape would have a width determined by the carrier recombination rate. (Decay of the induced grating by spatial diffusion of the carriers is not included, since the size of microcrystallites is small compared with the grating spacing and microcrystallites are surrounded by insulating glass.) However, if electrons (or holes) can be trapped, the remaining electrons and holes can still contribute to band filling. The time constant for the decay of this system would have a fast component owing to

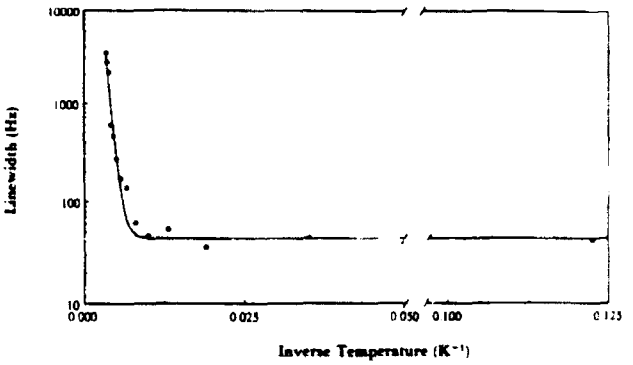

Fig. 2. FWMp linewidth as a function of inverse temperature.

free-carrier recombination and a slow component determined by the rate of electron (or hole) escape from the trap.

In the limit that the dynamics of the nonlinear response are determined by trap kinetics, this simplified model can be used to obtain a more quantitative understanding by considering the rate equations for the electron density n and trap density n_t:

$$\dot{n} = \Phi - \gamma_{cv}n - K(N_t - n_t)n + \gamma_{tc}n_t, \quad (1)$$

$$\dot{n}_t = K(N_t - n_t)n - \gamma_{tc}n_t - \gamma_{rec}n_t, \quad (2)$$

where Φ represents the optical generation rate of electron–

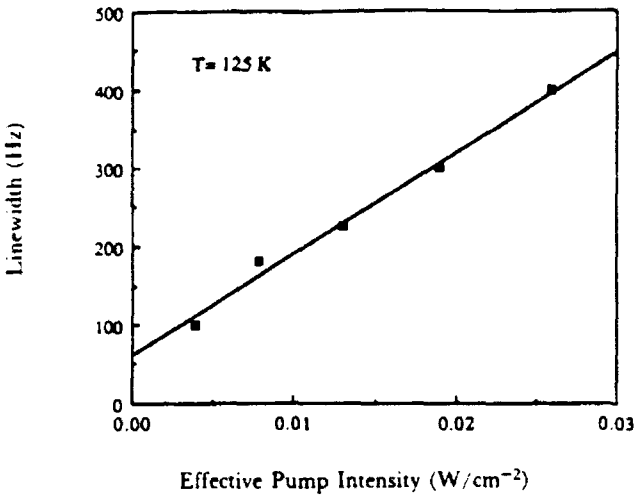

Fig. 3. FWMp linewidth as a function of pump intensity.

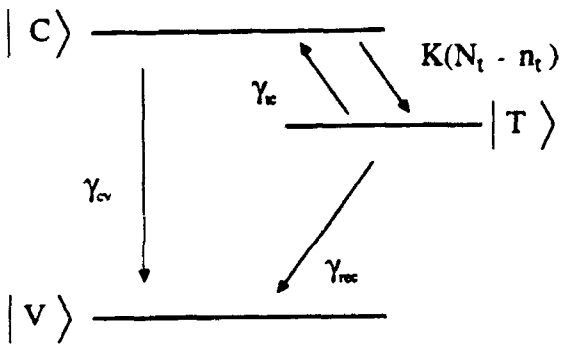

Fig. 4. Energy-level diagram describing the optical interaction believed responsible for the nonlinear response in CdSSe-doped glass. See text for definitions.

hole pairs. The possibility of trap saturation is included through the term $K(N_t - n_t)$. The nonlinear response of this material is the result of band filling, so that we take the nonlinear susceptibility to be proportional to the density of free electrons and holes.[40] However, since experimentally we detect only a slow component of the nonlinear response owing to the presence of holes that persist because of the presence of electron traps, we take the dominant term in the nonlinear susceptibility to be proportional to the filled-trap density. The above set of rate equations can be solved in the presence of strong pumps. However, the essential features of importance to spectroscopy can be seen from the solution obtained in the limit of perturbation theory and in the absence of trap saturation. (Trap saturation effects are discussed below.) Taking $\Phi = (\alpha_{abs}/\hbar\omega)I$, where

$$I = \frac{C}{4\pi}\left\langle\left[\sum_i E_i \cos(k_i x - \omega_i t + \phi_i)\right]^2\right\rangle_t,$$

we obtain an expression for the nonlinear polarization for the FWMp response for the interaction described above in the limit $\delta = \omega_f - \omega_p \ll \gamma_{cv}, KN_t$:

$$P^{NL} = \xi \mathcal{E}_f \mathcal{E}_p^* \mathcal{E}_b \exp[i(k_f - k_p + k_b)x - i(\delta + \omega_b)t \times \frac{N_t}{i\delta + \gamma_{rec} + \gamma_{tc}[\gamma_{cv}/(\gamma_{cv} + KN_t)]} + \text{c.c.}, \quad (3)$$

where ξ is a constant and

$$E_i \cos(k_i x - \omega_i t + \phi_i) = \tfrac{1}{2}\mathcal{E}_i \exp[i(k_i x - \omega_i t)] + \text{c.c.}$$

Thus, in the case of a single trap (i.e., no distribution of trap lifetimes) the linewidth at zero intensity measured in a FWMp experiment is given by an effective trap lifetime

$$\gamma_{eff} = \gamma_{rec} + \gamma_{tc}\left(\frac{\gamma_{cv}}{\gamma_{cv} + KN_t}\right).$$

When the effects of trap saturation are included, the model predicts a rolloff in the nonlinear response at high pump intensities as well as a linear increase in the linewidth with pump intensity in the low-pump-intensity limit. In particular, the above equations can be solved in the presence of strong pumps (standing-wave effects are ignored since the pump polarizations are orthogonal.) In the limit that the dominate decay channel from the trap is γ_{tc}, the above polarization describes the intensity-dependent nonlinear response if we replace N_t with $N_t - n_{t(dc)}$ and replace γ_{tc} with $\gamma_{tc} + Kn_{(dc)}$, where

$$n_{t(dc)} = \frac{Kn_{(dc)}N_t}{\gamma_{tc} + Kn_{(dc)}}, \quad (4)$$

$$n_{(dc)} = \frac{\alpha_{abs}I_0}{\hbar\omega}\frac{1}{\gamma_{cv}}, \quad (5)$$

and I_0 is the pump intensity. These equations show the linear dependence of the linewidth on intensity and the rollover at high intensity; however, by using the single-trap level model presented above, it is not possible to reconcile the low-intensity linewidth broadening rate with the observed saturation intensity. Estimation of the saturation intensity from the low-intensity linewidth broadening rate predicts a value of saturation intensity that is much lower than that observed experimentally. Currently, we believe the explanation for this difference is that this material is characterized by a range of trap lifetimes with correspondingly different concentrations and positions within the band gap. As the intensity of the pumps is increased, the traps begin to fill, and different groups of traps in the distribution then contribute to the response. Thus at low pump intensities the response most likely results from one group of traps, and the values of trap relaxation time and activation energy thus pertain only to this group of traps. However, at the higher intensities different parts of the trap distribution contribute to the signal, resulting in an effective saturation intensity that will differ from the prediction based on the assumption of a single trap and use of the measured low-intensity linewidth broadening rate. Such an interpretation is supported by recent measurements by Tomita *et al.*,[37] which have shown nonexponential decays in luminescence lifetimes with time constants ranging from 2 μsec up to lifetimes beyond 20 μsec at liquid-nitrogen temperatures. These multiple exponential decays are consistent with our non-Lorentzian line shapes.

In summary, these measurements provide further insight into the nature of the nonlinear response obtained by using cw excitation in CdSSe-doped glass. Using frequency-domain nonlinear laser spectroscopy methods, we have determined the effects of temperature and pump intensity on the dynamical behavior of the nonlinear response. There is strong evidence that traps are responsible for the dynamics of the cw nonlinear response and that trap saturation is responsible for the observed rolloff of the response.

ACKNOWLEDGMENTS

This research was supported by U.S. Air Force Office of Scientific Research grant 85-0280. In addition, M. D. Webb was supported by an Army Research Office Fellowship from the University Research Initiative program.

REFERENCES AND NOTES

1. For example, from Corning, Schott, Hoya, and Toshiba.
2. N. F. Borrelli, D. W. Hall, H. J. Holland, and D. W. Smith, J. Appl. Phys. **61**, 5399 (1987).
3. J. Warnock and D. D. Awschalom, Phys. Rev. B **32**, 5529 (1985).
4. F. Moshary and S. R. Hartmann, Department of Physics, Columbia University, New York, New York 10027 (personal communication).
5. L. Banyai and S. W. Koch, Phys. Rev. Lett. **57**, 2722 (1986); see also S. Schmitt-Rink, Phys. Rev. Lett. **60**, 1205 (1988); L. Banyai and S. W. Koch, Phys. Rev. Lett. **60**, 1206.
6. A. I. Ekimov and A. A. Onushchenko, Pis'ma Zh. Eksp. Teor. Fiz. **40**, 337 (1984) [JETP Lett. **40**, 1136 (1984)]; Pis'ma Zh. Eksp. Teor. Fiz. **34**, 363 (1981) [JETP Lett. **34**, 343 (1981)]; A. I. Ekimov, Al. L. Efros, and A. A. Onushchenka, Solid State Commun. **56**, 921 (1985).
7. G. Bret and F. Gires, Appl. Phys. Lett. **4**, 175 (1964).
8. S. L. McCall and H. M. Gibbs, J. Opt. Soc. Am. **68**, 1378 (1978).
9. H. M. Gibbs, G. R. Olbright, N. Peyghambarian, H. E. Schmidt, S. W. Koch, and H. Haug, Phys. Rev. A **32**, 692 (1985); see also H. Gibbs, *Optical Bistability, Controlling Light with Light* (Academic, Orlando, Fla., 1985).
10. G. Thibault and M.-M. Denariez-Roberge, Can. J. Phys. **63**, 198 (1985).
11. R. K. Jain and R. C. Lind, J. Opt. Soc. Am. **73**, 647 (1983).
12. S. S. Yao, C. Karaguleff, A. Gabel, R. Fortenbuery, C. T. Seaton, and G. Stegeman, Appl. Phys. Lett. **46**, 801 (1985).
13. P. Roussignol, D. Ricard, K. C. Rustagi, and C. Flytzanis, Opt. Commun. **55**, 143 (1985).
14. B. Danielzik, K. Natterman, and D. von der Linde, Appl. Phys. B **38**, 31 (1985).
15. G. R. Olbright and N. Peyghanbarian, Appl. Phys. Lett. **48**, 1184 (1986).
16. D. Cotter, presented at the XIV International Quantum Electronic Conference, San Francisco, California, 1986.
17. G. R. Olbright, N. Peyghambarian, S. W. Koch, and L. Banyai, Opt. Lett. **12**, 413 (1987).
18. F. Hache, P. Roussignol, D. Ricard, and C. Flytzanis, Opt. Commun. **64**, 200 (1987).
19. F. de Rougemont, R. Frey, P. Roussignol, D. Ricard, and C. Flytzanis, Appl. Phys. Lett. **50**, 1619 (1987).
20. P. Roussignol, M. Kull, D. Ricard, F. de Rougemont, R. Frey, and C. Flytzanis, Appl. Phys. Lett. **51**, 1881 (1987).
21. P. Roussignol, D. Ricard, J. Lukasik, and C. Flytzanis, J. Opt. Soc. Am. B **4**, 5 (1987).
22. D. W. Hall and N. F. Borrelli, J. Opt. Soc. Am. B **5**, 1650 (1988).
23. K. C. Rustagi and C. Flytzanis, Opt. Lett. **9**, 344 (1984).
24. C. Flytzanis, F. Hache, D. Ricard, and P. Roussignol, "Optical nonlinearities in small particles and composite materials," in *The Physics and Fabrication of Microstructures and Microdevices*, M. J. Kelly and C. Weisbuch, eds. (Springer-Verlag, Berlin, 1986), p. 331.
25. Eiichi Hanamura, Phys. Rev. B **37**, 1273 (1988).
26. J. Warnock and D. D. Awschalom, Appl. Phys. Lett. **48**, 425 (1986).
27. S. C. Hsu and H. S. Kwok, Appl. Phys. Lett. **50**, 1782 (1987).
28. K. Shum, G. C. Tang, M. R. Junnarkar, and R. R. Alfano, Appl. Phys. Lett. **51**, 1839 (1987).
29. M. Tomita, T. Matsumoto, and M. Jatsuoka, "Ultrafast optical nonlinearity in semiconductor-doped glasses controlled through the trapping state," in *Ultrafast Phenomena VI*, T. Yajima, K. Yoshihara, C. B. Harris, and S. Shionaga, eds. (Springer-Verlag, Berlin, 1988), p. 340.
30. M. C. Nuss, W. Zinch, and W. Kaiser, Appl. Phys. Lett. **49**, 1717 (1986).
31. N. Peyghambarian and S. W. Koch, Rev. Phys. Appl. **22**, 1711 (1987).
32. P. Roussignol, D. Ricard, C. Flytzanis, and N. Neuroth, Phys. Rev. Lett. **62**, 312 (1989).
33. A. P. Alivisatos, A. L. Harris, N. J. Levinos, M. L. Steigerwald, and L. E. Brus, J. Chem. Phys. **89**, 4001 (1988).
34. J. T. Remillard, H. Wang, M. D. Webb, D. G. Steel, IEEE J. Quantum Electron. **25**, 408 (1989).
35. N. I. Zheludev, I. S. Ruddock, and R. Illingworth, Jr. Mod. Opt. **34**, 1257 (1987).
36. J. T. Remillard and D. G. Steel, Opt. Lett. **13**, 30 (1988).
37. M. Tomita, T. Matsumoto, and M. Maysuoka, J. Opt. Sci. Am. B **6**, 165 (1989).
38. D. G. Steel and J. T. Remillard, Phys. Rev. A **36**, 4330 (1987).
39. Jing Liu, "Effects of state-specific reservoir coupling on four-wave mixing spectroscopy," Ph.D. dissertation (University of Michigan, Ann Arbor, Mich., 1989).
40. H. Haug, J. Lumin **30**, 171 (1985); J. F. Müller, R. Mewis, and H. Haug, Z. Phys. B **69**, 231 (1987); S. Schmitt-Rink, D. A. B. Miller, and D. S. Chemla, Phys. Rev. B **35**, 8113 (1987); S. Schmitt-Rink, D. S. Chemla, and H. Haug, Phys. Rev. B **37**, 941 (1988); M. Lindberg and S. W. Koch, Phys. Rev. B **38**, 3342 (1988).
41. Contributions from thermal effects have been eliminated for two reasons: (1) An estimate of the signal strength expected from thermal effects can be obtained from a knowledge of the temperature dependence of the refractive index and absorption coefficient (i.e., from dn/dt and $d\alpha/dt$.) At temperatures of the order of 125 K (corresponding to the data in Fig. 1,) the change in absorption with temperature was measured along with the corresponding change in index of refraction. [Our measured values of dn/dt ($\approx 8 \times 10^{-6}$) and $d\alpha/dt$ ($\approx 0.055\ cm^{-1}\ K^{-1}$) at 125 K do not differ appreciably from the reported values at room temperature. See G. Thibault and M.-M. Denariez-Roberge, Can J. Phys. **63**, 198 (1985) and the Schott Glass Technologies, Inc., catalog for optical glass filters.] Using these results, we determined that the nonlinear signal caused by thermal effects is of the order of 10^{-8} times weaker than the measured response. (2) A second reason to rule out thermal effects is that lateral thermal diffusion would result in a four-wave mixing linewidth that would have a $\sin^2\theta$ dependence (θ represents the angle between the forward pump and probe beams), which is not observed.
42. N. Chestnoy, T. D. Harris, R. Hull, and L. W. Brus, J. Phys. Chem. **90**, 3393 (1986).
43. J. Jortner, J. Chem. Phys. **64**, 4860 (1976).

Comment on "Nonlinear Magneto-optics of Vacuum: Second-Harmonic Generation"

In an interesting Letter, Ding and Kaplan propose that the four-wave interaction induced by quantum-electrodynamic vacuum fluctuations can be observed as second-harmonic generation in an external dc magnetic field.[1] Unfortunately, the effect they consider vanishes identically. Indeed, there is no second-harmonic generation for any combination of external dc magnetic or electric fields. While this fact is implicit in a well-known paper of McKenna and Platzman,[2] it might be useful to repeat the calculation with a few more details.

The calculation is based on the nonlinear effective Lagrangian density, which in Gaussian units takes the following form:[3]

$$L=-\frac{1}{16\pi}F_{\mu\nu}F^{\mu\nu}-\frac{\xi}{64\pi}[5(F_{\mu\nu}F^{\mu\nu})^2-14F_{\mu\nu}F^{\nu\kappa}F_{\kappa\lambda}F^{\lambda\mu}]$$
$$=\frac{1}{8\pi}(E^2-B^2)+\frac{\xi}{8\pi}[(E^2-B^2)^2+(\mathbf{E}\cdot\mathbf{B})^2]. \quad (1)$$

Here $\xi=e^4\hbar/45\pi m^4c^7$ and the electromagnetic-field tensor $F_{\mu\nu}=\partial_\mu A_\nu-\partial_\nu A_\mu$. Forming the action and taking the variation with respect to the four-vector potential A_μ, one gets equations that can be put in the familiar classical Maxwell form:

$$\nabla\cdot\mathbf{B}=0,\quad \nabla\times\mathbf{E}+\frac{1}{c}\frac{\partial\mathbf{B}}{\partial t}=0,$$
$$\nabla\cdot\mathbf{D}=0,\quad \nabla\times\mathbf{H}-\frac{1}{c}\frac{\partial D}{\partial t}=0. \quad (2)$$

Now, however, in the last two equations (the usual inhomogeneous equations) the dielectric displacement and magnetic intensity are given by the nonlinear expressions

$$\mathbf{D}=\frac{\partial L}{\partial\mathbf{E}}=\mathbf{E}+4\pi\mathbf{P},$$
$$\mathbf{P}=\frac{\xi}{4\pi}[2(E^2-B^2)\mathbf{E}+7(\mathbf{E}\cdot\mathbf{B})\mathbf{B}],$$
$$\mathbf{H}=-\frac{\partial L}{\partial\mathbf{B}}=\mathbf{B}-4\pi\mathbf{M}, \quad (3)$$
$$\mathbf{M}=-\frac{\xi}{4\pi}[2(E^2-B^2)\mathbf{B}-7(\mathbf{E}\cdot\mathbf{B})\mathbf{E}].$$

It is at this point that Ding and Kaplan seem to have the wrong expression; they appear to have the opposite sign for M.

We now solve the nonlinear Maxwell equations perturbatively.[2] In zeroth approximation the incident fields satisfy the usual linear Maxwell equations. That is, in the relations (3) one sets P and M equal to zero. In the first approximation these zeroth-order fields are put in the nonlinear expressions for P and M. The corresponding terms are then taken to the right-hand side and treated as a source for the first-order fields. The result is that the first-order fields are solutions of the linear Maxwell equations in the presence of sources. That is, in Eqs. (2) one puts $\mathbf{D}=\mathbf{E}$ and $\mathbf{H}=\mathbf{B}$, and in the last two equations adds, respectively, source terms $4\pi\rho$ and $4\pi\mathbf{j}/c$, with

$$\mathbf{j}=\partial\mathbf{P}/\partial t+c\nabla\times\mathbf{M},\quad \rho=-\nabla\cdot\mathbf{P}. \quad (4)$$

Inserting the nonlinear expressions (3) for P and M evaluated with the zeroth-order fields, and eliminating the time derivatives using the zeroth-order equations in the absence of sources, we find for the current density

$$\mathbf{j}=\frac{c\xi}{4\pi}[4(\mathbf{E}\cdot\nabla\times\mathbf{B}+\mathbf{B}\cdot\nabla\times\mathbf{E})\mathbf{E}+2\mathbf{B}\times\nabla(E^2-B^2)$$
$$+7(\mathbf{B}\cdot\nabla\times\mathbf{B}-\mathbf{E}\cdot\nabla\times\mathbf{E})\mathbf{B}-7\mathbf{E}\times\nabla(\mathbf{E}\cdot\mathbf{B})]. \quad (5)$$

For second-harmonic generation in the presence of uniform dc fields, the zeroth-order field is a superposition of these dc fields and an optical field. Following Ding and Kaplan,[1] we assume the optical field is of the form of a wave propagating in the y direction; the zeroth-order field is of the form

$$\mathbf{E}=\mathbf{E}_0+\mathbf{e}(y-ct),\quad \mathbf{B}=\mathbf{B}_0+\mathbf{b}(y-ct), \quad (6)$$

where $\mathbf{b}=\hat{\mathbf{y}}\times\mathbf{e}$ and $\mathbf{e}=-\hat{\mathbf{y}}\times\mathbf{b}$. With this form, the current density (5) becomes

$$\mathbf{j}=-\frac{c\xi}{4\pi}[4(\mathbf{B}_0\cdot\mathbf{b}'-\mathbf{E}_0\cdot\mathbf{e}')(\mathbf{E}_0+\hat{\mathbf{y}}\times\mathbf{B}_0)$$
$$-7(\mathbf{B}_0\cdot\mathbf{e}'+\mathbf{E}_0\cdot\mathbf{b}')(\mathbf{B}_0-\hat{\mathbf{y}}\times\mathbf{E}_0)], \quad (7)$$

where the prime denotes the derivative with respect to y. This term corresponds to a weak dc-field-induced birefringence. There is no term quadratic in the optical field and, therefore, no second-harmonic generation. There is no term of third order in the optical field either, so there is no third-harmonic generation. Note that this result holds for an arbitrary superposition of collinear fields. Hence, sum- and difference-frequency contributions also vanish. There is, however, nonvanishing four-wave mixing of noncollinear fields.[2]

This work was supported by the Air Force Office of Scientific Research.

George W. Ford and Duncan G. Steel
Department of Physics
The University of Michigan
Ann Arbor, Michigan 48109-1120

Received 7 June 1990
PACS numbers: 42.50.Wm, 42.65.Ky

[1]Y. J. Ding and A. E. Kaplan, Phys. Rev. Lett. 63, 2725 (1989).
[2]J. M. McKenna and P. M. Platzman, Phys. Rev. 129, 2354 (1963).
[3]J. M. Jauch and F. Rohrlich, *The Theory of Photons and Electrons* (Springer-Verlag, New York, 1976), 2nd ed., p. 298.

Ding and Kaplan Reply: In the preceding Comments by Raizen and Rosenstein[1] (hereafter RR) and by Ford and Steel[2] (hereafter FS) on our recent Letter,[3] RR state that the QED box diagram for second-harmonic generation (SHG) in a dc magnetic field vanishes identically, whereas using phenomenological results, FS state that although nonlinearity of the respective order does not vanish, SHG vanishes in the case of collinear propagation.

We agree with RR that the result for the box diagram vanishes only for *collinear* photons[4] and when dispersion is absent. The main reason for the box diagram vanishing is nonconservation of four-momentum in such an interaction.[4,5] However, in the case of weak dispersion in vacuum (which always exists intrinsically[5]), the condition of four-momentum conservation is less restrictive for SHG. This results in the fact that even in the box approximation, SHG does not vanish (although the box-diagram contribution is smaller than that from the hexagonal diagram); see the Appendix in Ref. 5 which points out that dispersion can enhance the SHG amplitude. Our preliminary calculations show that the effect proposed in Ref. 3 can still be observed if one spatially modulates the amplitude of the dc magnetic field, by using, e.g., wigglers, which changes the dispersion of the system. Regarding the statement in RR that "more complicated diagrams" must be used even in the case of noncollinear photons, we want to stress again that essentially the box approximation is still valid and nonvanishing in the case of slight noncollinearity (see the discussion below as well as FS's Comment that still uses results of the box approximation).

Regarding the comments by FS we want to point out that the sign in the nonlinear constitutive relations used by us was based on Eqs. (54.30) in Ref. 6. Other sources, in particular the original publications[7] and those cited in FS, seem to use the opposite sign for **M**, the difference being attributed to the fact that the notations for **H** and **B** have been interchanged in Ref. 6. Presuming the propagation equations in vacuum in the standard form of Maxwell's equations,[8]

$$\nabla\cdot\mathbf{B}=0,\quad \nabla\times\mathbf{E}+(1/c)\,\partial\mathbf{B}/\partial t=0, \tag{1}$$

$$\nabla\cdot\mathbf{D}=0,\quad \nabla\times\mathbf{H}-(1/c)\,\partial\mathbf{D}/\partial t=0, \tag{2}$$

with the nonlinear constitutive relations in the form in Eqs. (3) in FS, we agree with FS that if one chooses **E** and **B** as base vectors describing the wave propagation, and use nonlinear components of vectors **D** and **H** as driving terms for Maxwell's equations, then the driving terms for collinear propagation vanish as in FS. However, although **E** and **B** are fundamental vectors, the propagation of *energy* (and therefore energy flow in SHG) in classical electrodynamics seems to be based on the vectors **E** and **H** since only these vectors form the Poynting vector, $\mathbf{S}=(c/4\pi)(\mathbf{E}\times\mathbf{H})$,[9] not **E** and **B**. Using Eqs. (1) and (2), we obtain the equations for $\mathbf{E}_2$ and $\mathbf{H}_2$ at the second-harmonic frequency with nonvanishing driving terms; for a particular polarization configuration, in which the fundamental wave is polarized along the dc magnetic field, the driving terms are

$$\mathbf{D}^{(2)}=\hat{\mathbf{e}}_x A\exp[2i(k_1 y-\omega_1 t)]\,,$$
$$\mathbf{B}^{(2)}=\hat{\mathbf{e}}_z A\exp[2i(k_1 y-\omega_1 t)]\,, \tag{3}$$

where $A=\frac{7}{2}\xi E_1^2 H_0$, although these driving terms do not lead to the same results as in Ref. 3. The difference between results for the pairs **E**,**H** and **E**,**B** disappears for the noncollinear fundamental beams. Since the driving terms do not vanish for SHG in a dc magnetic field in the general case (as is also indicated in FS), they should give a nonvanishing result for noncollinear propagation, in which case the calculation[3] gives the estimate which we believe is correct to the order of magnitude.

We appreciate fruitful input by M. G. Raizen, B. Rosenstein, G. W. Ford, and D. G. Steel. This work is supported by the U.S. Air Force Office of Scientific Research.

Y. J. Ding and A. E. Kaplan
Department of Electrical and Computer Engineering
The Johns Hopkins University
Baltimore, Maryland 21218

Received 20 April 1990;
revised manuscript received 26 October 1990
PACS numbers: 42.50.Wm, 42.65.Ky

[1]M. G. Raizen and B. Rosenstein, preceding Comment, Phys. Rev. Lett. **65**, 2744 (1990).

[2]G. W. Ford and D. G. Steel, preceding Comment, Phys. Rev. Lett. **65**, 2745 (1990).

[3]Y. J. Ding and A. E. Kaplan, Phys. Rev. Lett. **63**, 2725 (1989).

[4]Z. Bialynicka-Birula and I. Bialyniciki-Birula, Phys. Rev. D **2**, 2341 (1970); S. L. Adler *et al.*, Phys. Rev. Lett. **25**, 1061 (1970); S. L. Adler, Ann. Phys. (N.Y.) **67**, 599 (1971).

[5]R. J. Stoneham, J. Phys. A **12**, 2187 (1979).

[6]A. I. Akhiezer and V. B. Berestetskii, *Quantum Electrodynamics* (Interscience, New York, 1965), pp. 764–792.

[7]H. Euler, Ann. Phys. (Leipzig) **26**, 398 (1936); W. Heisenberg and H. Euler, Z. Phys. **98**, 714 (1936); V. Weisskopf, Kgl. Danske Vidensk. Selsk. Mat. Fys. Medd. **14**, No. 6 (1936).

[8]J. McKenna and P. M. Platzman, Phys. Rev. **129**, 2354 (1963).

[9]J. D. Jackson, *Classical Electrodynamics* (Wiley, New York, 1975), Eq. (6.109).

Measurement of Phonon-Assisted Migration of Localized Excitons in GaAs/AlGaAs Multiple-Quantum-Well Structures

H. Wang, M. Jiang, and D. G. Steel

Harrison M. Randall Laboratory of Physics, The University of Michigan, Ann Arbor, Michigan 48109

(Received 18 May 1990)

We report high-resolution nonlinear-laser-spectroscopy measurements of relaxation of lowest-energy heavy-hole excitons in GaAs multiple-quantum-well structures. We show that excitons below the absorption line center are spatially localized, and migrate among localization sites with a time scale of order 100 ps. The measurements give the resultant quasiequilibrium energy distribution of the scattered excitons and, based on the temperature dependence of the migration rate, confirm the theoretical model for phonon-assisted migration.

PACS numbers: 71.35.+z, 42.65.−k, 78.47.+p, 78.65.Fa

Optical resonant excitation of excitons with nearly monochromatic light of energy E leads to an optically induced polarization (coherence) and a population of excitons within ΔE of E where $\Delta E \sim \hbar\Gamma_h$ (Γ_h is the homogeneous linewidth of the exciton). The decay of this excitation must be characterized by decay of the polarization (often called dephasing) as well as decay of the population about energy E. In a simple ideal quantum well, quasi-two-dimensional excitons are described by a Bloch type of wave function and are free to move in the well plane. At low exciton density, decay of the excitation is then expected to be predominantly due to exciton-phonon scattering along with exciton recombination. In practice, however, the problem becomes more complicated due to nonideal growth processes. Recent transport and chemical lattice-imaging measurements[1,2] have shown the interface of GaAs/AlGaAs multiple-quantum-well (MQW) samples exhibits islandlike structures with a height of one monolayer and a lateral size of order 50 Å. For an exciton confined to a thin GaAs layer in a MQW, its energy depends strongly on the well thickness. For example, well width fluctuations of one monolayer in a 100-Å GaAs/$Al_{0.3}Ga_{0.7}As$ MQW can result in a change of exciton energy on the order of several meV. Therefore, at low temperature in the low-energy region of the heavy-hole exciton (HH1) absorption spectrum, excitons can be localized in the well with an energy determined by the local environment[3] leading to inhomogeneous broadening of the linear absorption spectrum. Excitons in the high-energy region may still be delocalized.[3] These excitons are expected to experience additional dephasing due to elastic scattering from potential fluctuations in addition to the decay due to exciton-phonon scattering and exciton recombination.

Localized excitons are in a local minimum in energy, and at very low temperature, decay of the localized exciton at energy E is expected to be dominated by migration between localization sites. The migration is accompanied by absorption or emission of acoustic phonons to compensate for the energy difference. Indeed, phonon-assisted migration was proposed to explain the slow and nonexponential energy relaxation observed in time-resolved luminescence measurements in a GaAs MQW.[4] While the migration is due to the overlap of the exciton wave functions between different sites for small intersite distances, the intersite dipole-dipole interaction mediates the migration process when the intersite distance is much greater than the localization length.[5] It is estimated that the typical magnitude of participating phonon wave vectors is within a few times of the inverse of the localization length, which indicates the energy of participating phonons is on the order of 0.01–0.1 meV. At higher temperatures (> 10 K), thermal activation of localized excitons to delocalized states becomes important. This process is associated with phonon absorption, and has been observed in GaAs MQW structures using resonant Rayleigh scattering[3] and resonant Raman scattering.[6] The estimated activation energy indicates that the onset for the delocalized exciton is near the absorption line center.

A distinctive signature for phonon-assisted migration is the temperature dependence. Recent work by Takagahara[5] has shown the temperature dependence of the migration rate in MQW structures has a form given by $\exp(BT^{\alpha})$, and has been observed in transient hole-burning experiments in an InGaAs/InP MQW.[7] In this expression, B is positive and independent of temperature but is expected to increase with the exciton energy and depends on the details of interface roughness; α is estimated to be between 1.6 and 1.7. The predicted temperature dependence is quite different from that of variable-range hopping used by Mott to interpret electronic conduction in the localized regime,[8] and is attributed to the role of the long-range dipole-dipole interaction involved in the migration of the localized exciton.[5]

In this paper, we present results of high-resolution nonlinear laser spectroscopy of lowest-energy heavy-hole excitons in a GaAs/AlGaAs MQW at temperatures between 2.5 and 15 K. Using frequency-domain four-wave mixing (FWM), we are able to obtain relaxation rates

for the exciton population at a given energy E, and to directly measure the steady-state exciton redistribution under narrow-band cw excitation. The measurement shows that excitons below the absorption line center are localized and migrate among localization sites on a time scale of order 100 ps. The predicted temperature dependence of the migration rate is also confirmed.

The experimental configuration, discussed elsewhere,[9] is based on the use of two frequency stabilized tunable cw dye lasers. Three incident beams $\mathbf{E}_f(\omega_f,\mathbf{k}_f)$, $\mathbf{E}_b(\omega_b,\mathbf{k}_b)$, and $\mathbf{E}_p(\omega_p,\mathbf{k}_p)$ (f, b, and p represent forward, backward, and probe, respectively, and $\mathbf{E}_p \| \mathbf{E}_f \perp \mathbf{E}_b$) interact in the sample to generate a signal beam $\mathbf{E}_s(\omega_s,\mathbf{k}_s)$ which is proportional to $\chi^{(3)}\mathbf{E}_f\mathbf{E}_p^*\mathbf{E}_b$, where $\omega_s=\omega_f+\omega_b-\omega_p$. $\mathbf{E}_f\cdot\mathbf{E}_p^*$ results in a spatial and temporal modulation of the exciton population[10] which modifies the optical response of the sample through exciton phase-space filling and exchange effects.[11] The signal arises from coherent scattering of the backward beam from the modulation. Spectroscopic information related to the energy-level structure and relaxation of the system is obtained by measuring the nonlinear response as a function of the frequency of any of the three input beams. Depending on which frequency is tuned, the resultant line shape is designated the FWMi line shape ($i=f,b,p$). The physical meaning of the different line shapes can be understood based on the following simple picture (a more rigorous analysis based on effective optical Bloch equations is presented elsewhere[12]).

In the FWMb measurement, $\mathbf{E}_f\cdot\mathbf{E}_p^*$ ($|\omega_f-\omega_p| \ll \Gamma_h$) excites an exciton population in a spectral hole with a half-width $\Delta E=\hbar\Gamma_h$ within the inhomogeneous width. A resonance as a function of ω_b occurs when ω_s is resonant with the exciton dipoles induced by $\mathbf{E}_f\cdot\mathbf{E}_p^*$. This leads to a simple resonance represented by the hole-burning denominator $(\omega_s-\omega_p+2i\Gamma_h)^{-1}$ (note the extra factor of 2 over ordinary linear spectroscopy).[13,14] In addition, since $\mathbf{E}_b$ detects the exciton dipole, localized excitons that are scattered to other energy states will also contribute to the FWMb response, allowing for the direct measurement of the exciton spectral redistribution. While delocalized excitons can also be scattered to other energies by inelastic processes such as exciton-phonon interactions, these states have nonzero momentum, and, as a result, a zero dipole moment. In this case, the FWMb line shape simply provides a measure of the exciton homogeneous line shape.

In the FWMf measurement, we hold $\omega_p=\omega_b$ and tune ω_f by an amount $\delta=\omega_f-\omega_p$ producing a traveling-wave modulation of excitation. The nonlinear response as a function of δ then measures the decay rate Γ of the modulation formed by excitons that are resonant with ω_s; Γ includes contributions from exciton recombination as well as scattering of excitons from energy E to E' where $|E-E'|>\Gamma_h$. Spatial diffusion of the exciton also contributes to the decay and manifests itself as a dependence of the decay rate on the spatial period of the modulation.[15] In the limiting case where $\Gamma_h \ll \Gamma/2$, the FWMf line shape is complicated by the fact tuning ω_f tunes ω_s. The FWMf response then experiences an additional resonant effect from the hole-burning denominator appearing as $(\delta+2i\Gamma_h)^{-1}$, resulting in a deviation from a simple Lorentzian and requiring a small correction (of order 1) in relating Γ to the FWHM for *absolute* decay-rate measurements. The FWMp response provides a measurement similar to the FWMf response. However, since $\omega_f=\omega_b$, the hole-burning denominator appears as $(\delta+i\Gamma_h)^{-1}$ resulting in a slightly larger correction. In the case $\Gamma_h \gg \Gamma/2$, the FWMp and FWMf line shapes are the same and independent of Γ_h.

Samples consisted of 65 periods of 96-Å GaAs wells and 98-Å $Al_{0.3}Ga_{0.7}As$ barriers, grown at 630°C by molecular-beam epitaxy on semi-insulating (100) GaAs substrates with interrupted growth. They are mounted on a sapphire disk (c-axis normal) with the substrate removed. The data presented in this paper were obtained on a sample that is characterized by an absorption linewidth of 2.2 meV for the HH1 exciton, and a Stokes shift of 1 meV between the HH1 exciton absorption and emission. Similar results were also obtained on other samples. All the nonlinear measurements are carried out on the HH1 exciton with an exciton density on the order of $10^7/cm^2$.

The complex decay dynamics of the exciton population is seen in the FWMf response. A typical line shape below the absorption line center is shown in Fig. 1(a). The FWHM corresponds to a relaxation time of 60 ps, which is too slow to be due to phonon scattering of the delocalized exciton (typically[16] on a time scale of several ps), and is over an order of magnitude faster than the exciton recombination time. Furthermore, the FWHM is independent of the grating period, indicating the contribution from exciton diffusion is negligible and that excitons are localized in this spectral region. Hence, the data suggest that the decay is due to spectral diffusion as

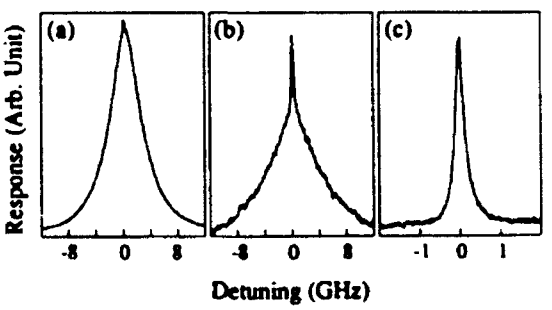

FIG. 1. The FWMf responses (where energy shifts are given, they refer to the absorption line center at 1.5508 eV): (a) at 1.5 meV below line center and at 2.5 K, (b) at 0.6 meV below line center and at 10 K, and (c) at 2 meV above line center and at 10 K.

a result of scattering of localized excitons from energy E to E' ($|E-E'|>\Gamma_h$). In fact, the decay rate is in agreement with a recent calculation based on phonon-assisted migration of the localized exciton.[5] In addition, excitons that are scattered from E to E' can later be scattered back to energy E establishing a quasiequilibrium exciton population about E before they eventually recombine. This quasiequilibrium population contributes to the FWMf response with a decay rate characterized by the exciton recombination rate.[12] The FWMf response shown in Fig. 1(a) indeed shows a small and narrow feature at the top of the line shape. The narrow feature becomes more pronounced at higher temperature due to faster exciton migration as shown in Fig. 1(b). The width associated with the feature corresponds to a decay time of 1.2 ns, consistent with the exciton recombination rate.[17]

We further examine the relaxation mechanism of the localized exciton by studying the temperature dependence of the exciton relaxation rate. Figure 2(a) shows the temperature dependence of the exciton relaxation rate obtained at 0.6 and 1.5 meV below the absorption line center using the FWMf response. The data are in good agreement with the theory of phonon-assisted migration discussed above with $\alpha=1.6$. The measurement indicates that the dominant contribution to relaxation of the localized exciton is phonon-assisted migration up to a temperature of 15 K. Note that earlier measurements[3,6] have reported observations of an activation type of temperature dependence for the localized exciton at temperatures between 7 and 20 K, indicating that in this temperature region, relaxation for the localized exciton is dominated by thermal activation to delocalized states. It has been suggested[18] that sample-dependent variations in the thermal activation energy are the result of differences in the nature of interface roughness. Hence, the effective activation energy can be much higher than simply the energy difference between the mobility edge and the localized exciton resulting, at low temperature (< 15 K), in a thermal activation rate much smaller than the phonon-assisted migration rate.

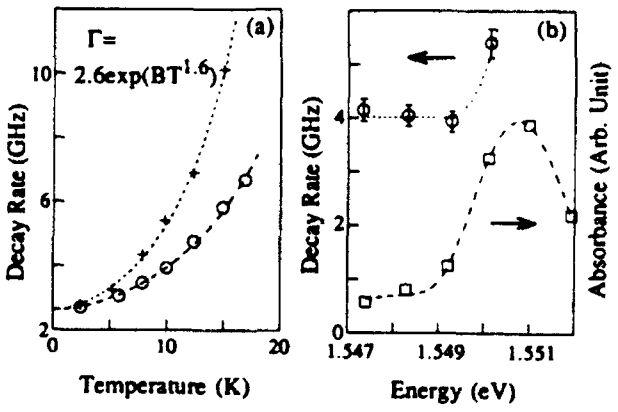

FIG. 2. (a) The temperature dependence of the exciton decay rate. Circles and crosses are data obtained at 1.5 and 0.6 meV below line center, respectively. Dashed lines are fits by the theory of phonon-assisted migration. (b) The energy dependence of the exciton decay rate at 10 K. The dashed line is only a guide to the eye.

The energy dependence of the decay of the exciton population below the absorption line center is shown in Fig. 2(b). For exciton energies less than 1.5 meV below the absorption line center, the decay rate depends very weakly on the energy. The rate increases rapidly when the exciton energy approaches the absorption line center, suggesting a transition from localized to delocalized excitons.[3]

If we imagine that localized excitons are optically excited at energy E and then migrate among localization sites to different energies, a quasiequilibrium exciton population over a broad spectral range can be established assuming the exciton migration rate is large compared with the recombination rate. As indicated earlier, it is the decay of this quasiequilibrium distribution that gives rise to the narrow features in Figs. 1(a) and 1(b). The spectral redistribution of the population can be directly measured in the FWMb response by scanning ω_b while keeping ω_f and ω_p fixed at E. Figure 3 shows a FWMb line shape where excitons are optically excited at 1.5 meV below the absorption line center. The nonlinear response is corrected for sample absorption, and is proportional to the quasiequilibrium exciton population assuming all excitons in the spectral region concerned give rise to the same cw nonlinear response.

To improve the qualitative understanding of the exciton migration process, we introduce a distribution kernel $f(E,E')$, the rate for an exciton to migrate from energy E to E'. $f(E,E')$ is analogous to collision kernels which are used to describe velocity-changing collisions in atomic vapor.[19] Decay of the exciton population can then be described by the following transport equation:

$$\dot{\rho}(E)=-(\gamma+\Gamma_E)\rho(E)+\int f(E',E)\rho(E')dE',$$

where $\rho(E)$ is the density of the excitons at E, γ is the

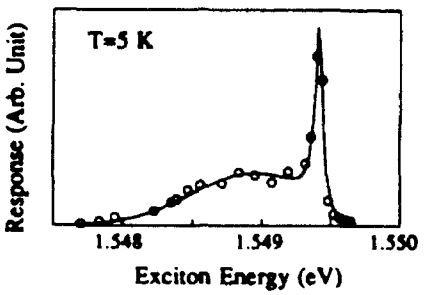

FIG. 3. The FWMb response with the frequencies of the forward and probe beams at 1.5 meV below line center.

recombination rate, $\Gamma_E = \int f(E,E')dE'$ is the overall rate at which excitons migrate out of states with energy E. In principle, the transport equation, together with the equation for the nonlinear polarization,[11,20] can provide a description for the FWMf and FWMb line shapes, though, in general, $f(E,E')$ is unknown and has to be determined by experiments. However, by assuming $f(E,E')$ to be independent of the initial-state energy, analytical solutions[12] can be obtained for standard distributions and can show that the FWMf response has an additional component with a width given by γ as anticipated based on physical arguments. The FWMb line shape in Fig. 3 can be described by a simple model which neglects migration to states above the excitation energy, and is based on the understanding of the solution to the above transport equation. The model assumes a Gaussian distribution for the quasiequilibrium population of excitons that have migrated to states below the excitation energy. The result is plotted as a solid line in Fig. 3.

Finally, we note that earlier measurements have suggested that excitons above the absorption line center are weakly delocalized.[3] Indeed, our measurements of the FWMf response show a quadratic dependence[15] of the modulation decay rate on the inverse of the spatial period of the modulation yielding a diffusion coefficient on the order of 4 cm^2/s. More strikingly, for large spatial modulation spacing where there is negligible contribution from exciton spatial diffusion, the FWMf line shape is completely dominated by the recombination component due to the rapid exciton-phonon scattering [on the order of several ps (Ref. 16)]. A typical FWMf line shape in this case is shown in Fig. 1(c). The FWHM of the line shape corresponds to an exciton recombination time of 1.2 ns. Using the FWMb response, we also determined the homogeneous width to be on the order 0.5 meV (corresponding to a dephasing time of 1.3 ps) at a temperature of 5 K, consistent with what is expected for the delocalized exciton.[16]

This work was supported by the Air Force Office of Scientific Research.

[1]R. Gottinger, A. Gold, G. Abstreiter, G. Weiman, and W. Schlapp, Europhys. Lett. 6, 183 (1988).

[2]A. Ourmazd, D. W. Taylor, J. Cunningham, and C. W. Tu, Phys. Rev. Lett. 62, 933 (1989).

[3]J. Hegarty, L. Goldner, and M. D. Sturge, Phys. Rev. B 30, 7346 (1984).

[4]Yasuaki Masumoto, Shigeo Shionoya, and Hitoshi Kawaguchi, Phys. Rev. B 29, 2324 (1984).

[5]T. Takagahara, J. Lumin. 44, 347 (1989); Phys. Rev. B 32, 7013 (1985).

[6]J. E. Zucker, A. Pinczuk, D. S. Chemla, and A. C. Gossard, Phys. Rev. B 35, 2892 (1987).

[7]J. Hegarty, K. Tai, and W. T. Tsang, Phys. Rev. B 38, 7843 (1988).

[8]N. F. Mott, and E. A. Davis, *Electronic Processes in Noncrystalline Materials* (Oxford Univ. Press, New York, 1979), 2nd ed.

[9]J. T. Remillard, H. Wang, D. G. Steel, J. Oh, J. Pamulapati, and P K. Bhattacharya, Phys. Rev. Lett. 62, 2861 (1989).

[10]For cw measurements, the orientational grating ($E_r \perp E_i \parallel E_t$) has not been observed.

[11]S. Schmitt-Rink, D. S. Chemla, and D. A. B. Miller, Adv. Phys. 38, 89 (1989).

[12]H. Wang and D. G. Steel (to be published).

[13]J. L. Oudar and Y. R. Shen, Phys. Rev. A 22, 1141 (1980).

[14]D. G. Steel and J. T. Remillard, Phys. Rev. A 36, 4330 (1987).

[15]J. T. Remillard, H. Wang, D. G. Steel, J. Oh, J. Pamulapati, and P. K. Bhattacharya, Opt. Lett. 14, 1131 (1989).

[16]L. Schultheis, A. Honold, J. Kuhl, K. Kohler, and C. W. Tu, Phys. Rev. B 34, 9027 (1986).

[17]J. Feldman, G. Peter, E. O. Gobel, P. Dawson, K. Moore, C. Foxon, and R. J. Elliott, Phys. Rev. Lett. 55, 2337 (1987).

[18]T. Takagahara (private communication).

[19]Paul R. Berman, Phys. Rep. 43, 102 (1978).

[20]M. Lindberg and S. W. Koch, Phys. Rev. B 38, 3342 (1988).

HIGH RESOLUTION NONLINEAR LASER SPECTROSCOPY MEASUREMENTS OF EXCITON DYNAMICS IN GaAs QUANTUM WELL STRUCTURES

Duncan G. Steel, Hailin Wang, Jeffrey T. Remillard, Min Jiang

Departments of Electrical Engineering and Physics
Randall Laboratory of Physics
University of Michigan
Ann Arbor, Michigan

The optical properties of GaAs/$Al_xGa_{1-x}As$ multiple quantum well structures are dominated by strong sharp excitonic resonances near the band edge which are observable in both absorption and luminescence spectra[1,2]. The quasi 2-dimensional excitons are confined in the GaAs layer by the $Al_xGa_{1-x}As$ barriers. The principal properties of the confined exciton include a binding energy which increases with decreasing well width and a blue shift in the exciton transition energy. Indeed the increase in binding energy due to confinement explains the clear observation of these resonances even at room temperature. These materials are grown by molecular beam epitaxy (MBE) methods and are important for application in high speed electronic and opto-electronic devices[3]. Moreover, the ability to fabricate crystals with dimensions controllable at the atomic level provides an excellent opportunity to study the basic physics giving rise to relaxation of the exciton with reduced dimensionality through the interaction of the exciton with the crystal lattice.

Optical resonant excitation of the exciton with quasi-monochromatic light with energy E leads to an optical induced coherence (the polarization) as well as a population of the excitons with energy between E and E+ΔE. Hence the decay of the coherent excitation must be characterized by decay of the coherence or polarization and the decay of the population at energy E. At room temperature, it is well known that LO phonons (E_{LO} ~ 37 meV) ionize the exciton (binding energy ~ 9 meV) on a time scale of a few hundred femtoseconds[4]. The decay rate of the coherence measured by the homogeneous linewidth or dephasing rate is then dominated by this ionization rate while the relaxation of the energy is then typically determined by electron-hole dynamics. At low temperature, the exciton is stable against phonon ionization and the predominant decay of the energy would be by recombination of the electron-hole pair of the exciton. In a perfect crystal at low temperature excitons are delocalized and described by Bloch type wave functions. The decay of the coherence is then expected to be due predominantly to elastic scattering by acoustic phonons along with contributions due to decay of the exciton by recombination.

However, in a quantum well structure, the problem can become more complicated[5,6]. Nonideal growth conditions result in interface roughness between the GaAs well region and the AlGaAs barrier region. From transport measurements[7,8] and chemical lattice imaging methods[9], it is known that the island regions which form during growth are typically one monolayer high and of order 50 Å in lateral extent. Since the exciton has a Bohr radius of order 65 Å for a 100 Å well, the exciton experiences a shift in the transition energy due to this interface roughness. These shifts lead to inhomogeneous broadening of the exciton absorption resonance[5]. In the low energy region of the absorption spectrum, the excitons are considered to be spatially localized by the island like structures. At low temperature (<10K), it is expected that excitons can then migrate among the islands by emitting or absorbing acoustic phonons leading to decay of the excitons at energy E and dephasing of the induced coherence. At higher temperatures, the excitons (at energy E) will experience an additional contribution to their decay by thermal activation to higher lying quasi-delocalized states. The general process of energy migration is designated spectral diffusion. Above line center, the excitons are believed to be quasi-delocalized. The dephasing of the induced polarization is due to scattering along the 2-D dispersion curve by acoustic phonons and disorder due

Laser Optics of Condensed Matter, Vol. 2
Edited by E. Garmire *et al.*, Plenum Press, New York, 1991

to interface roughness. Evidence for this transition region designated the exciton mobility edge has been reported in the pioneering work of Hegarty and Sturge[10].

In this paper we describe the use of new precision frequency domain nonlinear laser spectroscopy methods for the general study of exciton dynamics[11,12]. The objective is to experimentally determine the completeness of the above description of exciton relaxation. The frequency domain methods are particularly well suited to this problem because the narrow bandwidth of the excitation permits improved resolution over the usual time domain measurements and it is straight forward to observe in a single measurement time scales ranging over twelve orders of magnitude associated with exciton dynamics. In addition the frequency domain methods allow us to eliminate contributions from inhomogeneous broadening and to obtain homogeneous line shapes along with information related to spectral diffusion kernels.

A complete analytical discussion of the basis for precision spectroscopy based on frequency domain four-wave mixing (FWM) in simple systems has been presented by us elsewhere[13,14]. However, the physical basis for interpretation of FWM lineshapes is understood by considering the basic details of the resonant nearly-degenerate FWM response in a semiconductor. The experiments are based on the backward FWM interaction shown in Fig. 1.

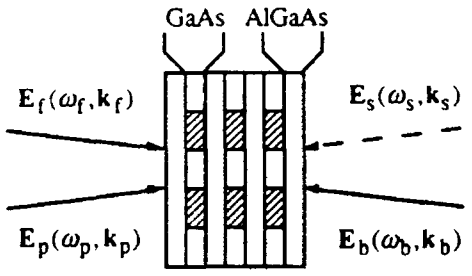

Figure 1: A schematic representation of the experimental configuration for frequency domain four-wave mixing spectroscopy in GaAs/AlGaAs *quantum* well structures. The cross hatched region represents the region of optically excited excitons which are confined by the AlGaAs barriers.

The three input fields (designated with subscript f, b, p representing forward, backward and probe fields, respectively) interact via the third order nearly degenerate resonant (i.e.,$\omega_i \approx \omega_j \approx \omega_o$) nonlinear susceptibility $\chi^{(3)}$ $(\omega_s = \omega_f - \omega_p + \omega_b)$ to produce a coherent signal field, E_s. Physically, the signal field arises from a coherent scattering of the p-polarized backward field from the spatial and temporal modulation of the optical absorption and dispersion created by the interference of the s-polarized forward pump and probe fields, given by $\mathbf{E}_f \cdot \mathbf{E}_p^*$ with a time and space dependent phase given by $(\omega_f - \omega_p)t - (\mathbf{k}_f - \mathbf{k}_p)\cdot\mathbf{x}$. (At low exciton densities, experiments show the absence of any tensor grating formed by $\mathbf{E}_b\mathbf{E}_p^*$)

Near resonance, it is well known now that the nearly degenerate third order susceptibility arises from many body effects due to the creation of excitons[15]. The effects include band filling, screening and exchange which modify the oscillator strength, the linewidth, and the resonance frequency. In a phenomenological description, these effects can be quantified by replacing the optical constants ξ_o, representing f_o, ω_o, and Γ_o, corresponding to the oscillator strength, resonant frequency, and linewidth, respectively in the linear susceptibility $\chi = \int d\omega_0 P(\omega_0) f_0 / [(\omega - \omega_0) - i\Gamma_0]$, with $\xi_0 \rightarrow \xi = \xi_0(1 + \xi_e n_e + \xi_A n_A)$ where n_i is the corresponding carrier density and expanding χ, keeping the terms first order in n_i[16]. The n_i are determined from their corresponding rate equations. At low temperature, the exciton is stable against phonon ionization and the parameters are modified to reflect the corresponding exciton density. The function $P(\omega_o)$ represents the distribution of resonant frequencies and gives rise to inhomogeneous broadening if the width of P is large compared to Γ_o.

Based on this discussion in the rate equation limit where energy relaxations are small compared to dephasing rate, Γ_o, (a reasonable approximation for many of the measurements discussed below, except where noted) it is easily seen that measuring the signal strength as function of $\omega_f - \omega_p$ while holding ω_f (or ω_p) = ω_b (designated the FWMp or FWMf response) provides a measure of the relaxation rate of the spatial modulation.

More specifically, the interference of E_f and E_p produces a traveling wave modulation of the excitation when $\omega_f \neq \omega_p$. When $|\omega_f - \omega_p|$ is larger than the spatial modulation decay rate, the signal intensity then decreases with increasing $|\omega_f - \omega_p|$. The lineshape function associated with this measurement is given by

$$L_{p(f)} = L \frac{1}{(\omega_f - \omega_p)^2 + (\gamma + D|\mathbf{k}_f - \mathbf{k}_p|^2)^2} \qquad (1)$$

where γ is the energy relaxation rate and $D|\mathbf{k}_f - \mathbf{k}_p|^2$ is the spatial diffusion rate which accounts for the fact that the excitation may diffuse in space, the rate being determined by diffusion coefficient and the reciprocal grating spacing $|\mathbf{k}_f - \mathbf{k}_p|^2 = (16\pi^2 \sin^2\theta/2)/\lambda^2$.

If the system is homogeneously broadened (i.e., $P(\omega_o)$ is a δ-function), tuning ω_b, designated the FWMb response, results in a lineshape closely related to the linear absorption profile. However, if the resonance is inhomogeneously broadened as is the contributions from localized excitons, then the linear absorption spectrum has little relation to the homogeneous lineshape. In this case, holding $\omega_f - \omega_p << \Gamma$ fixed results in creating excitons with energy in the region of $\hbar\omega_f$ ($\omega_f - \omega_p$). The energy spread is given by $\hbar\Gamma$; i.e., the interference of E_f and E_p produces a spatial modulation of a spectral hole in the inhomogeneous distribution. E_b only scatters from this spatial modulation when ω_b is tuned within the spectral hole. If $\chi(\omega - \omega_o)$ is the complex linear susceptibility associated with an excitation at a specific frequency ω_o, then in a simple hole burning picture, it is easily shown[14] that the lineshape function associated with the FWMb response in an inhomogeneously broadened system is given by:

$$L_b(\omega_b - \omega) = K\left|\int d\omega_o P(\omega_o)\chi(\omega_b - \omega_o)\,\mathrm{Im}\,\chi(\omega - \omega_o)\right|^2 \qquad (2)$$

where $\omega = \omega_f - \omega_p$ and $P(\omega_o)$ is the distribution function associated with the inhomogeneous broadening. Spectral diffusion effects are not included in this discussion. In this case, it can be shown that because χ must be analytic, even if $\chi(\omega - \omega_o)$ is asymmetric with respect to the maximum value at $\chi(\omega_o)$, $L_b(\omega_b - \omega) = L_b(\omega - \omega_b)$; i.e., L_b must be symmetric. In the data below, we see L_b is asymmetric at low temperature and is the result expected in the presence of spectral diffusion.

The experimental configuration for these experiments has been described in detail elsewhere[11], but is summarized here. A backward FWM geometry is used with two counterpropagating pump fields, described by $E_f(\omega_f,\mathbf{k}_f)$ and $E_b(\omega_b,\mathbf{k}_b)$, and the probe field, described by $E_p(\omega_p,\mathbf{k}_p)$. Phase matching conditions result in a signal field, $E_S(\omega_S,\mathbf{k}_S)$ which is counter propagating with respect to the probe field. The forward pump and probe fields are s-polarized while the backward pump and signal fields are p-polarized. The forward pump beam is chopped at a low frequency and the corresponding signal is phase sensitively detected and repeated scans of the signal as a function of frequency is averaged in a computer. In these experiments, two of the frequencies are held fixed (usually degenerate) while the third frequency is tuned. One frequency stabilized cw dye laser laser is used to provide the set of fixed frequencies while a second tunable frequency stabilized laser is used for scanning the remaining frequency. Two acousto-optic modulators driven by two phase locked digital frequency synthesizers are used to provide fixed frequency offsets between two different beams or to provide tuning in the $1\text{-}10^6$ Hertz region for high resolution measurements.

The sample consists of 65 periods of 96Å GaAs wells and 98Å $Al_{0.3}Ga_{0.7}As$ barriers grown by MBE methods and then mounted on a sapphire disk (c-axis normal to avoid birefringence problems and polarization mixing.)

The first line shapes we discuss were obtained at room temperature. As described above, the exciton is quickly ionized, producing an e-h plasma. Hence, the FWMb response provides little information of additional spectroscopic interest over the linear absorption spectrum. However, the FWMp response provides information on the e-h plasma dynamics, including e-h recombination and ambipolar diffusion, and is described by the line shape function L_p, given above. The result for a fixed angle between the forward pump and probe is shown in Fig. 2. The solid line is a least squares fit of L_p, showing a classical Lorentzian line shape, as expected. The presence of ambipolar diffusion of the spatially modulated e-h plasma results in an angle dependent decay of the grating. Figure 3 shows the measured angle dependence, varying as expected as $\sin^2\theta/2$. From the θ=0 intercept, we obtain the e-h recombination time (5 nsec), and from fitting the quadratic portion of the curve, we obtain the ambipolar diffusion coefficient ($18cm^2/sec$). These measurements are in good agreement with those reported earlier[16].

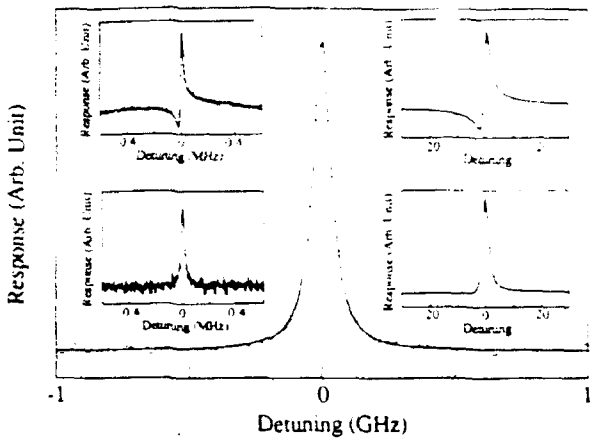

Figure 2: The FWMp response in the room temperature GaAs muluple quantum well. The solid line is a Lorentzian fit. The decay rate which determines the linewidth is due to recombination and ambipolar diffusion. The upper left inset is a high resolution scan of the FWMp response using the method of correlated optical fields. The interference dip is believed due to an excitation induced shift in the exciton resonance energy. The upper right inset is the theoretical FWMp response based on a phenomenological model. The curves in the lower insets represent experiment and theory when the back pump beam is detuned far from the exciton resonance energy, showing the disappearance of the interference effect.

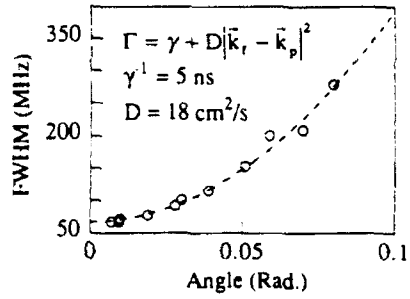

Figure 3: The FWMp response as a function of angle between the forward pump and probe beam in the room temperature GaAs multiple quantum well. The quadratic dependence on the sin of the angle is due to ambipolar diffusion of the carriers. The diffusion rate is determined by the fringe spacing which is angle dependent. The zero degree intercept is due to carrier recombination.

To determine the nature of dynamics corresponding to time scales below 1MHz (determined by interlaser jitter), we used the method of correlated optical fields which enables us to obtain precision line shapes by tuning one acousto-optic modulator with respect to the fixed modulator[17]. For this experiment, one laser is used, but ω_f an ω_b are provided by the first order Bragg deflected beam of one fixed ao modulator while ω_p is provided by tuning the first order beam from the other modulator. The upper left inset in Fig. 2 shows resultant line shape. From the bandwidth of this resonance, it is clear that there exists a component of the excitation characterized by a decay on the order of 10 μsec. Even more striking is the presence of a classical interference dip on the left side of the resonance. Using the phenomenological description for many body effects given above, we considered the possibility that the structure contained e- or h-traps that were long lived. Inserting this effect into simple rate equations for the electron and holes including only band filling effects on the oscillator strength and collisional broadening on the line width, we easily obtained a narrow resonance due to trap dynamics in addition to the ordinary resonance due to free e-h carrier dynamics. However, no interference effect is obtained. In contrast, when

a small shift in the exciton resonance due to many body effects is included in the calculation, the interference effect is observed in the scattering FWM signal, as shown in the upper right inset of Fig. 2. In addition, the simple theory showed that the interference effect would vanish if ω_b was tuned far away from ω_o, the exciton resonant frequency. Under this condition, the lower insets show agreement between experiment and the simple model. It is important to note that the time scale and signal magnitude is also roughly consistent with a temperature induced shift in ω_o, and we have calculated that such a shift would also give rise to this kind of profile. However, the thermal shift is red and would give a profile *reversed* from that in Fig. 2.

At low temperature, the linear absorption spectrum shows the clearly resolved HH1 and LH1 exciton peaks. HH1 has a width of order 2 meV and is inhomogeneously broadened. The luminescence shows a single emission peak corresponding to HH1 which is Stokes shifted by an amount varying between 10 and 20 cm^{-1}, depending on the sample. The degenerate FWM (DFWM) spectrum shows a single strong resonance also Stokes shifted by an amount comparable to the shift in the luminescence peak with a much weaker nonlinear signal being obtained at higher energies near the HH1 and LH1 absorption resonances. The Stokes shift in the luminescence and the DFWM response suggests that the cw low intensity nonlinear response in these samples is dominated by excitons localized by disorder. In contrast to many earlier measurements, the exciton density for these experiments was kept very low, near 10^7 excitons/cm^2/layer.

In a simple picture of the exciton dynamics, we would anticipate the FWMp response would be characterized by a simple Lorentzian line shape corresponding to L_p above with a width determined by the exciton recombination time (1-2 nsec for these structures[18]) along with contributions from phonon scattering on the psec time scale[19]. In fact, Fig 4 shows a much more complicated structure which was obtained at 5K. The spectrum shown in Fig. 4 is angle *independent*, suggesting that any spatial diffusion corresponds to a diffusion rate less than 1 cm^2/sec. The spectrum clearly indicates two obvious time scales corresponding to 15 nsec and 100 psec and clearly do not correspond to the expected 1-2 nsec time scale for recombination. The origin of the 15 nsec structure is currently under study and further discussion will be presented elsewhere. In the current paper, we will emphasize discussion of the 100 psec structure.

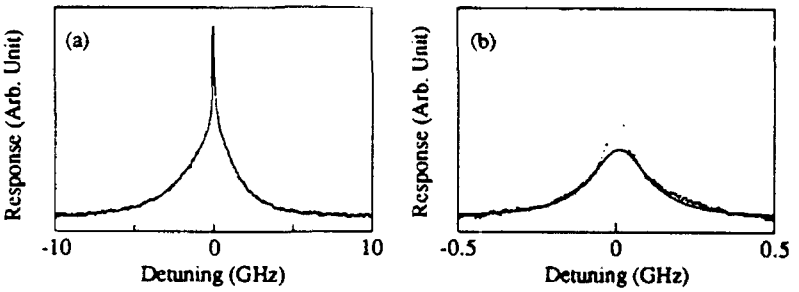

Figure 4a,b: The FWMp response in the GaAs multiple quantum well at 5K. (a) shows two major components to the spectrum corresponding to decay times of order 15nsec (the narrow component) and 100 psec (the broad component). A high resolution display of the central portion of the response is shown in 4b where a component corresponding to a 1.5 nsec decay is observed. The 100 psec component is believed due to spectral diffusion and the 1.5 nsec component is the radiative recombination time.

Earlier time domain work by Hegarty and Sturge[20] also showed the presence of fast decay components which they interpreted as arising from spectral diffusion, i.e., the scattering of the exciton at energy E to some energy E' outside the bandwidth of the spectral hole created by the forward pump and probe. Indeed, there has been recent work by Takagahara[21] suggesting that at low temperature, excitons localized by disorder spectrally diffuse to different localization sites by absorption and emission of acoustic phonons, changing their energy on the order of 0.01-0.1meV per scattering event. The process is identified as phonon assisted tunneling. In such a picture, we can imagine $\mathbf{E}_f$ and $\mathbf{E}_p$ create a spatial modulation of the exciton population at energy E in a narrow spectral hole with width $\Delta E = \hbar\Gamma$ within the inhomogeneous broadening profile. The narrow spectral hole decays at the scattering rate from E to E'. Since there is also scattering from E' to E, an equilibrium is established which

describes the resultant distribution in energy space of the exciton population. This equilibrium distribution also contributes to the scattering of E_b but is characterized by a decay time of the total exciton population, i.e., the recombination time. Such dynamics are described by an equation of the form[22]

$$\dot{\rho}(E) = -(\gamma_{rec} + \Gamma_{SD})\rho(E) + \Gamma_{SD}\int f(E' \rightarrow E)\rho(E')dE' \qquad (3)$$

where ρ(E) is the density of excitons at energy E, γ_{rec} is the recombination rate, Γ_{SD} is the integrated spectral diffusion rate or the rate at which excitons scatter from energy $E \rightarrow E' = E + \delta E$ and $f(E \rightarrow E')$ is the probability of scattering from E to E'. Such a model is analogous with the hard sphere collision model for velocity changing collisions in the gas phase. Analytical solutions assuming f to be independent of E' are easily obtained for standard distributions and show that the FWMp response has an additional component with a width given by γ_{rec} as anticipated based on physical arguments. The higher resolution experiment, shown in Figure 4b shows the expected component with a width corresponding to an inverse decay time of 1.5 nsec.

A more complete description of spectral diffusion is had, however, by making a direct measurement of the exciton scattered from energy E to E'. This measurement is made by scanning the backward pump. In the absence of spectral diffusion, the FWMb response is determined purely by the homogeneous linewidth associated with the spectral hole produced by the forward pump and probe. Recall from above (Eq. 2) that even if the hole were asymmetric, the FWMb response would be symmetric. However, excitons produced at energy E by the forward pump and probe and scattered to E'=E+δE will result in a scattering of the backward pump beam when $\hbar(\omega_f - \omega_b)=\delta E$, producing a lineshape broader than the homogeneous lineshape and lacking symmetry if the distribution function of scattered states, f, is asymmetric. Figure 5a shows the FWMb response in the low energy energy

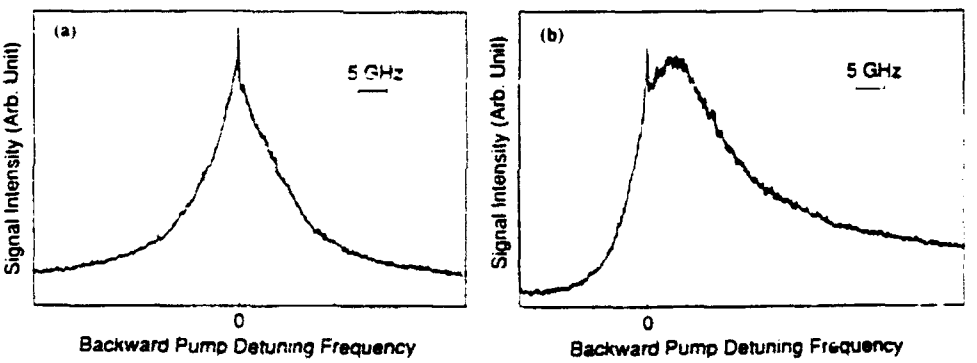

Figure 5a,b The FWMb response obtained at two different excitation energies. (a) is obtained 28cm^{-1} below absorption line center. (b) is obtained 5 cm^{-1} below line center.

region of the absorption spectrum, obtained 28cm^{-1} below absorption line enter. The line shape is characterized by a slight skew to the high energy side of the spectrum as clearly seen by the discontinuity just to the right of line center, but no large degree of scattering was observed. However, the degree of asymmetry is greatly increased when the measurement is made near absorption line center as seen in Fig. 5b, corresponding to greatly increased scattering leading to spectral diffusion. This data shows that indeed the excitons are scattering to different energy states, and that the degree of scattering depends strongly on the excitation energy.

Further confirmation of the mechanism of exciton spectral diffusion is had by comparing the analytical prediction of Takagahara with the experimentally determined tunneling rate as a function of temperature. Figure 6 shows the FWMf response as a function of temperature for two different excitation energies. (The FWMf response rather than the FWMp response was used to reduce contributions to the response from the homogeneous line width, an effect which must be considered when the dephasing rate is comparable to the excitation decay rate. The interference creates an uncertainty of at most a factor of 2 in the overall rate constants which are measured[13].) As predicted, the tunneling rate varies as $\exp(BT^{1.6})$ as seen by the solid line fit of this function to the data, where B depends on the excitation energy. The inset shows a rapid increase of the tunneling rate when the exciton energy approaches the absorption line center. The behavior is consistent with the assignment of the absorption line

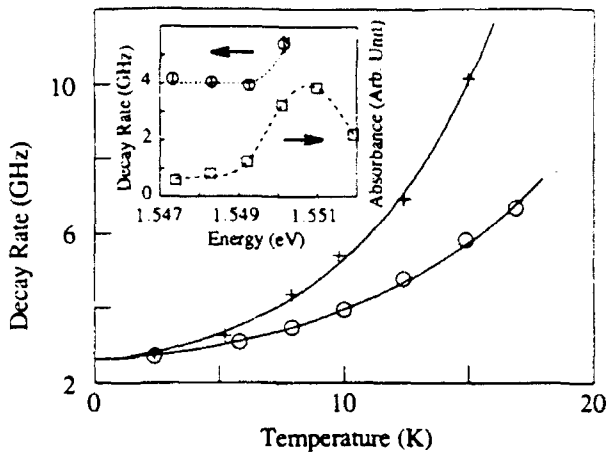

Figure 6 The measured exciton spectral diffusion rate as a function of temperature for two different excitation energies. Circles and crosses are data obtained at 1.5 meV and 0.6 meV below line center respectively. The solid curves are a fit of the theory for phonon assisted tunneling. The inset shows the energy dependence of the exciton decay rate at 10 K. The dash line is only a guide to the eye.

center as the exciton mobility edge. At higher temperatures, above 20K, we show in independent measurements made in the time domain that thermal activation dominates phonon assisted tunneling, in agreement with expectations.

In summary, we have examined the dynamics of excitons in room temperature and low temperature GaAs multiple quantum wells. Using a new kind of frequency domain nonlinear laser spectroscopy we have been able to make the first demonstration of phonon assisted tunneling in these structures. In addition, using the precision frequency domain capability of this method, we have also been able to make a direct measurement of the excitation lineshape which provide information on the redistribution kernel associated with spectral diffusion.

This work has been supported by the U.S. Army Research Office and the Air Force Office of Scientific Research.

REFERENCES

1. R. Dingle, W. Wiegmann and C.H. Henry, "Quantum states of confined carriers in very thin AlGaAs-GaAs-AlGaAs heterostructures," Phys. Rev. Lett. **33**, 827(1974).
2. R.C. Miller and D.A. Kleinman, "Excitons in GaAs quantum wells," J. Lumin. **30**, 520(1985).
3. D.S. Chemla and D.A.B. Miller, "Physics and applications of excitons confined in semiconductor quantum wells," in Heterojunctions: Band discontinuities and device applications, F. Capasso and G. Margaritondo, eds., (North-Holland, Amsterdam 1987).
4. W.H. Knox, R.L. Fork, M.C. Downer, D.A.B. Miller, D.S. Chemla, C.V. Shank, A.C. Gossard and W. Wiegmann, "Femtosecond. dynamics of resonantly excited excitons in room-temperature GaAs quantum wells," Phys. Rev. Lett. **54**, 1306(1985).
5. C. Weisbuch, R. Dingle, A.C. Gossard and W. Wiegmann, "Optical characterization of interface disorder in GaAs-GaAlAs multi-quantum well structures," Solid State Comm., **38**, 709 (1981).
6. T. Takagahara, "Excitonic relaxation processes in quantum well structures," J. Lumin. **44**, 347(1989).
7. R. Gottinger, A. Gold, G. Abstreiter, G. Weiman and W. Schlapp, "Interface roughness scattering and electron mobilities in thin GaAs quantum wells," Europhs. Lett., **6**, 183 (1988).
8. H. Sakaki, T. Noda, K. Hirakawa and T. Matsusue, "Interface roughness scattering in GaAs/AlAs quantumwells," Appl. Phys. Lett. **51**, 1934(1987).
9. A. Ourmazd, D.W. Taylor, J. Cunningham, and C.W. Tu, "Chemical mapping of semiconductor interfaces at near-atomic-resolution," Phys. Rev. Lett. **62**, 933 (1989).
10. J. Hegarty, L. Goldner and M.D. Sturge, "Localized and delocalized two-dimensional excitons in GaAs-AlGaAs multiple quantum well structures," Phys. Rev. **B30**, 7346(1984).

11. J.T. Remillard, H. Wang, D.G. Steel, J. Oh, J. Pamulapau and P.K. Bhattacharya, "High resolution nonlinear laser spectroscopy of heavy hole excitons in GaAs/AlGaAs quantum well structures: a direct measure of the exciton line shape," Phys. Rev. Lett. **62**, 2861(1989).
12. J.T. Remillard, H. Wang, M.D. Webb, D.G. Steel, J. Oh, J. Pamulapau and P.K. Bhattacharya, "High resolution nonlinear laser spectroscopy of room temperature GaAs quantum well structures: observation of interference effects," Opt. Lett. **14**, 1131(1989).
13. D.G. Steel and J.T. Remillard, "Resonant nearly degenerate four wave mixing in open and closed systems," Phys. Rev. A **36** 4330(1987).
14. H. Wang, and D.G. Steel, to be published.
15. S. Schmitt-Rink, D.S. Chemla and D.A.B. Miller, "Theory of transient excitonic optical nonlinearities in semiconductor quantum-well structures," Phys. Rev. B32, 6601(1985).
16. D.S. Chemla, D.A.B. Miller, P.W. Smith, A.C. Gossard and W. Wiegmann, "Room temperature excitonic nonlinear absorption and refraction in GaAs/AlGaAs multiple quantum well structures," IEEE J. Quant. Elec. **20**, 265(1984).
17. D.G. Steel and S.C. Rand, "Ultranarrow nonlinear optical resonances in solids," Phys. Rev. Lett. **55**, 2285(1985).
18. J. Feldmann, G. Peter, E.O. Gobel, P. Dawson, K. Moore, C. Foxon, and R.J. Elliott, "Linewidth dependence of radiative exciton lifetimes in quantum wells," Phys. Rev. Lett. **59**, 2337 (1987).
19. L. Schultheis, A. Honold, J. Kuhl, K. Kohler and C.W. Tu, "Optical dephasing of homogeneously broadened two dimensional exciton transition in GaAs quantum wells," Phys. Rev. B**34**, 9027(1986).
20. J. Hegarty and M.D. Sturge, "studies of exciton localization in quantum-well structures by nonlinear optical techniques," J. Opt. Soc. Am. B**2**, 1143(1985).
21. T. Takagahara, "Localization and homogeneous dephasing relaxation of quasi-two-dimensional excitons in quantum-well heterostructures," Phys. Rev. B32 7013(1985).
22. P.R. Berman, "Validity conditions for the optical Bloch equations," J. Opt. Soc. Am. B3, 564(1986).

Effects of spectral diffusion on frequency-domain four-wave-mixing spectroscopy

Hailin Wang and Duncan G. Steel
Randall Laboratory of Physics, University of Michigan, Ann Arbor, Michigan 48109
(Received 4 September 1990)

We report the results of a theoretical study of line shapes obtained in frequency-domain four-wave mixing in systems inhomogeneously broadened due to random fields in the presence of spectral diffusion. The results are based on a solution of the modified optical Bloch equations solved perturbatively to third order in the applied optical fields, assuming a strong redistribution model for the spectral diffusion. The results show that the redistribution of excitation can be directly observed in the line-shape function and can also lead to the presence of interference effects in the line shape.

I. INTRODUCTION

Coherent nonlinear optical spectroscopy has provided a convenient method for studying complex relaxation in materials. Transient spectroscopy methods such as time-resolved absorption and photon echoes have been commonly used in part because of the apparent ease in interpretation of experimental results. However, frequency-domain four-wave mixing (FWM) has also been shown to be a powerful method for such studies,[1] and in some systems can provide information more easily than time domain methods. Line shapes obtained through frequency-domain FWM can provide detailed information about energy relaxation comparable to classical transient absorption spectroscopy as well as eliminate inhomogeneous broadening due, for example, to random crystal fields and provide a direct measure of the homogeneous line shape of the excitation. The latter measurement is similar to dephasing measurements using transient FWM or photon echoes. In the frequency-domain measurements, since the measurement is performed in energy space, the line shape is very sensitive to relaxation processes involving energy shifts of the excitation (referred to, in general, as spectral diffusion). Such results were recently demonstrated in measurements of spectral diffusion due to phonon-assisted migration of localized excitons in $GaAs/Al_{1-x}Ga_xAs$ multiple-quantum-well structures.[2]

The physical mechanisms of spectral diffusion depend on the specifics of the system under study. For example, spectral diffusion can be induced by relatively slow environmental fluctuations, such as observed in glasses[3,4] and in some crystals due to spin flips of neighboring sites.[5] Alternatively, for impurity-doped crystals, spectral diffusion can be a result of energy exchange between ions at different sites.[6] Similarly, excitons in quantum-well structures can be localized in islands formed during the growth process where migration of these excitons among localization sites also results in spectral diffusion.[7] In general, the microscopic description of the spectral diffusion process is based on statistical assumptions regarding the energy-shift process, and is a rather difficult task as is shown by the pioneering work of Klauder and Anderson.[8]

The physical basis that is presented in many dis sions of relaxation of optically excited systems is c based on the optical Bloch equations for two-level tems.[9] In this model, the system is characterized two relaxation parameters: a decay time for relaxatic the macroscopic polarization (the T_2 or transverse r ation time, commonly called the dephasing time) a decay time for relaxation of the excitation (the T_1 or gitudinal relaxation time). The model is based on Bloch equations for spin-relaxation studies by nuc magnetic resonance; however, it was recognized very ly that relaxation even in these systems is generally r complex.[10] Theoretical work extended the discussic relaxation to a more general reservoir of optically ex systems.[11] The inadequacy of the simpler models wa cently experimentally demonstrated in the extensive of Devoe and Brewer.[12] Their classic experiments on polarization decay in Pr^{3+} ions in the impurity-ion tal $Pr^{3+}:LaF_3$ showed that the presence of spe diffusion resulted in the breakdown of the convent optical Bloch equations.[13] In this system, spe diffusion is due to transition-frequency changes of Pr^{3+} ions arising from fluorine nuclear flip-flops. Si quent studies by Szabo and Muramoto have confi similar observations in $Cr^{3+}:Al_2O_3$.[14]

Several theoretical models were developed with th of describing optical interactions in these kinds o tems. Of interest in the current work is the study of of modified optical Bloch equations (MOBE) deve by modeling the frequency change as a Markovian cess.[13] These equations can be generalized to de other types of spectral diffusion processes, suc transfer of the excitation among neighboring site cussed above. The MOBE equations resemble the port equations used to characterize collision proces atomic vapor[15] since the energy-shift process is anal to the change of the Doppler-shifted atomic tran frequency induced by velocity-changing collisions. collisions in gas phase systems result in a redistribut the emitted radiation,[16] while in solids, a similar ef observed in the broadening of the luminescence spe due to spectral diffusion. The purpose of this pape explore solutions to the MOBE in order to unde qualitatively the effects of spectral diffusion on th

shapes in frequency-domain FWM.

Without loss of generality, we assume a backward FWM configuration (see Fig. 1) where two counterpropagating pump beams $\mathbf{E}_f(\mathbf{k}_f,\Omega_f)$ and $\mathbf{E}_b(\mathbf{k}_b,\Omega_b)$ (f and b stand for forward and backward pump, respectively) interact with a probe beam $\mathbf{E}_p(\mathbf{k}_p,\Omega_p)$ in the sample with $\mathbf{E}_f\parallel\mathbf{E}_p\perp\mathbf{E}_b$ through the resonant third-order susceptibility to generate a coherent signal beam $\mathbf{E}_s(\mathbf{k}_s,\Omega_s)$. Spectroscopic information related to relaxation rates and energy-level structure of the resonant system is obtained by measuring the signal as a function of the frequency of any of three input beams. The resultant line shape is designated by FWMi, where i stands for f,p,b depending on which beam is tuned.[2] In general, FWMp and FWMf line shapes provide a measure of energy relaxation similar to transient absorption measurements, while FWMb line shapes eliminate the effects of inhomogeneous broadening and provide information on the homogeneous line shape and, as we discuss below, on the spectral redistribution of the excitation.

The paper is organized as follows: In Sec. II we discuss the modified optical Bloch equations for a two-level system solved perturbatively to third order in the applied optical fields. The system undergoes spectral diffusion by excitation transfer to neighboring sites. This model may provide insight into potential experiments in impurity-doped crystals and is also analogous to the model of migration of localized excitons in a quantum-well structure.[7] In Sec. III we consider effects of the excitation redistribution on the FWMb, FWMf, and FWMp line shapes, respectively. In the absence of spectral diffusion, we show that the FWMb line shape is symmetric with respect to the peak of the nonlinear response. Our calculation further shows that asymmetries in the FWMb line shape can be a signature of the presence of spectral diffusion and can provide a direct measure of the spectral redistribution of the optical excitation. In addition, spectral diffusion also leads to multiple decay components in FWMf and FWMp line shapes, and results in interference line shapes in most cases. The appearance of the interference line shape is shown to be associated with a preferred energy-transfer direction. In general, FWMf and FWMp responses can provide information on the spectral diffusion rate and the spontaneous emission rate of the excited states.

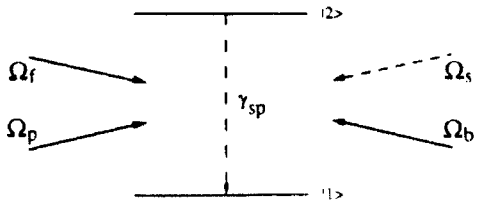

FIG. 1. Energy-level diagram for a two-level system, and configuration for backward four-wave mixing.

II. MODEL

A simple two-level system whose relaxation is characterized by spontaneous emission of the excited state to the ground state is shown in Fig. 1. The resonant frequency of the system is ω. The interaction of the system with radiation fields is then described by the following density-matrix equations assuming a classical representation for the optical fields:

$$i\hbar\frac{\partial}{\partial t}\rho_{11}(\omega)=\{V\rho_{21}(\omega)-\text{c.c.}\}+i\hbar\gamma_{sp}\rho_{22}(\omega), \tag{1}$$

$$i\hbar\frac{\partial}{\partial t}\rho_{22}(\omega)=-\{V\rho_{21}(\omega)-\text{c.c.}\}-i\hbar\gamma_{sp}\rho_{22}(\omega), \tag{2}$$

$$i\hbar\frac{\partial}{\partial t}\rho_{12}(\omega)=V[\rho_{22}(\omega)-\rho_{22}(\omega)]-\hbar\omega\rho_{12}(\omega)-i\hbar\gamma\rho_{12}(\omega), \tag{3}$$

where $\rho_{ij}(\omega)$ is the usual population density-matrix[17] element for systems with a resonant frequency ω, and γ_{sp} is the spontaneous emission rate. $V=-\boldsymbol{\mu}\cdot\mathbf{E}$ is the interaction Hamiltonian with $\boldsymbol{\mu}$ the dipole moment (assumed to be real), and

$$\mathbf{E}=\tfrac{1}{2}\sum_j \mathbf{E}_j\exp(i\mathbf{k}_j\cdot x-i\Omega_j t)+\text{c.c.}$$

is summed over all applied electric fields. These equations take into consideration pure dephasing of the optically induced coherence by letting the dephasing rate $\gamma=\frac{1}{2}\gamma_{sp}+\gamma_{ph}$, where γ_{ph} is the pure dephasing rate, due, for example, to elastic scattering. The FWMi line shape obtained in systems described by these equations has been discussed elsewhere.[18]

To develop a qualitative understanding of the effects of spectral diffusion on the FWMi response, we use a simple model based on the modified optical Bloch equations developed by Berman.[13] The model allows transfer of the excitation at an individual site to neighboring sites through the intersite interaction (such as dipole-dipole interaction). In this model, there is also the constraint that the system is quantum-mechanically closed, i.e., the probability that an atom is in the ground or the excited state is unity. This leads to the condition $\rho_{11}(\omega)+\rho_{22}(\omega)=G(\omega)$ where $G(\omega)$ is the density of atoms at frequency ω. Such a model is related to the problem of excitation transfer between ions embedded in a crystal,[19] or energy migration of localized excitons in semiconductor heterostructures.[20] In addition, the excitation transfer is likely to be associated with emission or absorption of thermal phonons to compensate for the energy difference. In this case, at the new site, the excitation transfer does not induce a superposition state of the ground and excited state that is coherent with the input fields. Hence, for the off-diagonal matrix elements related to the optical-induced coherence, the transfer process results only in additional dephasing. The corresponding equations of motion for the population density matrix have the form

$$i\hbar\frac{\partial}{\partial t}\rho_{22}(\omega)=-[V\rho_{21}(\omega)-\text{c.c.}]$$
$$-i\hbar[\gamma_{sp}+\Gamma_{22}(\omega)]\rho_{22}(\omega)$$
$$+i\hbar\int W_{22}(\omega',\omega)\rho_{22}(\omega')d\omega' , \quad (4)$$

$$i\hbar\frac{\partial}{\partial t}\rho_{12}(\omega)=V[\rho_{22}(\omega)-\rho_{11}(\omega)]$$
$$-\hbar\omega\rho_{12}(\omega)-i\hbar[\gamma+\Gamma_{12}(\omega)]\rho_{12}(\omega) , \quad (5)$$

where $W_{22}(\omega,\omega')$ is the redistribution kernel representing the rate for population in state $|2\rangle$ to be transferred from a site with resonant frequency ω to sites with resonant frequency ω', and $\Gamma_{22}(\omega)=\int W_{22}(\omega,\omega')d\omega'$ is the overall spectral diffusion rate. $\Gamma_{12}(\omega)$ is the dephasing rate of systems with resonant frequency ω due to spectral diffusion. The equation for ρ_{11} follows from Eq. (4) and the earlier constraint for $\rho_{11}(\omega)+\rho_{22}(\omega)$.

To obtain an analytical solution for the frequency-domain FWM line shapes, we further simplify the MOBE by using a strong redistribution model for the spectral diffusion process.[21] In this model, the kernel is independent of the resonant frequency of the initial site, $W_{22}(\omega,\omega')=\Gamma F(\omega')$, with $F(\omega)$ satisfying $\int d\omega F(\omega)=1$, and Γ is the overall spectral diffusion rate for the excited state. In this limit, $\Gamma_{22}(\omega)=\Gamma$, and each transfer, on average, leads to a complete redistribution of the excited-state population. The scattering giving rise to spectral diffusion also contributes to the dephasing at a rate we designate by $\Gamma_{12}(\omega)$. For the qualitative discussions of this work, we set $\Gamma_{12}(\omega)=\Gamma/2$ (recall, the coupling giving rise to spectral diffusion may also lead to pure dephasing effects that would be included in γ_{ph}). Under the above assumptions, the much simplied MOBE has the following form:

$$i\hbar\frac{\partial}{\partial t}\rho_{22}(\omega)=-[V\rho_{21}(\omega)-\text{c.c.}]-i\hbar(\gamma_{sp}+\Gamma)\rho_{22}(\omega)$$
$$+i\hbar\Gamma F(\omega)\int\rho_{22}(\omega)d\omega , \quad (6)$$

$$i\hbar\frac{\partial}{\partial t}\rho_{12}(\omega)=V[2\rho_{22}(\omega)-G(\omega)]$$
$$-\hbar\omega\rho_{12}(\omega)-i\hbar\gamma_t\rho_{12}(\omega) , \quad (7)$$

where $\gamma_t=\gamma_{sp}/2+\Gamma/2+\gamma_{ph}$ is the total dephasing rate. Although the solution to the MOBE depends on the specifics of the kernel and the assumptions we have made here, we expect the FWM line shapes obtained based on these equations to reflect the qualitative feature of the line shapes in more complicated systems. We also note that the deviation of the MOBE from the density-matrix equation of a simple two-level system occurs only in the equation for the diagonal matrix element. Hence, the linear absorption of the system, which is associated with the first order off-diagonal matrix element, *does not provide any information on the redistribution kernel and a higher-order optical probe is required to examine these effects.*

To obtain the frequency-domain FWM line shapes, we solve the MOBE, in the rotating wave approximation, using perturbation theory to third order in the applied optical fields. The effect of inhomogeneous broadening is included in the equation by assuming a frequency-dependent zeroth-order population $\rho_{11}^{(0)}(\omega)=G(\omega)$. In the scalar approximation for the optical fields, the third-order nonlinear polarization is then given by

$$P^{(3)}=\int d\omega\,\mu[\rho_{21}^{(3)}(\omega)+\text{c.c.}] . \quad (8)$$

The third-order off-diagonal matrix element for a signal nearly counterpropagating to the probe (proportional to $E_f E_p^* E_b$) giving rise to the third-order nonlinear polarization of interest follows from the general perturbation sequence:

$$\begin{Bmatrix}\rho_{11}^{(0)}\\ \rho_{22}^{(0)}\end{Bmatrix}\xrightarrow{E_f,E_p^*}\begin{Bmatrix}\rho_{12}^{(1)}\\ \rho_{21}^{(1)}\end{Bmatrix}\xrightarrow{E_p^*,E_f}\begin{Bmatrix}\rho_{11}^{(2)}\\ \rho_{22}^{(2)}\end{Bmatrix}\xrightarrow{E_b}\begin{Bmatrix}\rho_{12}^{(3)}\\ \rho_{21}^{(3)}\end{Bmatrix} . \quad (9)$$

Assuming the system is dilute, i.e., ignoring interactions between the resonant systems,[22] $\rho_{12}^{(3)}$ is given by (see Appendix A for brief outline of derivation):

$$\rho_{21}^{(3)}(\omega)=-2\left[\frac{\mu}{2\hbar}\right]^3 E_f E_p^* E_b\exp[i(\mathbf{k}_f+\mathbf{k}_b-\mathbf{k}_p)\cdot\mathbf{x}-i\Omega_s t]\frac{1}{\Omega_s-\omega+i\gamma_t}\frac{1}{\Delta_{fp}+i(\Gamma+\gamma_{sp})}$$
$$\times\left[G(\omega)\left[\frac{1}{\Omega_f-\omega+i\gamma_t}-\frac{1}{\Omega_p-\omega-i\gamma_t}\right]+\frac{i\Gamma}{\Delta_{fp}+i\gamma_{sp}}F(\omega)[A(\Omega_f)-A^*(\Omega_p)]\right] , \quad (10)$$

where $\rho_{ij}=\rho_{ji}^*$, $\Omega_s=\Omega_f+\Omega_b-\Omega_p$ is the signal frequency, and $\Delta_{ij}=\Omega_i-\Omega_j$ with $i,j=f,b,p$. $A(\Omega)$ is given by

$$A(\Omega)=\int\frac{1}{\Omega-\omega+i\gamma_t}G(\omega)d\omega . \quad (11)$$

The imaginary part of the $A(\Omega)$ is related to the inhomogeneous linear absorption profile of the system and the real part corresponds to the dispersion. Note that in the usual case where $G(\omega)$ is taken to be a Gaussian, the integral reduces to the familiar plasma dispersion function.[23] In the limit that the width of the Gaussian is large compared to γ_t, $A(\Omega)=i\sqrt{\pi\ln 2}N/\Delta\omega_{inh}$ for Ω near the center frequency of $G(\omega)$ where N is the density of atoms. As discussed in Appendix A, we have included only those terms that are proportional in second order to (E,E_p^*) where either field can act in perturbation in either first or second order. Second-order terms proportional to $(E_b E_p^*)$ have been excluded because we have chosen $\mathbf{E}_p\perp\mathbf{E}_b$ and in materials of interest, contributions to the

nonlinear response from these terms is usually small. (Experimentally, this is easily verified by showing that the third-order nonlinear response obtained when all fields are copolarized is large compared to the measured response when the probe polarization is orthogonal to the copolarized pump beams.)

The corresponding third-order polarization follows from the integral in Eq. (8):

$$P^{(3)}(\Omega_s)=-2\mu\left|\frac{\mu}{2\hbar}\right|^3 E_f E_p^* E_b \exp[i(\mathbf{k}_s+\mathbf{k}_b-\mathbf{k}_p)\cdot\mathbf{x}-i\Omega_s t]\frac{1}{\Delta_{fp}+i(\gamma_{sp}+\Gamma)}$$
$$\times\left|\frac{1}{\Delta_{sp}+2i\gamma_t}[A(\Omega_s)-A^*(\Omega_p)]-\frac{1}{\Delta_{sf}}[A(\Omega_s)-A(\Omega_f)]\right.$$
$$\left.+\frac{i\Gamma}{\Delta_{fp}+i\gamma_{sp}}Q(\Omega_s)[A(\Omega_f)-A^*(\Omega_p)]\right|+\text{c.c.}\,, \tag{12}$$

where $Q(\Omega_s)$ is related to the redistribution kernel by

$$Q(\Omega_s)=\int\frac{1}{\Delta_s-\omega+i\gamma_t}F(\omega)d\omega\,. \tag{13}$$

Again, it is useful to note that if $F(\omega)$ is taken to be a Gaussian, $Q(\Omega)$ is related to the plasma dispersion function.

In a more rigorous discussion, spectral diffusion due to intersite energy transfer is also accompanied by a corresponding change in location of the excitation. However, if the effective mean free path for excitation transfer is small, then the effect would be described by a spatial diffusion process. Since we have assumed that the optical coherence is destroyed by the transfer process, this effect can be phenomenologically included as a spatial diffusion decay term in the equations for ρ_{ij}, and the decay rate is given by $\Gamma_d=4\pi^2D/\Lambda^2$ where D is the diffusion coefficient and Λ is the spatial period of the modulation. For the purposes of this discussion, this effect is not considered.

III. DISCUSSION OF FWM LINE SHAPES

The generation of the nonlinear signal can be associated with a simple physical picture. The forward pump and probe interfere in the sample to form a spatial and temporal modulation of the ground-state as well as excited-state population. This modulation further results in a modulation of the optical absorption and dispersion. The backward pump Bragg scatters off this modulation and produces a signal beam with frequency $\Omega_s=\Omega_f+\Omega_b-\Omega_p$. From a solution to Maxwell's equations, it is easily seen that the signal propagates in a direction determined by the phase-matching conditions which for the simple case of degenerate FWM are given by $\mathbf{k}_s=\mathbf{k}_b+\mathbf{k}_f-\mathbf{k}_p$. For small-frequency detunings or thin samples, the phase mismatch that occurs for nondegenerate beams is small and does not effect the spectroscopic line shapes. In the limit that all fields are weak and there is no depletion of any of the applied fields, the nonlinear signal is then simply determined by a solution of the appropriate wave equation where the nonlinear polarization is the source term. The nonlinear signal is then simply proportional to $|P^{(3)}(\Omega_s)|^2$.

With the exception of the last term, Eq. (12) is nearly identical to the results obtained for the simple two-level system discussed earlier.[18] The resonant denominator $[\Delta_{fp}+i(\gamma_{sp}+\Gamma)]^{-1}$ in Eq. (12) arises in the calculation of $\rho_{22}^{(2)}-\rho_{11}^{(2)}$. The width of the denominator is determined by decay dynamics of the excitation modulation, and includes an additional contribution from spectral diffusion. The resonant denominator associated with $2\gamma_t$ represents the familiar hole-burning resonance that occurs when the signal is resonant with the dipole excited by $E_fE_p^*$ (i.e., when $\Omega_s=\Omega_p$), and also shows an additional broadening due to the dephasing that occurs through spectral diffusion. The term inversely proportional to Δ_{sf} is not singular, but rather goes to 0 in the limit of $\Delta_{sf}=0$. Note that contributions from this term are negligible in the limit of strong inhomogeneous broadening when the detuning Δ_{ij} is small compared with the inohomogeneous width.

The last term in Eq. (12) is not present in the earlier calculation and is the result of spectrally diffused excitation. It is proportional to Γ and, because of the strong redistribution assumption, is also proportional to $Q(\Omega_s)$, which is related to the redistribution kernel. In general, due to the resonant enhancement which occurs when the signal is resonant with the optical transition, as reflected by the denominator $(\Omega_s-\omega+i\gamma_t)^{-1}$ in Eq. (10), the dominant contribution to the nonlinear response comes from systems that are resonant with the signal. Hence, we see that even though the excitation has scattered by spectral diffusion to other frequency groups, there is a strong contribution to the polarization when Ω_s is near the maximum of Q.

We first discuss the FWMb line shape. In this measurement, $E_fE_p^*$ (with $|\Omega_f-\Omega_p|\ll\gamma_{sp}$) excites a narrow spectral hole in the sample about the excitation energy with a width $\Delta=2\hbar\gamma_t$. The FWMb line shape is obtained by measuring the nonlinear signal as a function of the frequency of the backward pump beam. This measurement is analogous to the cw hole-burning measurements and is closely related to standard transient FWM experiments. The FWMb signal includes contributions from both real and imaginary parts of the nonlinear response.

Compared to earlier work in the absence of spectral diffusion,[18] the FWMb line shape is significantly modified by the presence of the spectral diffusion process. In the

absence of spectral diffusion, the FWM*b* line shape simply reflects the details of the hole excited by $E_f E_p^*$. The line shape reduces to a simple Lorentzian with a width *twice* the homogeneous width. In the presence of the spectral diffusion, the hole excited by $E_f E_p^*$ diffuses in energy space resulting in a spectral redistribution of the excitation. Since tuning Ω_b effectively changes Ω_r, the FWM*b* response provides a direct measure of the spectral redistribution of the excitation, as determined by $Q(\Omega)$. In particular, with the strong redistribution model, the contribution to the FWM*b* response due to spectral diffusion is proportional to the convolution of the homogeneous response with the redistribution kernel.

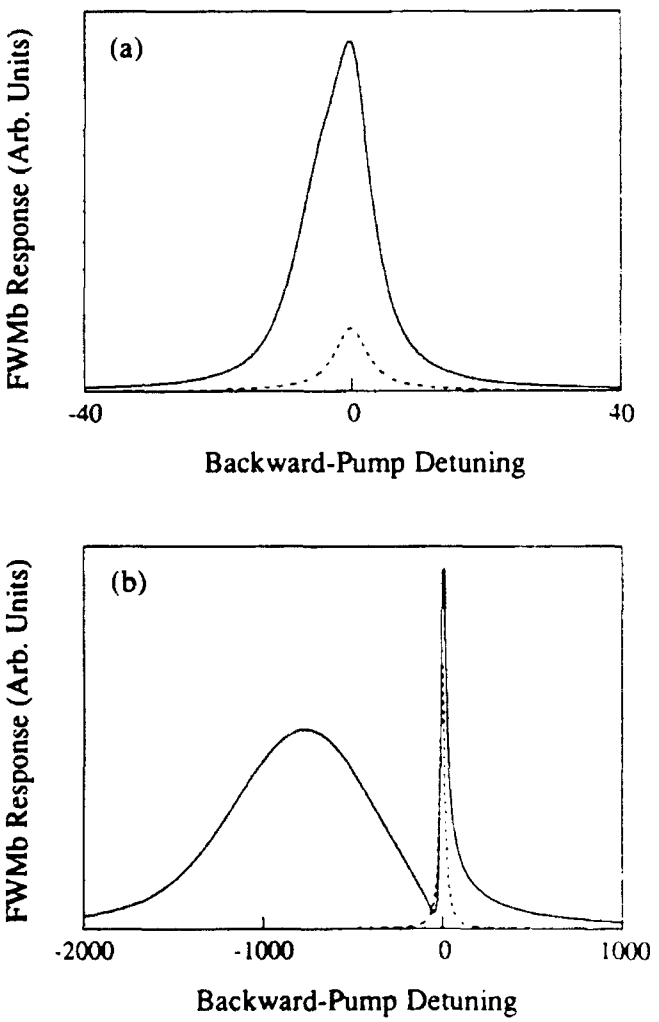

FIG. 2. FWM*b* responses. All the frequency and decay rates are normalized to the spontaneous emission rate (a) $\Gamma=2$, $\Delta\omega_{inh}=1000$, $\Delta\omega_0=4$, $\Omega_p-\omega_{inh}=-100$, and $\Omega_r-\omega_0=3$, where ω_{inh} and $\Delta\omega_{inh}$ are the center and width of the inhomogeneous distribution, respectively, and ω_0 and $\Delta\omega_0$ are the center and width of the redistribution kernel, respectively. The line shape is asymmetric signaling the effects of spectral diffusion. (b) $\Gamma=15$, $\Delta\omega_{inh}=1000$, $\Delta\omega_0=400$, $\Omega_p-\omega_{inh}=-100$, and $\Omega_p-\omega_0=750$. The line shape reflects a direct measure of the steady-state redistribution of the optical excitation. In both figures, dashed lines represent contribution to the nonlinear response due to the hole-burning effects.

Figure 2 shows two typical FWM*b* line shapes obtained by assuming a Gaussian distribution for both the strong distribution kernel and the inhomogeneous distribution.[24] Figure 2(a) corresponds to a kernel where the peak of the kernel is very close to the initial excitation energy. The line shape is asymmetric, a direct result of spectral diffusion. The asymmetry is associated with a preferred energy-transfer direction. Since the width of the kernel here is on the same order of magnitude as the homogeneous width of the system, it is difficult to separate contributions to the nonlinear line shape due to spectral diffusion from those contributions resulting from hole burning. In this case, spectroscopic information, such as the homogeneous width of the system, can be extracted only with an assumption of the functional form for the redistribution kernel. Figure 2(b) corresponds to a kernel where the peak of the redistribution function is far from the excitation energy, and the width of the redistribution function is much larger than the homogeneous width of the system. The narrow peak around zero detuning is the result of spectral hole burning while the broad peak in the line shape represents the spectral redistribution of the excitation created about the forward pump frequency. The dashed line in both figures represents the hole created by the forward pump and probe and the FWM*b* response without the contribution from diffused excitation. The backward pump detuning is measured with respect to the forward pump and probe frequency, $\Omega_b-\Omega_f$.

Analytical solutions to the MOBE without assuming that the redistribution kernel is independent of the initial state are very difficult to obtain. However, we expect that the FWM*b* response in general contains contributions from excitations that have spectrally diffused as well as contributions due to spectral hole burning. In particular, in the limit that the homogeneous width is small compared with the characteristic width of the redistribution kernel, the FWM*b* response directly maps out the steady-state spectral redistribution of the excitation.

The asymmetry seen in Fig. 2 is associated with the presence of spectral diffusion, however, it is interesting to consider whether the FWM*b* line shape can be asymmetric in the absence of spectral diffusion. In general, in the absence of any spectral diffusion process, the nonlinear polarization of interest is proportional to the following function:

$$P^{(3)}(\Omega_r)=K\int d\omega\, G(\omega) f(\Omega_r,\omega)\,\mathrm{Im}[f(\Omega,\omega)]+\text{c.c.}, \tag{14}$$

where K is a constant, $\Omega=\Omega_f=\Omega_p$, and $\Omega_r=\Omega_p$. $f(\Omega,\omega)$ is the complex optical response for a system with resonant frequency ω, and the imaginary part of $f(\Omega,\omega)$ represents the homogeneous line shape of the system. For Ω near the center of $G(\omega)$ and in the limit that the system is strongly inhomogeneously broadened, the nonlinear response is due to spectral hole burning, and $G(\omega)$ can be treated as a constant inside the integral. The FWM*b* line shape is then determined solely by the homogeneous line shape. Furthermore, assuming the line shape of the optical response function is independent of the resonant frequency of the system and using the

causality requirement of the response function, it can be shown (see Appendix B) that the FWM*b* line shape is a symmetric function of the detuning Δ_{bp}, *regardless of whether the homogeneous line shape of the system is symmetric or asymmetric.* Hence, the experimental observation of asymmetry in the FWM*b* line shape is indeed a likely indication of the presence of spectral diffusion.

Spectral diffusion processes can clearly complicate the extraction of spectroscopic information such as the homogeneous width and the spectral diffusion rate from the FWM line shapes, especially when the characteristic width of the redistribution kernel is comparable with the homogeneous width of the system. Within the strong redistribution model, this is primarily due to the change of the signal frequency when the frequency of only one beam is tuned. This type of complication can be avoided by scanning the frequencies of two input beams simultaneously. Similar to the FWM*b* response, we can scan Ω_p and $\Omega_f(\Omega_f \approx \Omega_p)$ while we keep Ω_b fixed, and we designate the line shape obtained as FWM*b'*. In the FWM*b* measurements, we create an excitation modulation at a specific frequency and probe the subsequent steady-state spectral redistribution of the excitation. In contrast, the FWM*b'* response measures the nonlinear signal at a fixed frequency as a function of the initial excitation frequency. In the absence of spectral diffusion the FWM*b* and FWM*b'* measurements are equivalent. In the limit of the strong redistribution model, the spectral diffusion process is independent of the initial-state frequency; therefore the contribution due to spectral diffusion remains constant in the FWM*b'* response, which also enables us to measure the homogeneous response of the system through hole-burning effects. This difference results from the fact that the forward pump and probe act in first and second order in perturbation, before the effects of spectral diffusion, while the backward pump acts in third order. Physically, in the strong redistribution model, spectral diffusion to any one frequency (say, $\omega=\Omega_b$) is independent of the excitation frequency. Hence, the effect of spectral diffusion on the FWM*b'* response is to simply add an offset to the signal that is independent of forward pump and probe frequencies. It is interesting to note here that if the FWM*b'* line shape shows a frequency dependence in the offset, then it is quite likely that the strong spectral redistribution assumption is not appropriate. Hence, both measurements are important in order to complete the understanding of the FWM line shapes.

The presence of spectral diffusion also greatly changes the FWM*f* and FWM*p* line shapes from earlier discussions.[18] In these measurements, detuning the pump or probe results in a traveling-wave modulation oscillating with the detuning $\Delta_{fp}=\Omega_f-\Omega_p$. The nonlinear response as a function of Δ_{fp} provides a measure of the decay of the modulation formed by excitations resonant with the signal beam. In addition to the contribution from spontaneous emission, the decay rate obtained includes contributions from the decay of the excitation out of the spectral region about the signal frequency, that is, $\Gamma_m=\gamma_{sp}+\Gamma$ where Γ_m is the overall decay rate of the modulation. Note that tuning Ω_f or Ω_p changes the frequency of the signal beam as well as the frequency of the first-order excitation, causing the interpretation of the measurements to become complicated when the decay rate of the modulation is comparable with the homogeneous width of the system. However, in the limit that the homogeneous width is large compared with the energy relaxation rate, the above complication is negligible.

Based on the general expression for the third-order nonlinear polarization given in Eq. (12), the polarization associated with the FWM*f* response can be simplified to

$$P^{(3)}=K'\frac{1}{\Delta_{fp}+i\Gamma_m}\left[\frac{1}{\Delta_{fp}+2i\gamma_t}+\frac{i\Gamma}{\Delta_{fp}+i\gamma_{sp}}Q(\Omega_f)\right]\times[A(\Omega_f)-A^*(\Omega_p)]+\text{c.c.}\,, \tag{15}$$

where we have assumed $\Omega_p=\Omega_b$, and K' is a constant. Since we are dealing with a strongly inhomogeneously broadened system, the inhomogeneous response function $A(\Omega)$ can be treated as a constant in the detuning range in which we are interested. The FWM*f* line shape is then determined by three relaxation processes: Γ_m, $2\gamma_t$, and γ_{sp}. The appearance of the hole-burning denominator associated with the homogeneous width is due to the change of the frequencies of the signal and the first-order excitation when the frequency of the forward pump is tuned. In the limit where the dephasing is large compared to all other relaxation rates, this term does not change significantly compared to the other terms as a function of Ω_f. Hence, the dominant term is a broad resonance with a width determined by the total decay rate Γ_m. However, as a result of excitation diffusion between different energy states, a quasiequilibrium is established due to this dynamic process, extending over all states. This is expected regardless of the functional form of the redistribution kernel. The quasiequilibrium population contributes to the nonlinear response, and decay of this population is determined by the spontaneous emission of the excited states. If the spontaneous emission rate is slow compared to the spectral diffusion rate, or more generally Γ_m, then a narrow resonance will be observed on top of the broad resonance with a width given by γ_{sp}. It is important to note here that in time-resolved luminescence of this transition, the measured decay rate would be given by γ_{sp}. However, because of the hole burning achieved in FWM, it is possible to separately measure both decay rates.

Figure 3(a) shows a FWM*f* line shape obtained with the excitation energy at the peak of the redistribution kernel. As anticipated, it clearly shows a prominent narrow peak sitting on top of a broad base. The broad base is the result of the fast spectral diffusion process ($\Gamma=15\gamma_{sp}$). The narrow peak corresponds to the excited-state spontaneous emission rate. More interestingly, if we move the excitation energy to the low-energy side of the kernel, an interference type of line shape develops as is shown in Fig. 3(b). In this case, the excitation transfer to the higher-energy states dominates the transfer to the lower-energy states. Physically, the interference results between the field radiated by the dipoles in the spectral hole, and the dipoles associated with

the spectrally diffused excitation.

More specifically, in the limit that the width of the redistribution kernel is much larger than the homogeneous width of the system, the function $Q(\Omega)$ can be treated as a constant for the FWMf measurement. For a symmetric redistribution kernel and when the excitation energy is at the peak of the kernel, the real part of the function $Q(\Omega)$ goes to zero, and the nonlinear response due to the spectral diffusion has the same phase as the nonlinear response due to spectral hole burning. However, any presence of a nonzero real part for $Q(\Omega)$ can result in a phase difference between the two components of the nonlinear response. A direct consequence of this difference is an interference type of FWMf line shapes. Appearances of the interference line shape are determined by the local property of the redistribution kernel in the vicinity of signal frequency Ω. In the limit of the strong redistribution model discussed here, the phase shift occurs when the excitation energy is off the peak of the redistribution kernel. In fact, the interference profile can be reversed if we move the excitation frequency to the high-energy side of the redistribution kernel. Recall that in the FWMb measurement, a preferred energy-transfer direction leads to an asymmetric FWMb line shape. We can conclude that the interference line shape in the FWMf response will be associated with an asymmetric FWMb line shape.

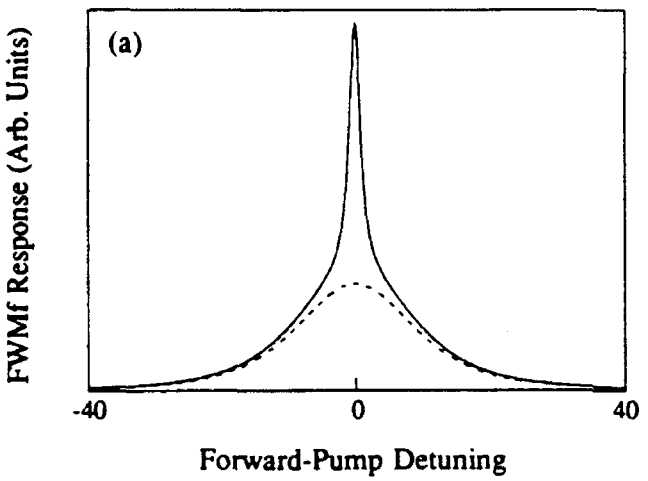

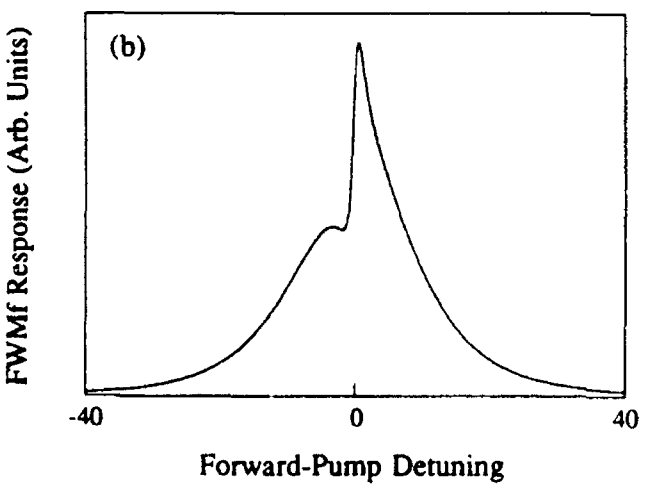

FIG. 3. FWMf responses. (a) $\Gamma=15$, $\Delta\omega_{inh}=1000$, $\Delta\omega_0=400$, $\omega_0-\omega_{inh}=-100$, and $\Omega_p=\omega_0$. The response shows a prominent narrow component due to the spectral diffusion process. The width of this component is determined by the spontaneous emission rate. The dashed line represents the nonlinear response without contribution from the spectrally diffused excitations. (b) $\Gamma=15$, $\Delta\omega_{inh}=1000$, $\Delta\omega_0=400$, $\omega_0-\omega_{inh}=-100$, and $\Omega_p-\omega_0=-750$. The FWMf response shows interference types of line shapes.

The same analysis also applies to the FWMp line shape, and features of the FWMf response are all present in the FWMp response. The main difference is that the hole-burning denominator, $(\Delta_{sp}+2i\gamma_t)^{-1}$ appears in the FWMp response (where $\Omega_f=\Omega_b$) as $(\Delta_{fp}+i\gamma_t)^{-1}$ instead of $(\Delta_{fp}+2i\gamma_t)^{-1}$ as it does in the FWMf response (where $\Omega_b=\Omega_p$). Hence, in the limiting case where γ_t is on the order of $(\gamma_{sp}+\Gamma)$, the rate obtained from the width of the FWMf response will be less affected by this denominator than will the FWMp response. Assuming $\gamma_{ph}=0$, $\Gamma\gg\gamma_{sp}$, and the characteristic width of the redistribution kernel to be much larger than the homogeneous width of the system, appearance of the hole-burning denominator is expected to introduce only an overall correction factor for rates obtained from the width of FWMp or FWMf responses.

In summary, we see that the problem of obtaining a quantitative understanding of a resonant system in a solid is greatly complicated by the presence of spectral diffusion processes. However, the results of these calculations show that line shapes obtained through frequency-domain FWM can provide additional understanding, though it is clear that, except in some simple-limiting cases, the interpretation of these results must be made with care.

ACKNOWLEDGMENTS

The authors wish to acknowledge helpful discussions with Professor P. R. Berman. This work was supported by the U.S. Air Force Office of Scientific Research.

APPENDIX A

In this work, we are interested in the nonlinear polarization giving rise to an electromagnetic wave counterpropagating with regard to the probe wave. This implies that the third-order off-diagonal matrix element $\rho_{21}^{(3)}(\omega)$ of interest is proportional to $E_f E_p^* E_b$. Since we use the geometry of $\mathbf{E}_f\|\mathbf{E}_p\perp\mathbf{E}_b$, we assume that the excitation modulation formed by fields with orthogonal polarization can be neglected. We then calculate the matrix element $\rho_{21}^{(3)}(\omega)$ using the perturbation sequence in Eq. (9), in which the forward pump and probe interact in the sample forming a modulation of the ground-state and excited-state population, and the backward pump beam acts only

in third order.

The first-order off-diagonal matrix element, which is also related to the linear optical response, is easily obtained in the rotating wave approximation from Eq. (7) by taking $\rho_{11}^{(0)}(\omega)=G(\omega)$:

$$\rho_{21}^{(1)}(\omega)=-\frac{\mu}{2\hbar}\sum_i \frac{G(\omega)}{\Omega_i-\omega+i\gamma_i}E_i\exp[i(\mathbf{k}_i\cdot\mathbf{x}-\Omega_i t)], \tag{A1}$$

where the sum is over all the applied optical fields. To obtain $\rho_{22}^{(2)}(\omega)$, we first define the matrix element $\rho_{\alpha\beta}=\int\rho_{\alpha\beta}(\omega)d\omega$, integrated over all frequencies, where α and $\beta=1,2$. In the strong redistribution limit, the redistribution kernel is independent of the frequency of the initial excitation. Hence, we integrate Eq. (6) over ω, yielding the equation for ρ_{22},

$$i\hbar\frac{\partial}{\partial t}\rho_{22}=-(V\rho_{21}-\text{c.c.})-i\hbar\gamma_{sp}\rho_{22}\ . \tag{A2}$$

As expected, decay of the overall spectrally integrated excited-state population is determined by the spontaneous emission rate. Solving the above equation to second order in the applied field and taking the slowly varying component (i.e., the term proportional to $E_iE_j^*$), we obtain

$$\rho_{22}^{(2)}=-\left|\frac{\mu}{2\hbar}\right|^2\sum_{i,j}\frac{A(\Omega_i)}{\Delta_{ij}+i\gamma_{sp}}E_iE_j^*\times\exp[i(\mathbf{k}_i-\mathbf{k}_j)\cdot\mathbf{x}-(\Omega_i-\Omega_j)t]+\text{c.c.}\ , \tag{A3}$$

where $\Delta_{ij}=\Omega_i-\Omega_j$, i and $j=f,p$, and $A(\Omega_i)$ is defined in Eq. (11). The second-order matrix element $\rho_{22}^{(2)}(\omega)$ follows directly from Eq. (6):

$$\rho_{22}^{(2)}(\omega)=-\left|\frac{\mu}{2\hbar}\right|^2\sum_{i,j}E_iE_j^*\exp[i(\mathbf{k}_i-\mathbf{k}_j)\cdot\mathbf{x}-(\Omega_i-\Omega_j)t]\times\frac{1}{\Delta_{ij}+i(\gamma_{sp}+\Gamma)}\left[\frac{G(\omega)}{\Omega_i-\omega+i\gamma_i}+\frac{i\Gamma F(\omega)}{\Delta_{ij}+i\gamma_{sp}}A(\Omega_i)\right]+\text{c.c.}\ , \tag{A4}$$

where again, i and $j=f,p$. Using Eq. (A4) and substituting in Eq. (7), we find the expression for $\rho_{21}^{(3)}(\omega)$ given in Eq. (10).

APPENDIX B

In the absence of spectral diffusion, the FWM*b* line shape of an inhomogeneously broadened system is described by the square of the induced polarization, given in general for classical hole burning by Eq. (14). This leads to a general line shape described by

$$L_b(\Delta)=\left|\int d\omega\, f(\Omega+\Delta,\omega)\,\mathrm{Im}[f(\Omega,\omega)]\right|^2, \tag{B1}$$

where for FWM, $\Omega=\Omega_f=\Omega_p$ and $\Delta=\Omega_b-\Omega$. We have also assumed that the inhomogeneous width is much greater than the homogeneous width of the system, and Ω is near the center of the inhomogeneous distribution so that $G(\omega)$ can be assumed constant within the integral and has been removed. Within the rotating wave approximation and with the assumption that the functional form of the homogeneous response function $f(\Omega,\omega)$ is independent of the transition frequency ω, the response function can be written as a function of the difference between the response frequency Ω and the transition frequency ω, that is, $f(\Omega,\omega)=f(\Omega-\omega)$. The causality condition further requires that the response function is an analytical function of Ω in the upper half of the complex plane, and therefore an analytical function of ω in the lower half of the complex plane.[25]

To show that $L_b(\Delta)$ is symmetric for $\Delta\rightarrow-\Delta$, we begin by defining

$$V(\Delta)=\int d\omega\, f(\Omega+\Delta-\omega)f(\Omega-\omega)\ . \tag{B2}$$

The integrand is also an analytical function of ω in the lower half of the complex plane. We now follow the usual procedure and use Cauchy's integral theorem, choosing a contour to include the real axis and the semicircle in the lower half plane (there is no contribution to the integral from this part of the contour[25]). Since f is analytic in ω in the lower half plane, we get $\oint d\omega\, f(\Omega+\Delta,\omega)f(\Omega,\omega)=0$ and hence, $V(\Delta)=0$. Since $\mathrm{Im}f=f-f^*$, the line-shape function reduces to

$$L_b(\Delta)=\left|\int d\omega\, f(\Omega+\Delta-\omega)f^*(\Omega-\omega)\right|^2. \tag{B3}$$

It is easily seen that $L_b(\Delta)=L_b(-\Delta)$, which means the FWM*b* line shape in the absence of spectral diffusion is a symmetric function of the backward pump detuning.

[1] T. Yajima and H. Souma, Phys. Rev. A **17**, 309 (1978).
[2] H. Wang, M. Jiang, and D. G. Steel, Phys. Rev. Lett. **65**, 1255 (1990).
[3] J. Hegarty, J. Lumin. **36**, 273 (1987).
[4] M. Berg, C. A. Walsh, L. R. Narasimhan, K. A. Littau, and M. D. Fayer, J. Chem. Phys. **88**, 1564 (1988).
[5] P. Hu and S. R. Hartmann, Phys. Rev. B **9**, 1 (1974).
[6] D. L. Dexter, J. Chem. Phys. **21**, 836 (1953).
[7] T. Takagahara, J. Lumin. **44**, 347 (1989).
[8] J. R. Klauder and P. W. Anderson, Phys. Rev. **125**, 912 (1962).
[9] R. P. Feynman, F. L. Vernon, and R. W. Hellwarth, J. Appl. Phys. **28**, 49 (1957).

[10]C. P. Slichter, *Principles of Magnetic Resonance* (Harper and Row, New York, 1962). Even a simple two-level system requires a minimum of four decay parameters: one each for the upper and lower states and a complex parameter for the decay and frequency shift of the polarization. If the upper state decays into the lower state, an additional source term is then required to account for this dynamics in the lower state.

[11]C. Cohen-Tannoudji, *Frontiers in Laser Spectroscopy*, edited by R. Balian, S. Haroche, and S. Liberman (North-Holland, Amsterdam, 1977).

[12]R. G. DeVoe and R. G. Brewer, Phys. Rev. Lett. **50**, 1269 (1983).

[13]P. R. Berman, J. Opt. Soc. Am. B **3**, 564 (1986).

[14]A. Szabo and T. Muramoto, Phys. Rev. A **39**, 3992 (1989); A. Szabo, in *Proceedings of the Nonlinear Optics Conference, Vavilov, 1990* (Nova Sicence, New York, in press).

[15]For review, see P. R. Berman, in *New Trends in Atomics Physics*, edited by G. Grynberg and R. Stora (North-Holland, Amsterdam, 1984), pp. 453–514.

[16]J. Cooper, R. J. Ballagh, K. Burnett, and D. G. Hummer, Astrophys. J. **260**, 299 (1982).

[17]W. E. Lamb, Jr., Phys. Rev. A **134**, 1429 (1964).

[18]D. G. Steel and J. T. Remillard, Phys. Rev. A **36**, 4330 (1987). [See especially Eq. (7). Note that in this discussion, terms proportional to $(E_b E_p^*)$ in second order are included, along with a general decay to the reservoir.]

[19]T. F. Soules and C. B. Duke, Phys. Rev. B **3**, 262 (1971).

[20]E. Cohen and M. D. Sturge, Phys. Rev. B **25**, 3828 (1982).

[21]P. R. Berman and R. G. Brewer, Phys. Rev. A **32**, 2784 (1985).

[22]R. Friedberg, S. R. Hartmann, and J. T. Manassah, Phys. Rep. **7**, 101 (1973). Interactions between resonant systems are known to be very important in dense systems. Recent results show novel behavior in transient FWM in semiconductors due to this effect [K. Leo *et al.*, Phys. Rev. Lett. **65**, 1340 (1990)].

[23]B. D. Fried and S. D. Conte, *The Plasma Dispersion Function* (Academic, New York, 1961). For $b>0$, the plasma dispersion function is defined as

$$Z(a+ib)=(\sqrt{\pi})^{-1}\int_{-\infty}^{\infty} dx \frac{\exp(-x^2)}{[x-(a+ib)]} .$$

It is also useful to note that

$$(\sqrt{\pi})^{-1}\int_{-\infty}^{\infty} dx \frac{\exp(-x^2)}{[x-(a-ib)]} = -Z(-a+ib) .$$

For small argument $\xi=a+ib$, the first term in the power series is given by $i\sqrt{\pi}\exp(-\xi^2)$. In general, this integral must be numerically evaluated and then it is helpful to note that the plasma dispersion function is closely related to the integral representation of the w function and the complex complimentary error function in *Handbook of Mathematical Functions*, Natl. Bur. Stand. Appl. Math. Ser. No. 55, edited by M. Abramowitz and I. A. Stegun (U.S. GPO, Washington, D.C., 1965). This latter function is numerically evaluated in many standard software libraries.

[24]The form of the redistribution kernel was chosen for convenience and represents a model used to describe earlier experimental results given in Ref. 2 above.

[25]J. D. Jackson, *Classical Electrodynamics* (Wiley, New York, 1975), p. 309.

Appl. Phys. A 53, 514–522 (1991)

Applied Physics A Solids and Surfaces

High-Resolution Nonlinear Laser Spectroscopy of Exciton Relaxation in GaAs Quantum Wells

H. Wang and D. G. Steel

H. M. Randall Laboratory of Physics, The University of Michigan, Ann Arbor, MI 48109, USA

Received 1 May 1991/Accepted 11 September 1991

Abstract. This paper describes measurements of exciton relaxation in GaAs/AlGaAs quantum well structures based on high resolution nonlinear laser spectroscopy. The nonlinear optical measurements show that low energy excitons can be localized by monolayer disorder of the quantum well interface. We show that these excitons migrate between localization sites by phonon assisted migration, leading to spectral diffusion of the excitons. The frequency domain measurements give a direct measure of the quasi-equilibrium exciton spectral redistribution due to exciton energy relaxation, and the temperature dependence of the measured migration rates confirms recent theoretical predictions. The observed line shapes are interpreted based on solutions we obtain to modified Bloch equations which include the effects of spectral diffusion.

PACS: 71.35.+z, 42.65.–k, 78.47.+p, 78.65.Fa

The linear and nonlinear optical properties of GaAs quantum well (QW) structures are dominated by strong excitonic resonances near the band edge. In these materials, quasi-two-dimensional excitons are confined in the thin GaAs layer by the larger band gap of the $Al_xGa_{1-x}As$ layers. The enhancement of the electron-hole correlation due to confinement leads to an increase in both the exciton oscillator strength and the exciton binding energy. The resultant appearance of well-resolved excitonic resonances even at room temperature has generated considerable interests in studies of excitonic nonlinear optical properties in QW structures [1]. It is now understood that effects of the Pauli exclusion principle inciuding phase space filling and exchange dominate the nonlinear optical response of the exciton while effects of the Coulomb screening are significantly reduced due to the reduced dimensionality [2].

In adition to the exciton manybody interactions, the nonlinear optical property of the exciton also strongly depends on the dynamical interaction of the exciton with the surrounding crystal lattice and vacuum radiation. Relaxation of the exciton and the associated polarization (i.e., the induced coherence) due to these interactions can significantly alter the nonlinear optical response of the exciton. Measurements of the excitonic nonlinear optical response not only determine the effect of relaxation on the nonlinear optical property of the material, but also provide us a quantitative description of the exciton relaxation process. As we discuss below, details of exciton relaxation in a QW also in part reflect properties of the interface between GaAs and AlGaAs.

Relaxation of excitonic excitation is characterized by decay of the exciton population about energy E and decay of the optically induced polarization or coherence (often called dephasing which determines the homogeneous line width, Γ_h). In an ideal crystal, excitons are described by a Bloch wave function and are free to move in the crystal. At low exciton density, decay of the excitation is expected to be predominantly due to exciton–phonon scattering along with exciton recombination.

However, in a QW the problem becomes more complicated. Non-ideal growth conditions can result in interface roughness between the GaAs well and AlGaAs barrier. Recent transport and chemical lattice imaging investigations have shown the interface of GaAs/AlGaAs multiple quantum well samples may be characterized by island-like structures with a height of one mononlayer and a lateral size of order 50 Å [3]. Details of the interface roughness also depend on specific growth processes, such as interrupted or non-interrupted growth [4, 5], or whether GaAs is grown on AlGaAs or AlGaAs is grown on GaAs [5]. The effects of interface roughness are significant. For example, an exciton confined to a thin GaAs layer (typically 100 Å) experiences an energy shift of the

order of several meV for a monolayer well-width change. As the exciton moves inside the well, it will be scattered by the random potential due to the interface roughness. As a result, low energy excitons are expected to become localized, i.e. the envelope of the wave function decays exponentially in space. In this case, the energy of the exciton also depends on the local environment leading to inhomogeneous broadening of the linear absorption spectrum.

Localized and delocalized excitons have qualitatively different relaxation properties [6]. Even at very low temperature (< 10 K), localized excitons do not remain truly localized, instead they can migrate among localization sites by emitting or absorbing acoustic phonons (phonon assisted migration). Phonon assisted migration was first proposed to explain the slow and non-exponential energy relaxation observed in time resolved luminescence measurements in a GaAs QW structure [6, 7]. At higher temperatures, excitons can absorb phonons of enough energy and be activated to delocalized states at higher energies. The activation process has been observed in a number of measurements such as spectral hole burning [8], resonant Rayleigh scattering [9], and resonant Raman scattering [10]. Estimations of the activation energy have suggested that the onset for the delocalized exciton in GaAs QW structures is near the absorption line center [8, 9]. In contrast, decay of the delocalized exciton is determined by the exciton–phonon scattering along the energy–momentum dispersion curve and the exciton recombination. Furthermore, delocalized excitons also experience elastic scattering from potential fluctuations, which introduces additional dephasing to the decay of the polarization.

In this paper, we discuss high resolution nonlinear optical measurements of the exciton relaxation in GaAs quantum well structures. The measurements are based on frequency domain four wave mixing (FWM) [11]. The primary objective of these measurements has been to further the physical understanding of relaxation of excitonic excitations in QW structures. Particular emphasis has also been given to the understanding of nonlinear optical measurements in semiconductors, and to how relaxation manifests itself in the frequency domain nonlinear optical response of the material. High resolution nonlinear measurements can provide detailed information on the population relaxation similar to transient nonlinear absorption measurements as well as eliminate the inhomogeneous broadening due to the interface roughness leading to a measure of the homogeneous line shape or the steady state spectral redistribution of the excitation. Since these measurements are performed in the energy space, they are particularly sensitive to relaxation processes involving energy shifts of the excitation (referred to in general as spectral diffusion) such as the exciton migration discussed above. The narrow band-width of the excitation also permits improved resolution over the usual time domain measurements. In addition, the frequency domain methods are able to observe in a single measurement time scales ranging over twelve orders of magnitude [12].

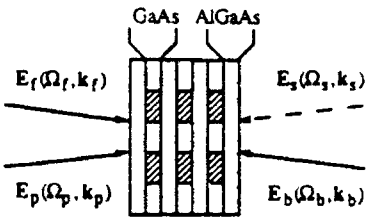

Fig. 1. A schematic representation of the experimental configuration for frequency domain backward four-wave mixing spectroscopy in GaAs/AlGaAs QW structures. The cross hatched region represents the region of optically excited excitons which are confined by the AlGaAs barriers

1 Frequency Domain FWM Line Shapes

The experimental configuration is based on the backward FWM geometry, which is closely related to optical phase conjugation [13], and on the use of two frequency stabilized tunable cw dye lasers. As shown in Fig. 1, two counter-propagating pump beams $\mathbf{E}_f(\Omega_f, \mathbf{k}_f)$ and $\mathbf{E}_b(\Omega_b, \mathbf{k}_b)$ (f and b stand for forward and backward respectively) interact in the sample with a probe beam $\mathbf{E}_p(\Omega_p, \mathbf{k}_p)$ with $\mathbf{E}_p \| \mathbf{E}_f \perp \mathbf{E}_b$ through the resonant third order susceptibility to generate a signal beam $\mathbf{E}_s(\Omega_s, \mathbf{k}_s)$ proportional to $\chi^{(3)}(\mathbf{E}_f \cdot \mathbf{E}_p^*)\mathbf{E}_b$. Physically, $\mathbf{E}_f \cdot \mathbf{E}_p^*$ results in a spatial and temporal modulation of the exciton population, which modifies the optical response of the sample. The coherent nonlinear signal arises from scattering of the backward beam from the modulation [14]. Spectroscopic information can be obtained by studying the dependence of the nonlinear optical response on the relative frequency detuning, the electric field polarization, or the relative angle of the different input beams. For the measurements in this paper, information related to relaxation of the system is obtained by measuring the nonlinear response as a function of the frequency of any of the three input beams. The resultant line shape is designated the FWMi response where i = f, b, p depending on which beam is tuned. In general, FWMp and FWMf responses provide details of population relaxation, while the FWMb response reflects a measure of the homogeneous line shape and of the spectral redistribution of the excitation as we discuss below.

To illustrate the measurement ability of the frequency domain nonlinear measurement and understand the effects of spectral diffusion on line shapes of the nonlinear optical response, we have examined the FWM response of a simple two level system undergoing spectral diffusion [15]. In this model, the excitation at an individual site can transfer to neighboring sites through an intersite interaction (such as dipole–dipole interaction). The excitation transfer is assumed to be characterized by a redistribution kernel $W(\omega, \omega')$ representing the rate for populations in the excited state to be transferred from a site with resonant frequency ω to sites with resonant frequency ω'. The overall spectral diffusion rate is then $\Gamma(\omega) = \int W(\omega, \omega')\, d\omega'$. $W(\omega, \omega')$ is analogous to collision kernels that are used to describe velocity changing collisions in atomic vapor [16]. In addition, since the

excitation transfer is likely to be associated with emission or absorption of thermal phonons, we assume that at the new site the excitation transfer does not induce a superposition state of the ground and excited state that is coherent with the input fields. Such a model has been discussed in detail elsewhere [15], and is closely related to the problem of excitation transfer between ions embedded in a crystal [17].

The interaction of the system with optical fields can be described by the following modified optical Bloch equations (MOBE) assuming a classical representation for the optical fields:

$$i\hbar \frac{\partial}{\partial t} \varrho_{22}(\omega) = -[V\varrho_{21}(\omega) - \text{c.c.}] - i\hbar[\gamma_{sp} + \Gamma(\omega)]\varrho_{22}(\omega) + i\hbar \int W(\omega', \omega)\varrho_{22}(\omega')\, d\omega', \tag{1}$$

$$i\hbar \frac{\partial}{\partial t} \varrho_{12}(\omega) = V[\varrho_{22}(\omega) - \varrho_{11}(\omega)] - \hbar\omega\varrho_{12}(\omega) - i\hbar[\gamma + \Gamma_{12}(\omega)]\varrho_{12}(\omega), \tag{2}$$

where level $|2\rangle$ is the excited state and level $|1\rangle$ is the ground state, $\varrho_{ij}(\omega)$ is the usual population density matrix element for systems with a resonant frequency ω [18], $\Gamma_{12}(\omega)$ represents the dephasing rate of the system due to spectral diffusion, $V = -\boldsymbol{\mu} \cdot \mathbf{E}$ is the interaction energy with $\boldsymbol{\mu}$ the dipole moment (assumed to be real) and $\mathbf{E} = \frac{1}{2} \sum \mathbf{E}_j \exp(i\mathbf{k}_j \cdot \mathbf{x} - i\Omega_j t) + \text{c.c.}$ summed over all applied electric fields. Equation (2) takes into consideration pure dephasing of the optically induced coherence by letting the dephasing rate $\gamma = \gamma_{sp}/2 + \gamma_{ph}$, where γ_{sp} is the spontaneous emission rate, and γ_{ph} is the pure dephasing rate, due for example to elastic scattering. In addition, we have also assumed that the system is quantum mechanically closed, i.e., the probability that an atom is in the ground or the excited state is unity. This leads to the condition $\varrho_{11}(\omega) + \varrho_{22}(\omega) = G(\omega)$ where $G(\omega)$ is the density of atoms at frequency ω. Note that spectral diffusion due to intersite energy transfer is also accompanied by a corresponding change in location of the excitation. However, if the effective mean free path for excitation transfer is small, then the effect would be described by a spatial diffusion process. This effect can be phenomenologically included as a spatial diffusion decay term in the equation for ϱ_{22}, and the decay rate is given by $\Gamma_d = 4\pi^2 D/\Lambda^2$ where D is the diffusion coefficient and Λ is the spatial period of the modulation.

The model discussed above may not accurately represent the physical process of exciton migration during nonlinear optical interaction, since a simple two level model does not reflect many-body nature of the excitonic nonlinear optical response. Moreover, description of the spectral diffusion process in general, and exciton migration in particular is much more complicated than a simple transfer of the excited state population [19]. Nevertheless, recent theoretical work has shown that in the limit that phase space filling dominates the exciton nonlinear optical response, the equation of motion governing the nonlinear optical process in semiconductors is nearly identical to the optical Bloch equation of an atomic system [20]. Hence, we expect predictions from the above simple two level model to reflect the qualitative features of FWM line shapes of more complicated systems, in particular excitons in QW structures, and provide a guidance for more detailed studies.

Even with the above assumptions, it is rather difficult to obtain analytical solutions for frequency domain FWM line shapes for a general distribution kernel. However, using a strong redistribution model for the spectral diffusion process we may further simplify the above equations. In this model, the spectral diffusion process is independent of the resonant frequency of the initial site, and each transfer on average leads to a complete redistribution of the excited state population [21], i.e. $W(\omega', \omega) = \Gamma F(\omega)$ with $F(\omega)$ satisfying $\int d\omega F(\omega) = 1$ where Γ is the overall spectral diffusion rate for the excited state. For the qualitative discussions of this work, the dephasing rate due to spectral diffusion is taken to be $\Gamma_{12}(\omega) = \Gamma/2$ (the coupling giving rise to spectral diffusion may also lead to pure-dephasing effects which could be included in γ_{ph}).

With these simplifications, the off diagonal matrix element to the third order in applied fields for a signal nearly counter-propagating to the probe (proportional to $(\mathbf{E}_f \cdot \mathbf{E}_p^*)\mathbf{E}_b$) can be obtained [15]:

$$\varrho_{21}^{(3)}(\omega) = -2\left(\frac{\mu}{2\hbar}\right)^3 E_f E_p^* E_b \exp[i(\mathbf{k}_f + \mathbf{k}_b - \mathbf{k}_p)\cdot\mathbf{x} - i\Omega_s t] \times \frac{1}{\Omega_s - \omega + i\Gamma_h} \cdot \frac{1}{\Delta_{fp} + i(\Gamma + \gamma_{sp})} \times \left\{ G(\omega)\left(\frac{1}{\Omega_f - \omega + i\Gamma_h} - \frac{1}{\Omega_p - \omega - i\Gamma_h}\right) + \frac{i\Gamma}{\Delta_{fp} + i\gamma_{sp}} F(\omega)\,[A(\Omega_f) - A^*(\Omega_p)] \right\}, \tag{3}$$

where $\Gamma_h = \gamma_{sp}/2 + \Gamma/2 + \gamma_{ph}$ is the total dephasing rate, $\Omega_s = \Omega_f + \Omega_b - \Omega_p$ is the signal frequency, and $\Delta_{ij} = \Omega_i - \Omega_j$ with $i, j = f, b, p, s$. $A(\Omega)$ is given by

$$A(\Omega) = \int \frac{1}{\Omega - \omega + i\Gamma_h} G(\omega)\, d\omega. \tag{4}$$

The imaginary part of the $A(\Omega)$ is related to the inhomogeneous linear absorption profile of the system and the real part corresponds to the dispersion. The corresponding third order polarization can be easily obtained by integrating $\varrho_{21}^{(3)}(\omega)$ over the inhomogeneous distribution, yielding

$$P^{(3)}(\Omega_s) = -2\mu\left(\frac{\mu}{2\hbar}\right)^3 E_f E_p^* E_b \exp[i(\mathbf{k}_f + \mathbf{k}_b - \mathbf{k}_p)\cdot\mathbf{x} - i\Omega_s t] \times \frac{1}{\Delta_{fp} + i(\gamma_{sp} + \Gamma)} \left\{ \frac{1}{\Delta_{sp} + 2i\Gamma_h}\,[A(\Omega_s) - A^*(\Omega_p)] - \frac{1}{\Delta_{sf}}\,[A(\Omega_s) - A(\Omega_f)] + \frac{i\Gamma}{\Delta_{fp} + i\gamma_{sp}} \times Q(\Omega_s)\,[A(\Omega_f) - A^*(\Omega_p)] \right\} + \text{c.c.}, \tag{5}$$

where $Q(\Omega_s)$ is related to the redistribution kernel by

$$Q(\Omega_s) \doteq \int \frac{1}{\Omega_s - \omega + i\Gamma_h} F(\omega)\, d\omega. \tag{6}$$

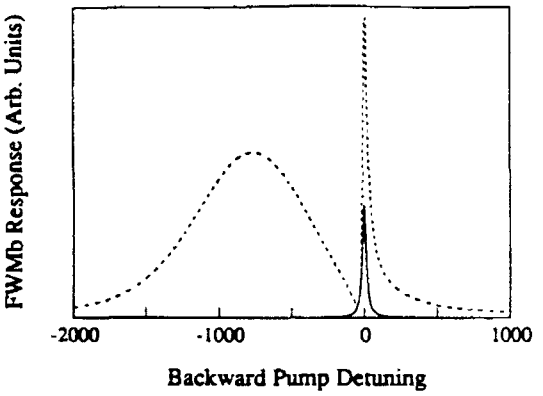

Fig. 2. The FWMb response. All the frequency and decay rates are normalized to the spontaneous emission rate. $\Gamma = 15$, $\Delta\omega_{inh} = 1000$, $\Delta\omega_0 = 400$, $\Omega_p - \omega_{inh} = -100$, $\omega_0 - \omega_{inh} = -850$, where ω_{inh} and $\Delta\omega_{inh}$ are the center and half-width of the inhomogeneous distribution respectively, and ω_0 and $\Delta\omega_0$ are the center and half-width of the redistribution kernel respectively. The backward pump detuning is measured with regard to $\Omega_p - \Delta_{fp}$. The solid line is the line shape obtained with $\Delta_{fp} = \Gamma$. The dashed line is the line shape obtained with $\Delta_{fp} = 0$

The nonlinear optical signal is determined by a solution of the appropriate Maxwell wave equation where the nonlinear polarization is the source term. In the limit that all fields are weak and there is no depletion of any of the applied fields, the nonlinear signal is simply proportional to $|P^{(3)}(\Omega_s)|^2$.

Equation (5) is nearly identical to the results obtained for a two level system without spectral diffusion with the exception of the last term [22]. The resonant denominator $[\Delta_{fp} + i(\gamma_{sp} + \Gamma)]^{-1}$ arises in the calculation of the second order diagonal matrix element. The width of the denominator measures the decay rate of the excitation modulation, and includes an additional contribution from spectral diffusion. The familiar hole burning resonant denominator associated with $2\Gamma_h$ results when the signal is resonant with the dipole excited by $\mathbf{E}_f \cdot \mathbf{E}_p^*$ (i.e., when $\Omega_s = \Omega_p$), and also shows an additional broadening due to the dephasing that occurs through spectral diffusion. The term inversely proportional to Δ_{sf} is not singular, but rather goes to 0 in the limit of $\Delta_{sf} = 0$. Contributions from this term are negligible in the limit of strong inhomogeneous broadening when the detuning Δ_{ij} is small compared with the inhomogeneous width.

The last term in (5) results from spectrally diffused excitation. It is proportional to $Q(\Omega_s)$ reflecting a measure of the redistribution kernel. Because of the resonant enhancement which occurs when the signal is resonant with the optical transition as represented by the denominator $(\Omega_s - \omega + i\Gamma_h)^{-1}$ in (3), the dominant contribution to the nonlinear response is expected to come from systems that are resonant with the Ω_s. In the presence of spectral diffusion, the signal coming from the last term can be observed even when the signal frequency is tuned away from the frequency of the initial excitation (the frequency of the forward pump and the probe beams) and resonant with excitations transferred to energy $E = \hbar\Omega_s$.

We first discuss the FWMb line shape. In this measurement, nearly degenerate forward pump and probe beams interfere in the sample to excite population modulation of a narrow spectral hole with a half-width Γ_h within the inhomogeneous profile. The FWMb line shape is obtained by measuring the nonlinear signal as a function of the frequency of the backward pump beam. This measurement is analogous to the cw hole burning measurements and also closely related to the standard two pulse photon echo measurement [23]. In hole burning measurements, a pump beam modulates the absorption in a narrow bandwidth compared to the inhomogeneous width whereas in FWM, a population grating is created. In the absence of spectral diffusion ($\Gamma = 0$), the FWMb line shape simply reflects the spectral details of the hole excited by $\mathbf{E}_f \cdot \mathbf{E}_p^*$. The line shape reduces to a simple Lorentzian with a width *twice* the homogeneous width. In the presence of spectral diffusion, the hole excited by $\mathbf{E}_f \cdot \mathbf{E}_p^*$ diffuses in energy space resulting in a spectral redistribution of the excitation. Since tuning Ω_b effectively changes Ω_s, this redistribution can be directly mapped out by the FWMb response. In this case, the FWMb response results from both the spectral hole burning and the spectrally diffused excitations.

It is important to note that while there are similarities between the FWMb line shape and the line shape obtained in ordinary spectral hole burning, there are two important differences. Hole burning basically measures the imaginary part of the optical response while the FWMb response measures the modulus square of the response, hence including both imaginary and real parts. More significantly, however, is that in frequency domain FWM, it is possible to control the amount of contributions from the spectrally diffused excitation by using a fixed forward pump and probe frequency offset as we can see from (5). In particular, in the limit of a large offset (much greater than the spontaneous emission rate), the FWMb response reflects only the homogeneous line shape. In practice, by choosing an appropriate offset, the contribution from spectrally diffused excitation may be eliminated without significant reduction of the nonlinear signal strength. Furthermore, while the current discussion has focused on a simple resonant system, it is not difficult to imagine that there are different systems characterized by different excitation and dephasing relaxation rates but having nearly the same resonant frequency. By examining the homogeneous line width measured in the FWMb response as a function of different forward pump and probe offsets, it is possible to differentiate between the different resonant systems [12].

Figure 2 shows two FWMb line shapes obtained from the nonlinear polarization in (5). Here, the strong redistribution kernel and the inhomogeneous distribution are taken to be Gaussian. The strong redistribution kernel is characterized by a center frequency ω_0 and a half-width $\Delta\omega_0$. Similarly, the inhomogeneous distribution is characterized by a center frequency ω_{inh} and a half-width $\Delta\omega_{inh}$. The dashed line in the figure is the response obtained with $\Delta_{fp} = 0$. The narrow peak around zero detuning is predominantly the result of spectral hole burning while the broad peak reflects the spectral redistribution of the exci-

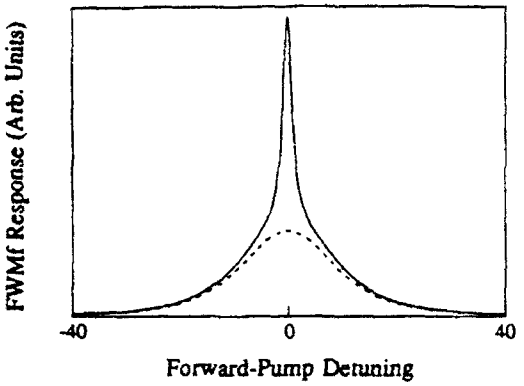

Fig. 3. The FWMb response. $\Gamma = 15$, $\Delta\omega_{inh} = 1000$, $\Delta\omega_0 = 400$, $\omega_0 - \omega_{inh} = -100$, $\Omega_p = \omega_0$. The response shows a prominent narrow component due to the decay of the quasi-equilibrium population. The width of this component is determined by the spontaneous emission rate. The dashed line represents the nonlinear response without contribution from the spectrally diffused excitations

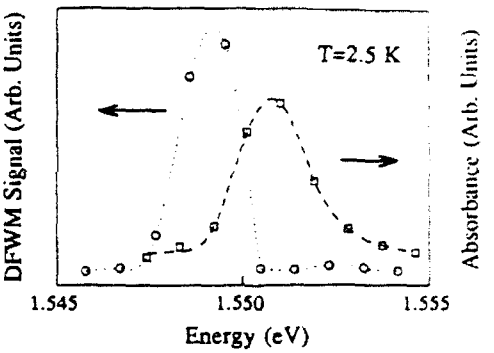

Fig. 4. The degenerate FWM (DFWM) and absorption spectra of HH1 excitons obtained at 2.5 K

tation created at the forward pump and probe frequency. The solid line in the figure represents the FWMb line shape using a forward pump and probe offset $\Delta_{fp} = \Gamma$. The line shape is *Lorentzian* and reflects the homogeneous line shape of the system. Note that the strength of the nonlinear signal has only been reduced by a factor of order 2.

In the FWMf measurement, we hold $\Omega_p = \Omega_b$. Detuning the forward pump frequency by an amount $\delta = \Omega_f - \Omega_p$ produces a traveling wave modulation of excitation with the amplitude proportional to $[\delta + i(\Gamma + \gamma_{sp})]^{-1}$. The nonlinear response as a function of δ then measures the decay rate of the modulation formed by excitations that are resonant with the signal beam. The decay rate, $\Gamma_m = \Gamma + \gamma_{sp}$, includes contributions from spontaneous emission as well as transfer of excitations from energy E to E' where $|E - E'| > \Gamma_h$. Spatial diffusion of the excitation, which is not included in (5), also contributes to the decay and manifests itself as a dependence of the decay rate on the spatial period of the modulation. Note that in the limiting case where $\Gamma_h \sim \Gamma_m/2$, the FWMf line shape is complicated by the fact that tuning Ω_f also changes the frequency of the signal beam and the frequency of the first order polarization. The FWMf response then experiences an additional resonant effect from the hole burning denominator appearing as $(\delta + 2i\Gamma_h)^{-1}$ [see (5)], resulting in a deviation from a simple Lorentzian and requiring a small correction (of order 1) in relating Γ_m to the HWHM for *absolute* decay rate measurements. The FWMp response provides a measurement similar to the FWMf response. However, since $\Omega_f = \Omega_b$, the hole burning denominator appears as $(\delta + i\Gamma_h)^{-1}$ resulting in a slightly larger correction as we can see from (5). In the case of $\Gamma_h \gg \Gamma_m/2$, the FWMp and FWMf line shapes are the same and independent of Γ_h.

Spectral diffusion of the excitation between different energy sites also leads to the establishment of a quasi-equilibrium redistribution of the excited state population as we have discussed earlier. This is expected regardless of the functional form of the redistribution kernel. This quasi-equilibrium population contributes to the nonlinear response, and decay of this population is determined by the spontaneous emission of the excited states. If the spontaneous emission rate is slow compared to the spectral diffusion rate, then a narrow resonance can be observed on top of the broad resonance with a half-width given by γ_{sp}. In the limit of a very large spectral diffusion rate, the narrow resonance may even become dominant. In time resolved luminescence of this transition, the measured decay rate would be given by γ_{sp}. However, because of the hole burning achieved in frequency domain FWM, it is possible to separately measure both decay rates. Figure 3 shows a FWMf line shape using the nonlinear polarization in (5). As anticipated, it clearly shows a prominent narrow peak sitting on top of a broad base. The broad base is the result of the fast spectral diffusion process ($\Gamma = 15\gamma_{sp}$). The narrow peak corresponds to the excited state spontaneous emission rate.

2 High-Resolution Nonlinear Measurements

Typical GaAs QW samples used in our measurements consisted of 65 periods of 96 Å GaAs wells and 98 Å $Al_{0.3}Ga_{0.7}As$ barriers, grown at 630° C by a Varian Gen II MBE machine on semi-insulating (100) GaAs substrate with interrupted growth. The samples are mounted on a sapphire disk (*c* axis normal) with the substrate removed for the nonlinear measurement. The data presented here were obtained on a sample that is characterized by an absorption line width of 2.2 meV for the HH1 exciton, and a Stokes shift of 1 meV between the HH1 exciton absorption and emission. Similar results were also obtained on other samples. In contrast to many earlier measurements, the exciton density for these measurements were kept low near 10^7 excitons/cm^2. All the nonlinear measurements are carried out on the HH1 exciton.

The excitonic nonlinear optical response is primarily due to phase space filling and exchange effects. Figure 4 shows the degenerate FWM response obtained at 2.5 K. The rapid decrease of the nonlinear response around the absorption line center is partly due to strong exciton absorption. However, the nonlinear response on the high energy side of the absorption line center is extremely

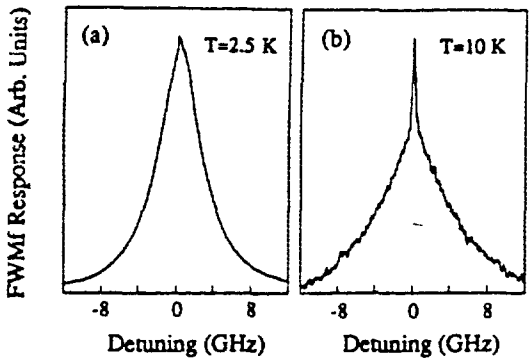

Fig. 5a, b. The FWMf response below the absorption line center. **a** At 2.5 K and at 1.5 meV below the exciton absorption line center. **b** At 10 K and at 0.6 meV below the exciton absorption line center. The line shapes show two decay components. The decay time associated with the line shape is $(2\pi \cdot \mathrm{HWHM})^{-1}$. Compare with Fig. 3

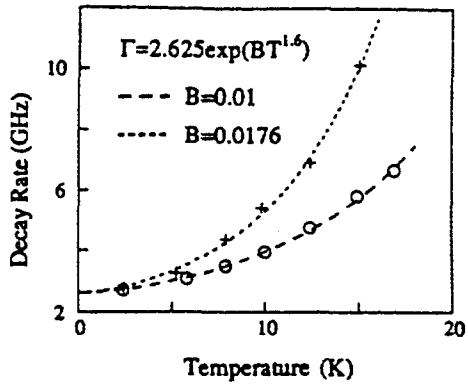

Fig. 6. The temperature dependence of the exciton population decay rate. Circles and crosses are data obtained at 1.5 meV and at 0.6 meV below the exciton absorption line center respectively. Dash lines are fit to the theory of phonon assisted migration

small compared to that on the low energy side signaling a change of the exciton relaxation properties across the absorption line center. The small cw nonlinear optical response indicates a much increased exiton relaxation rate above the absorption line center. The energy dependence of the relaxation rate will be discussed in more detail later.

Relaxation of the exciton population is first characterized using the FWMf response [23]. A typical line shape below the absorption line center is shown in Fig. 5a. Complex decay dynamics of the exciton is evidenced in the line shape. The HWHM of the line shape corresponds to a relaxation time of 60 ps, which is slow compared to acoustic-phonon scattering of the delocalized exciton (typically on a time scale of 10 ps), and is over an order of magnitude faster than the exciton recombination time. Furthermore, within experimental error, the spectrum shown in Fig. 5a is independent of the modulation spacing, indicating the contribution from exciton diffusion is negligible and inferring an upper limit of order 1 cm^2/s for the exciton diffusion coefficient. The above result indicates that excitons are strongly localized in this spectral region as suggested by earlier resonant Rayleigh scattering and transient FWM measurement of Hegarty and Sturge [9]. The measurements suggest that the decay of the exciton population is characterized by exciton spectral diffusion as a result of scattering of localized excitons from energy E to $E'(|E - E'| > \Gamma_h)$. The obtained decay rate is in agreement with the calculation based on phonon assisted migration of the localized exciton [6].

Excitons that have migrated out of sites with energy E also have a finite probability to come back leading to the establishment of a quasi-equilibrium exciton population at energy E before these ecitons eventually recombine, as discussed above. Decay of this quasi-equilibrium population should be characterized by the exciton recombination rate, and so is the nonlinear optical response due to this population. The FWMf response shown in Fig. 5a indeed shows a small and narrow feature at the top of the line shape. The narrow feature becomes more pronounced at higher temperature due to faster exiton migration rate which also leads to an increase of the quasi-equilibrium population, as shown in Fig. 5b. The width associated with the feature corresponds to a decay time of 1.2 ns consistent with the exciton recombination rate, which also confirms the above interpretation of the nonlinear measurements.

The mechanism of exciton migration can be best revealed by the temperature dependence of the migration rate since the migration process is likely to involve absorption or emission of acoustic phonons. The theoretical model for phonon assisted exciton mgiration was developed recently by Takagahara [6]. In this model, excitons resonantly excited are in a non-equilibrium state and can migrate to other sites by emitting or absorbing acoustic phonons. While the migration is due to the overlap of the exciton wave function in different sites when the inter-site distance is small, the inter-site dipole–dipole interaction mediates the migration process when the inter-site distance is much greater than the localization length. Typical magnitude of participating phonon wave vectors is within a few times of the inverse of the localization length corresponding to phonon energies of order 0.01 to 0.1 meV. The theory further predicts a distinctive temperature dependence for the migration rate. At low temperatures, the dependence is described by $\exp(BT^{\alpha})$. In this expression, B is positive and independent of temperature but is expected to increase with the exciton energy and depends on details of interface roughness; α is estimated to be between 1.6 and 1.7. The predicted temperature dependence is quite different from that of variable range hopping used by Mott to interpret electronic conduction in the localized regime. The difference has been attributed to the long-range nature of the inter-site interaction and the phonon emission process involved in the migration of the localized exciton [6]. The temperature dependence has been observed in transient hole burning experiments in an InGaAs/InP QW where all excitons are localized by alloy disorder [25].

Figure 6 shows the temperature dependence of the exciton migration rate obtained at 0.6 meV and 1.5 meV below the absorption line center using the FWMf re-

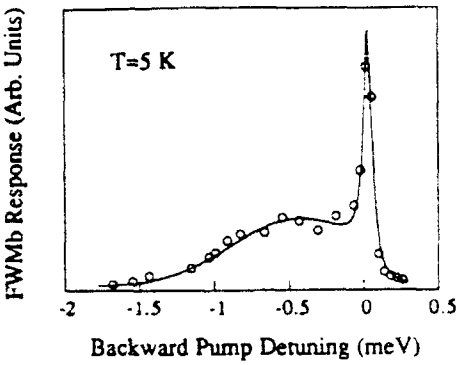

Fig. 7. The FWMb response at 5 K and with the frequencies of the forward pump and probe beams at 1.5 meV below the exciton absorption line center. The narrow resonance is due to spectral hole burning. The response also provides a measure of the steady state spectral redistribution of the exciton population. Compare with Fig. 2

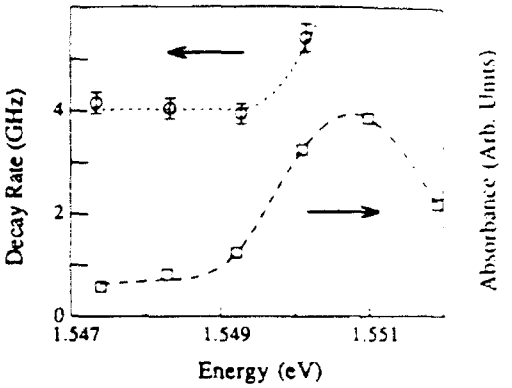

Fig. 8. The energy dependence of the exciton population decay rate at 10 K. Dash lines are only a guide to the eye

sponse. The data is in good agreement with the theory of phonon assisted migration discussed above with $\alpha = 1.6$. The measurement indicates that the dominant contribution to relaxation of the localized exciton is phonon assisted migration up to a temperature of 15 K. Note that earlier measurements have reported observations of an activation type of temperature dependence for the localized exciton at temperatures between 7 and 20 K, indicating that in this temperature region, relaxation for the localized exciton is dominated by thermal activation to delocalized states [8, 10]. It has been suggested that sample dependent variations in the thermal activation energy are the result of differences in the nature of interface roughness [26]. Hence, the effective activation energy can be much higher than simply the energy difference between the mobility edge and the localized exciton resulting, at low temperature (< 15 K), in a thermal activation rate much smaller than the phonon assisted migration rate. Note that thermal activation type of behavior in our samples has been observed above 15 K using stimulated photon echo methods [27, 28].

A more complete description of exciton spectral diffusion can be achieved by making a direct measurement of the excitons scattered from energy E to E' [24, 29]. If localized excitons are optically excited at energy E and then migrate among localization sites to different energies, a quasi-equlibrium exciton distribution over a broad spectral range can be established assuming the exciton migration rate is large compared with the recombination rate. The steady state redistribution of the exciton population can be directly probed in the FWMb response by scanning Ω_b while keeping Ω_f and Ω_p fixed at energy E, as anticipated in (5) and Fig. 2. Figure 7 shows a FWMb line shape where excitons are optically excited at 1.5 meV below the absorption line center. The nonlinear response is corrected for sample absorption. The narrow resonance in the response corresponds to exciton spectral hole burning, and the width of the hole gives an exciton homogeneous width of order $\Gamma_h \sim 0.01$ meV. The broad feature is due to the quasi-equilibrium redistribution of the exciton population, and the square root of the response is proportional to the steady state exciton population assuming all excitons in the spectral region concerned give rise to the same cw nonlinear response. The FWMb line shape in Fig. 7 can be fit to a simple model which neglects migration to states above the excitation energy, and is based on the understanding of the nonlinear optical response of a simple two-level system. The model assumes a Gaussian distribution for the quasi-equilibrium population of excitons that have migrated to states below the excitation energy. The spectral profile of the hole burning resonance is assumed to be Lorentzian. The result is plotted as the solid line in Fig. 7.

We further examine the energy dependence of the exciton relaxation rate using the FWMf response. For exciton energies less than 1.5 meV below the absorption line center, the exciton migration rate depends very weakly on the energy as is shown in Fig. 8. The migration rate increases rapidly approaching the absorption line center suggesting an increase of the localization length and an onset of the transition from localized to delocalized states. Physically, excitons can become delocalized when the localization length is comparable with or larger than the scale of inelastic cutoff given by $\sqrt{D\tau}$ [30], where D is the exciton diffusion coefficient and τ is the time between exciton–phonon scattering.

Earlier measurements using transient four wave mixing and resonant Rayleigh scattering have suggested that in a multiple QW, excitons above the exciton absorption line center may be weakly delocalized. Indeed, our measurements of FWMf and FWMb responses above the exciton absorption line center are qualitativeiy differen from that below the absorption line center. The nonlinea response is completely dominated by the recombinatio component even at the lowest temperature (1.8 K) w can achieve. This behavior is expected from the earlie analysis of the FWMf response if excitons experience a extremely rapid inelastic scattering such as in the case a delocalized exciton. Figure 9a shows a typical FWM line shape above the exciton absorption line center. large modulation spacing is used in this measurement s that contributions from exciton diffusion are negligibl The dashed line in the figure is a Lorentzian fit to the lir shape. The FWHM of the line shape corresponds to a

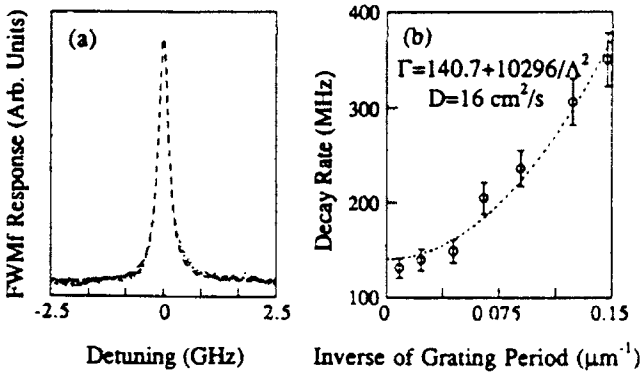

Fig. 9. a The FWMf response at 10 K and 2 meV above the exciton absorption line center. The dashed line is a fit to the Lorentzian. **b** The dependence of decay rates of the exciton population modulation on the modulation spacing. The dashed line is a fit to the equation of modulation decay due to diffusion

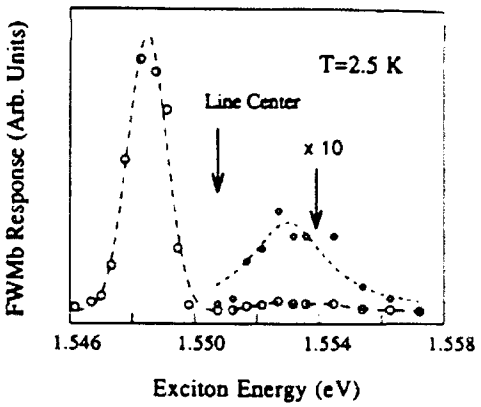

Fig. 10. The FWMb response at 2.5 K with the frequencies of the forward pump and probe beams at 2 meV above the exciton absorption line center. Dashed lines are guide to the eye

exciton recombination time of 1.2 ns. Furthermore, the measurement of the FWMf response as a function of the modulation spacing shows a quadratic dependence of the modulation decay rate on the inverse of the modulation spacing, yielding an exciton diffusion coefficient of order 16 cm^2/s (see Fig. 9b).

The FWMb response from the delocalized excitons needs more clarification. As we have discussed earlier, in a FWMb measurement, tuning the frequency of the backward pump probes the steady state distribution of the exciton population. While delocalized excitons can be scattered along the two dimensional energy–momentum dispersion curve to other delocalized states by inelastic processes such as exciton–phonon interactions, these states have nonzero momentum, and in the limit of a strict K-selection rule, a zero optical dipole moment. In this case, the FWMb line shape in the vicinity of the excitation energy simply provides a measure of the exciton homogeneous line shape. Note that at very low temperature, delocalized excitons scattered to the bottom of the dispersion curve will continue to lose energy by emitting acoustic phonons and eventually become localized as we show below.

The FWMb line shape for excitons resonantly excited 2 meV above the absorption line center is shown in Fig. 10. Narrow hole burning resonances are not observed in this line shape. The nonlinear signal above the absorption line center is extremely small compared to that below the line center, which is due to rapid dephasing of the polarization as well as the much increased exciton population decay rate. A magnified version of the FWMb spectrum above the absorption line center is also shown in the figure, from which we determine the homogeneous line width to be of order 1.5 meV (corresponding to a dephasing time of 0.5 ps). The large dephasing rate for the delocalized exciton is expected [6, 9] since these excitons are expected to experience rapid elastic scattering from interface potential fluctuations in addition to the exciton–acoustic-phonon scattering. The strong nonlinear optical signal below the absorption line center indicates that most of the excitons created above the absorption line center become localized before they eventually recombine.

In summary, frequency domain nonlinear measurements have revealed features of various physical mechanisms of exciton relaxation in GaAs QW structures. In particular, phonon assisted migration has been found to dominate relaxation of the localized exciton at very low temperature. The high resolution measurements have also enabled us to directly determine the redistribution of the exciton population due to exciton migration. In addition, these measurements clearly demonstrated the effects of relaxation on frequency domain nonlinear optical response of the exciton.

Acknowledgements. This work has been supported by the U.S. Army Research Office and the Air Force Office of Scientific Research. MBE samples were provided by Prof. P.K. Bhattacharya.

References

1. See for example, S. Schmitt-Rink, D.S. Chemla, D.A.B. Miller: Adv. Phys. **38**, 89 (1989)
2. S. Schmitt-Rink, D.S. Chemla, D.A.B. Miller: Phys. Rev. B **32**, 6601 (1985)
3. See for example, H. Sakaki, T. Noda, K. Hirakawa, M. Tanaka, M. Matsusue: Appl. Phys. Lett. **51**, 1934 (1987)
   R. Gottinger, A. Gold, G. Abstreiter, G. Weiman, W.Schlapp: Europhys. Lett. **6**, 183 (1988)
   A. Ourmazd, D.W. Taylor, J. Cunningham, C.W. Tu: Phys. Rev. Lett. **62**, 933 (1989)
4. See for example, C.W. Tu, R.C. Miller, B.A. Wilson, P.M. Petroff, T.D. Harris, R.F. Kopf, S.K. Sputz, M.G. Lamont: J. Cryst. Growth **81**, 159 (1987)
5. See for example, M. Tanaka, H.Sakaki: J. Cryst. Growth **81**, 153 (1987)
6. T. Takagahara: Phys. Rev. B **31**, 6552 (1985); B **32**, 7013 (1985)
7. Y. Masumoto, S. Shionoya, H. Kawaguchi: Phys. Rev. B **29**, 2324 (1984)
8. J. Hegarty, L. Goldner, M.D. Sturge: Phys. Rev. B **30**, 7346 (1984)
9. J. Hegarty, M.D. Sturge: J. Opt. Soc. Am. B **2**, 1143 (1985)
10. J.E. Zucker, A. Pinczuk, D.S. Chemla, A.C. Gossard: Phys. Rev. B **35**, 2829 (1987)
11. T. Yajima, H. Souma: Phys. Rev. A **17**, 309 (1978)

12. J.T. Remillard, H. Wang, D.G. Steel, J. Oh, J. Pamulapati, P.K. Bhattacharya: Phys. Rev. Lett. **62**, 2861 (1989)
13. See for example, Optical Phase Conjugation, ed. by R.A. Fisher (Academic,New York 1983)
14. For cw measurements, the orientational grating ($\mathbf{E}_p \perp \mathbf{E}_r \| \mathbf{E}_b$) has not been observed, and hence there is no back grating due to $\mathbf{E}_b \cdot \mathbf{E}_p^*$ if $\mathbf{E}_p \perp \mathbf{E}_b$
15. H. Wang, D.G. Steel: Phys. Rev. A **43**, 3823 (1991)
16. P.R. Berman: Phys. Rep. **43**, 102 (1978)
17. T.F. Soules, C.B. Duke: Phys. Rev. B **3**, 262 (1971)
18. W.E. Lamb, Jr.: Phys. Rev. A **143**, 1429 (1964)
19. J.R. Klauder, P.W. Anderson: Phys. Rev. **125**, 912 (1962)
20. M. Lindberg, S.W. Koch: Phys. Rev. B **38**, 3342 (1988)
21. P.R. Berman, R.G. Brewer: Phys. Rev. A **32**, 2784 (1985)
22. D.G. Steel, J.T. Remillard: Phys. Rev. A **36**, 4330 (1987)
23. I.D. Abella, N.A. Kurnit, S.R. Hartmann: Phys. Rev. **141**, 391 (1965); see also T. Yajima, Y. Taira: J. Phys. Soc. Japan **47**, 1620 (1979)
24. H. Wang, M. Jiang, D.G. Steel: Phys. Rev. Lett. **65**, 1255 (1990)
25. J. Hegarty, K. Tai, W.T. Tsang: Phys. Rev. B **38**, 7843 (1988)
26. T. Takagahara: Private communication
27. M.D. Webb, S.T. Cundiff, D.G. Steel: Phys. Rev. Lett. **66**, 934 (1991)
28. M.D. Webb, S.T. Cundiff, D.G. Steel: Phys. Rev. B **43**, 12658 (1991)
29. H. Wang, J.T. Remillard, M.D. Webb, D.G. Steel, J. Pamulapati, J. Oh, P.K. Bhattacharya: Surf. Sci. **228**, 69 (1990)
30. D.J. Thouless: Phys. Rev. Lett. **39**, 1167 (1977)

Spin-Flip-Induced Hole Burning in GaAs Quantum Wells: Determination of the Exciton Zeeman Splitting

H. Wang, M. Jiang, R. Merlin, and D. G. Steel

Harrison M. Randall Laboratory of Physics, The University of Michigan, Ann Arbor, Michigan 48109-1120

(Received 18 February 1992)

A new method of four-wave-mixing spectroscopy in GaAs quantum wells reveals spectral hole burning due to spin relaxation of magnetoexcitons. The measurements resolve the Zeeman doublet of the lowest-energy heavy-hole exciton where the doublet splitting is much less than the exciton inhomogeneous width. The Zeeman splitting depends nonlinearly on the magnetic field and is small compared with that of bulk GaAs. The results reflect effects of the complex band structure of quantum wells. Information on exciton spin relaxation is also provided by the hole-burning measurements.

PACS numbers: 71.35.+z, 71.70.Ej, 73.20.Dx, 78.65.Fa

The electronic energy spectrum of quantum well structures is fully quantized under a magnetic field parallel to the growth axis. Optical absorption reveals a ladder of magnetoexcitons corresponding to transitions between electron and hole Landau levels [1]. Magnetic fields also lift the Kramers degeneracy with the resultant Zeeman splitting depending on details of the band structure. The removal of this degeneracy is also expected to lead to a substantial increase of the spin relaxation time between Zeeman-split Landau levels since now spin relaxation can only take place via inelastic processes.

The electron g factor in GaAs heterostructures has been extensively studied. Earlier magnetotransport measurements have shown large exchange-induced enhancement of the electron g [2]. Recent electron-spin-resonance studies have revealed the magnetic field dependence of the electron g for different Landau levels [3]. These results were explained in terms of the nonparabolicity of the conduction band [4]. Determination of the exciton Zeeman splitting has proven to be more elusive [5–7]. Earlier magnetoreflectance measurements were able to resolve Zeeman splittings for the light-hole but not the heavy-hole exciton [5]. More recent measurements have inferred the exciton g from nonlinear quantum-beat spectroscopy [6]. A precise determination of the exciton Zeeman splitting in a quantum well using linear optical spectroscopy is difficult since interface disorder leads to exciton localization and subsequent inhomogeneous broadening of the absorption profile [8]; the resultant inhomogeneous broadening varies from 1 meV to several meV, much larger than the splitting in moderate fields.

A related area is relaxation of carrier and exciton spins in semiconductor heterostructures. Polarization-dependent measurements of interband optical transitions have shown an interesting dependence of spin relaxation on growth conditions, carrier confinement, and temperature [9]. Various physical mechanisms for spin relaxation have also been discussed [9,10]. In addition, luminescence measurements at high magnetic fields have revealed a much larger spin relaxation time due to the full quantization of the energy spectrum [11].

In this paper, we report frequency-domain nonlinear optical studies of exciton Zeeman splitting and spin relaxation in GaAs quantum wells. Using selective optical excitation and nonlinear optical methods similar to spectral hole burning (SHB, also referred to as saturation spectroscopy or differential transmission), we are able to probe spin relaxation of magnetoexcitons and measure directly their Zeeman splitting. The measurements reveal a heavy-hole splitting much smaller than that reported for bulk GaAs at low magnetic field and show a nonlinear dependence of the splitting on magnetic field strength. The results reflect effects of the complex band structure of a quantum well.

Nonlinear optical methods such as SHB have the advantage of being able to eliminate inhomogeneous broadening and accurately measure small energy separations as shown in precision measurements in atomic vapors [12]. For GaAs/AlGaAs quantum wells, a nearly monochromatic optical beam with $\sigma-$ circular polarization can be used to excite a narrow spectral hole (say at energy E_- within the inhomogeneous absorption profile) of the lowest heavy-hole (HH1) exciton associated with the $\frac{1}{2}$ to $\frac{1}{2}$ transition (see the inset in Fig. 1 for the energy-level diagram in a magnetic field). The width of the spectral hole is determined by the homogeneous linewidth. Spin flips of electrons and holes associated with these excitons generate a spectral hole at the energy of the $-\frac{1}{2}$ to $-\frac{1}{2}$ exciton transition, designated E_+. The *spin-flip-induced* SHB at E_+ results from the reduced absorption due to the presence of carriers that have flipped their spins from E_-. This SHB can be probed using an optical beam with σ_+ circular polarization. Zeeman splitting can then be obtained by measuring the energy spacing between the spin-flip-induced SHB and the original SHB resonance.

In practice the measurements proposed above are complicated by strong spectral diffusion of the localized excitons. Once created, localized excitons migrate rapidly among localization sites with different energies leading to *a broad quasiequilibrium distribution in energy* as we demonstrated earlier using four-wave mixing [13]. In the normal SHB measurement discussed above, the nonlinear

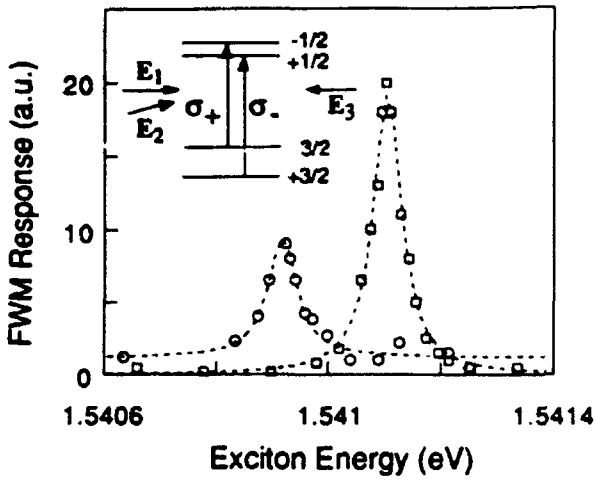

FIG. 1. Hole-burning FWM responses at 4 T. All three beams are circularly polarized with E_1 and E_2 exciting the $\sigma-$ exciton. Squares represent the response when the probe beam E_3 interacts with the $\sigma-$ exciton. Circles represent the response when E_3 interacts with the $\sigma+$ exciton. Dashed lines are Lorentzian fits to the response. Inset: Conduction-band and heavy-hole valence-band energy levels in a GaAs quantum well for a magnetic field parallel to the growth axis.

optical signal may be dominated by this distribution. In the limit that the spin relaxation time is long compared with the spectral diffusion time, nearly all spin-flipped excitons have diffused in energy. Hence, the spin-flip-induced SHB resonance will be overwhelmed by the spectral diffusion process.

To avoid the above complications, we have used a new method of SHB based on nearly degenerate four-wave mixing (FWM) [14,15]. This method can significantly reduce the contribution of the quasiequilibrium exciton distribution to the nonlinear optical response and, hence, allows us to recover the spin-flip-induced SHB resonance. The experimental configuration is based on backward FWM and uses three optical beams. Two nearly degenerate beams designated $E_1(\omega_1,\mathbf{k}_1)$ and $E_2(\omega_2,\mathbf{k}_2)$ interact in the sample with a third probing beam designated $E_3(\omega_3,\mathbf{k}_3)$. The SHB response is obtained by measuring the backward FWM signal (propagating in a direction determined by $\mathbf{k}_1-\mathbf{k}_2+\mathbf{k}_3$) as a function of ω_3. Detailed analytical discussions of frequency-domain FWM spectroscopy have been presented elsewhere [14,15]; however, the underlying physics can be understood as follows: Nearly degenerate beams E_1 and E_2 interfere in the sample to excite a traveling-wave grating which oscillates at a frequency equal to the detuning between the two beams $\delta=|\omega_1-\omega_2|$ ($\ll$homogeneous linewidth). The grating is a spatially modulated pattern of spectral hole burning at ω_1 ($\approx\omega_2$) with amplitude proportional to $(\delta+i\gamma)^{-1}$, where γ is the grating decay rate determined by relaxation and spatial transport of excitons. Measuring the FWM signal as a function of ω_3 probes the spectral profile of the grating within the inhomogeneous profile. In the absence of spectral diffusion, the *spectral* width of the grating is given by the exciton homogeneous linewidth as expected from SHB, and the width of the FWM response is twice the homogeneous linewidth [15]. Note that although both FWM and the traditional SHB (i.e., differential transmission) signals result from the induced nonlinear optical polarization, the FWM signal includes contributions from both the real and the imaginary part of the nonlinear susceptibility while the traditional SHB measures only the imaginary part [12].

In the presence of spectral diffusion, the spectral hole excited by $E_1\cdot E_2^*$ diffuses in energy resulting in a spectral redistribution of the excitation. In this case, the FWM response arises from both the spectral hole and the quasiequilibrium distribution of the exciton population as discussed above. The decay of the SHB population is determined by the sum of the exciton spectral diffusion, spin relaxation, and recombination rates. However, the lifetime of the quasiequilibrium distribution is determined by the *recombination time of the exciton* [13]. In the limit that the spectral diffusion rate is much larger than the rate for exciton recombination, setting δ large compared with the recombination rate (but still smaller than or comparable with the spectral diffusion rate) significantly decreases the relative amplitude of the grating associated with the quasiequilibrium distribution. Hence, the FWM response will be dominated by the SHB resonance [14].

The quantum well samples used in our measurements consist of ten periods of 100-Å GaAs wells and 100-Å $Al_{0.3}Ga_{0.7}As$ barriers, grown at 750°C by molecular-beam epitaxy on semi-insulating (100) GaAs substrates using interrupted growth. The structures show a 1-meV absorption linewidth with a Stokes shift of the luminescence of order 0.3 meV for the HH1 exciton. The nonlinear measurements were carried out at 2.5 K using a split-coil superconducting magnet. δ was set at 140 MHz using two acousto-optic modulators. The exciton density was of order $10^7/cm^2$.

In the first set of measurements, we used three circularly polarized optical beams rotating in the same direction in the laboratory frame. The nonlinear optical response, shown as squares in Fig. 1, involves only the $\sigma-$ excitons associated with the $\frac{3}{2}$ to $\frac{1}{2}$ transition. The width of the response corresponds to a homogeneous linewidth of 0.03 meV. The small linewidth confirms the localized and inhomogeneous broadening nature of the magnetoexciton [8,13].

As discussed earlier, if electrons or holes associated with $\sigma-$ excitons created with $E_1\cdot E_2^*$ flip their spin at the same localization site, it will produce SHB at the energy of the $\sigma+$ exciton. Experimentally, spin-flip-induced SHB can be probed by reversing the polarization direction of E_3. The resulting resonance, shown as circles in Fig. 1, clearly shows narrow SHB at a lower energy with

the energy difference being the exciton Zeeman splitting: 0.19 meV at 4 T. The small signal at the original SHB position is most likely due to the residual ellipticity of the circularly polarized beams. The nearly constant background signal in the inset in Fig. 1 is due to excitons that have spectrally diffused. Nonlinear signals due to the spectrally diffused excitons overwhelm the spin-flip-induced SHB when $\delta=0$. Note that spin relaxation of σ_+ excitons requires absorption of acoustic phonons and is slower than spin relaxation of σ_- excitons. The observed spin-flip-induced SHB is considerably weaker at 4 T when $\mathbf{E}_1\cdot\mathbf{E}_2^*$ excites σ_+ excitons.

In further experiments, we used linearly polarized light for the third beam. With $\mathbf{E}_1\cdot\mathbf{E}_2^*$ exciting only the σ_- excitons, we can simultaneously probe the SHB and the spin-flip-induced SHB resonance. The FWM response (Fig. 2) shows the well-resolved Zeeman doublet. Because of possible interference between the two resonances, the Zeeman splitting determined from Fig. 2 is less accurate than that from Fig. 1.

Recent measurements have shown that at low and intermediate magnetic field, the electron g factor at the lowest Landau level in GaAs quantum wells is close to the value for bulk GaAs [3,16]. In contrast, the Zeeman splitting of the HH1 exciton obtained above is very small in comparison with that reported for bulk GaAs [17]. Our results seem to be in agreement with the earlier magnetoreflectance measurements where the heavy-hole Zeeman doublet was not resolved. The small Zeeman splitting attributed to the strong valence-band mixing in quantum well structures has been recently predicted by numerical calculations of magnetoexcitons using the Luttinger Hamiltonian [18]. In particular, the mixing of σ_- excitons with excitons at higher energy pushes the σ_- exciton to lower energy. The above calculation also predicts an eventual sign change of the Zeeman splitting at higher magnetic fields where the band-mixing effects overcome those of the Zeeman interaction. However, theoretical determination of the magnetic field at which the zero crossing occurs is difficult since the cancellation of the two competing contributions depends strongly on parameters of the model [18]. The sign change of the splitting has not been observed in our measurements up to 6 T. It is interesting to note that disorder-induced localization is expected to enhance the band-mixing effects if the localization scale is smaller than the exciton Bohr radius. Using the recombination rate of the localized exciton, we have estimated the localization scale to be comparable to the exciton Bohr radius.

Figure 3 displays the magnetic field dependence of the Zeeman splitting for the HH1 exciton. The dashed line in the figure represents a quadratic dependence. Clearly the quadratic behavior may not extend into the high-field region. The observed field dependence is somewhat surprising since the calculations predict a field dependence slower than linear. The observed dependence may be due in part to the nonparabolicity of the conduction band [4], which was not included in the calculations. Note that our results differ considerably from those obtained from nonlinear quantum beats in a 30-Å stepwise GaAs quantum well [6]. Zeeman splittings reported in the quantum-beat measurement (0.5 meV at 4 T) are proportional to magnetic fields with a field strength ranging from 1 to 5 T, and are very close to those measured for impurity-bound excitons in bulk GaAs [19]. The sign of the Zeeman splitting cannot be determined in quantum-beat measurements.

The relative amplitude of the two SHB resonances shown in Fig. 2 is determined by the spin relaxation rates as well as the spectral diffusion rate of the exciton (assuming equal oscillator strengths). As expected, exciton spin relaxation rates decrease with increasing magnetic fields, resulting in a decrease in the relative peak height of the spin-flip-induced SHB. The ratio of σ_+ to σ_- exciton SHB amplitudes decreases approximately by a factor of 4 when the field increases from 2 to 6 T. Using a simple rate equation and a lifetime of 50 ps for the σ_+ exciton SHB (determined independently [20]), we are able to estimate an effective spin relaxation rate of 100 ps for the σ_- exciton at 4 T. The estimated spin relaxation

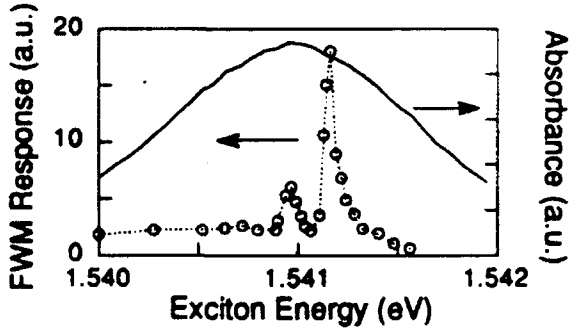

FIG. 2. FWM hole-burning response at 4 T with E_3 linearly polarized. E_1 and E_2 interact only with the σ_- exciton. The line shape shows the well-resolved Zeeman doublet. The solid line is the exciton absorption spectrum. The dotted line is a guide to the eye.

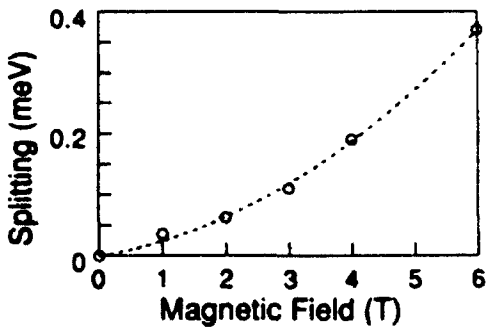

FIG. 3. Magnetic field dependence of the exciton Zeeman splitting. The dashed line is a least-squares fit with a quadratic dependence.

rate is smaller than the spectral diffusion rate, but is much larger than the rate for exciton recombination. Hence, most of the spectrally diffused $\sigma-$ excitons changed their spins before recombination, which explains the negligible nonlinear optical response from the spectrally diffused $\sigma-$ excitons in Fig. 1.

Finally, we note that although spin relaxation of magnetoexcitons in a quantum well is presumably an inelastic process, the relaxation may also proceed via an elastic process due to disorder-induced localization. A localized magnetoexciton with a specific spin orientation may have the same energy as magnetoexcitons at another localization site with different spin orientation. Strong resonant excitation transfer may occur between the two sites. The resonant transfer should depend strongly on the intersite distance as well as on the Zeeman splitting, providing a good probe for the interface disorder. In the SHB measurement, the resonant intersite transfer is characterized by a spin-flip-induced SHB resonance at the energy of the nearly degenerate E_1 and E_2 beams. However, conclusive evidence for the transfer has not been observed in samples used in our measurements.

This work was supported by the Army Research Office and the Air Force Office of Scientific Research.

[1] M. Shinada and K. Tanaka, J. Phys. Soc. Jpn. 29, 1258 (1970).

[2] See, for example, Th. Englert and K. von Klitzing, Surf. Sci. 73, 70 (1978); T. Ando and Y. Uemura, J. Phys. Soc. Jpn. 37, 1044 (1974).

[3] D. Stein, K. von Klitzing, and G. Weimann, Phys. Rev. Lett. 51, 130 (1983); M. Dobers, K. von Klitzing, and G. Weimann, Phys. Rev. B 38, 5453 (1988).

[4] G. Lommer, F. Malcher, and U. Rossler, Phys. Rev. B 32, 6965 (1985).

[5] P. Lefebvre, B. Gil, J. P. Lascaray, H. Mathieu, D. Bimberg, T. Fukunaga, and H. Nakashima, Phys. Rev. B 37, 4171 (1988).

[6] S. Bar-Ad and I. Bar-Joseph, Phys. Rev. Lett. 66, 2491 (1991).

[7] M. J. Snelling, E. Blackwood, C. J. McDonagh, R. T. Harley, and C. T. B. Foxon, Phys. Rev. B 45, 3922 (1992).

[8] J. Hegarty and M. D. Sturge, J. Opt. Soc. Am. B 2, 1143 (1985).

[9] M. Kohl, M. R. Freeman, D. D. Awschalom, and J. M. Hong, Phys. Rev. B 44, 5923 (1991); T. C. Damen, Luis Vina, J. E. Cunningham, Jagdeep Shah, and L. J. Sham, Phys. Rev. Lett. 67, 3432 (1991); T. C. Damen, Karl Leo, Jagdeep Shah, and J. E. Cunningham, Appl. Phys. Lett. 58, 1902 (1991).

[10] T. Uenoyama and L. J. Sham, Phys. Rev. Lett. 64, 3070 (1990); R. Ferreira and G. Bastard, Phys. Rev. B 43, 9687 (1991).

[11] M. Potemski, J. C. Maan, A. Fasolino, K. Ploog, and G. Weimann, Phys. Rev. Lett. 63, 2409 (1989).

[12] See, for example, Marc D. Levenson and Satoru S. Kano, *Introduction to Nonlinear Laser Spectroscopy* (Academic, Boston, 1988); S. Stenholm, *Foundations of Laser Spectroscopy* (Wiley, New York, 1984).

[13] H. Wang, M. Jiang, and D. G. Steel, Phys. Rev. Lett. 65, 1255 (1990).

[14] Hailin Wang and Duncan G. Steel, Appl. Phys. A 53, 514 (1991).

[15] D. G. Steel and J. T. Remillard, Phys. Rev. A 36, 4330 (1987); Hailin Wang and Duncan G. Steel, Phys. Rev. A 43, 3823 (1991).

[16] M. J. Snelling, G. P. Flinn, A. S. Plaut, R. T. Harley, A. C. Tropper, R. Eccleston, and C. C. Phillips, Phys. Rev. B 44, 11345 (1991).

[17] See, for example, D. Bimberg, Adv. Solid State Phys. 18, 195 (1977).

[18] G. E. W. Bauer, in *High Magnetic Fields in Semiconductor Physics II*, edited by G. Landwehr (Springer-Verlag, Berlin, 1989); G. E. W. Bauer and T. Ando, Phys. Rev. B 37, 3130 (1988).

[19] A. M. White, I. Hinchliffe, and P. J. Dean, Solid State Commun. 10, 497 (1972).

[20] Obtained by measuring the FWM signal as a function of the detuning between the two excitation beams. See also Ref. [13].

Nonlinear optical absorption and dynamics in quantum wells

Min Jiang, Hailin Wang, and Duncan G. Steel
Harrison M. Randall Laboratory of Physics, The University of Michigan, Ann Arbor, Michigan 48109-1120

(Received 24 April 1992; accepted for publication 6 July 1992)

We present measurements of differential transmission and four-wave mixing in GaAs quantum well structures at 1.8 K near the inhomogeneously broadened lowest heavy-hole ($hh1$) exciton resonance using narrow band cw excitation. The data show an *increase* in absorption and an excitation lifetime of order 1–10 μs outside the spectral hole produced by the pump. The long lifetime and the experimentally determined absence of excitation spatial diffusion in this region suggests that optical absorption produces electron-hole pairs that are correlated but separately localized due to disorder. A phenomenological model is proposed to explain the nonlinear response based on two-photon absorption.

The optical properties immediately below the band edge of direct band-gap semiconductors are dominated by excitonic effects. In a quantum well (QW), the strong transient nonlinear optical response associated with the exciton resonance has been shown by numerous theoretical and experimental studies to be due to many-body effects including phase space filling, exchange effects and to a lesser degree, screening.[1] However, the nonlinear response and exciton dynamics are greatly complicated and qualitatively changed by the presence of interface disorder in QW structures.[2] Early measurements suggested large atomically flat areas at the interface.[3] More recent measurements show the presence of monolayer flat island formation on a scale of 50 Å,[4] leading to the proposal that there is a bimodal distribution for island size.[5] At low temperature, excitons can be localized by the interface disorder which leads to strong inhomogeneous broadening of the optical absorption spectrum. Localized excitons, however, can migrate between localization sites by emitting and absorbing acoustic phonons.[6,7]

To improve the understanding of the intrinsic nonlinear optical response and the effects of disorder in GaAs quantum well structures, we present what we believe are the first measurements of the *cw nonlinear response* near the lowest heavy-hole ($hh1$) exciton at low temperature (1.8–5 K) where the effects of disorder is a dominating factor. The experiments are based on *nondegenerate* differential transmission (DT) and four-wave mixing (FWM). Nondegenerate DT measures the sign and magnitude of the imaginary part of the third-order susceptibility while nondegenerate FWM measures the magnitude (squared) of the third-order susceptibility and is useful for determining various relaxation rates.[8,9] While the results of many-body theory[1] have been highly successful in accounting for the nonlinear response observed using short pulse excitation at high excitation density ($>10^9$ excitons/cm^2/layer),[10] we show in this letter that the present understanding cannot account for the experimental results observed at low excitation density under cw excitation. We believe the discrepancy is due to the presence of disorder and propose a possible phenomenological model to explain the data.

The data reported in this letter are obtained in QW structures consisting of 65 periods of 96 Å GaAs wells and 98 Å $Al_{0.3}Ga_{0.7}As$ barriers, grown at 630 °C by molecular beam epitaxy on semi-insulating (100) GaAs substrates with interrupted growth. The $hh1$ exciton absorption linewidth is 2.3 meV [Fig. 1(a)] with a Stokes shift of 1 meV between the $hh1$ exciton absorption and emission. Similar experiment results have also been obtained on several $GaAs/Al_{0.3}Ga_{0.7}As$ samples differing in the number of layers and where the absorption line widths varied from 1.0 to 2.5 meV with a corresponding Stokes shift varying from <0.2 to 1.5 meV. Samples are mounted on a sapphire disk (c-axis normal) with the substrate removed and placed in a liquid helium immersion cryostat.

Measurements are performed using two frequency stabilized cw dye layers. For DT measurements, one laser supplies a pump beam at a fixed frequency Ω_1 while the second laser supplies a probe beam at Ω_2. Both beams are linearly and orthogonally polarized to avoid coherent effects. The nonlinear spectral response proportional to $\mathrm{Im}\chi^{(3)}$ is obtained by measuring the probe transmission as a function of Ω_2 where $\chi^{(3)}$ is the third-order susceptibility. For nondegenerate backward FWM, two nearly degenerate co-polarized beams $\mathbf{E}_1(\mathbf{k}_1,\Omega_1)$ and $\mathbf{E}_1'(\mathbf{k}_1',\Omega_1+\delta)$ with $\delta \ll \Omega_1$ intersect in the sample with a small angle θ between the beams producing a traveling-wave modulation of the absorption and dispersion with a period $\Lambda=\lambda/(2\sin\theta/2)$. The grating is probed by an orthogonally polarized beam $E_2(\mathbf{k}_2,\Omega_2)$ where $\mathbf{k}_2=-\mathbf{k}_1$ producing a coherent signal, proportional to $|\chi^{(3)}|^2$, propagating in the direction $-\mathbf{k}_1'$. Tuning Ω_2 again measures the spectral response.[9] Tuning δ provides information on the excitation decay dynamics probed at Ω_2.[9] This decay rate depends on γ, Γ_{sd}, and Γ_d where γ is the recombination rate, Γ_{sd} is the spectral diffusion rate and $\Gamma_d=4\pi^2D/\Lambda^2$ is the rate due to spatial diffusion where D is the diffusion coefficient.

Figure 1 shows a comparison between the FWM spectrum [Fig. 1(b)] and the DT spectrum [Fig. 1(c)] obtained by tuning Ω_2 [Fig. 1(b) is similar to that reported earlier[7,11]]. Ω_1 is given by the arrow in the $hh1$ linear absorption feature shown in Fig. 1(a). The sharp resonance at $\Omega_2=\Omega_1$ in Fig. 1(b) is the result of spectral hole burning of the inhomogeneously broadened localized excitons. The width of the hole is twice the homogeneous width.[8,9] The comparable DT spectrum [Fig. 1(c)], obtained at the same

 0003-6951/92/361301-03$03.00

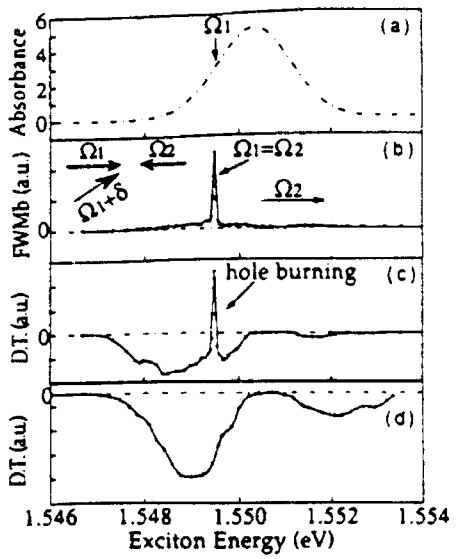

FIG. 1. A comparison of the cw four-wave mixing and differential transmission spectra. (a) The *hh*1 linear absorption spectrum. The arrow shows the location of Ω_1 for (b) and (c). (b) The four-wave mixing spectrum obtained by tuning Ω_2. (c) The corresponding differential transmission spectrum. (d) The differential transmission spectrum obtained when Ω_1 is set to 1.2 eV above the *hh*1 absorption peak

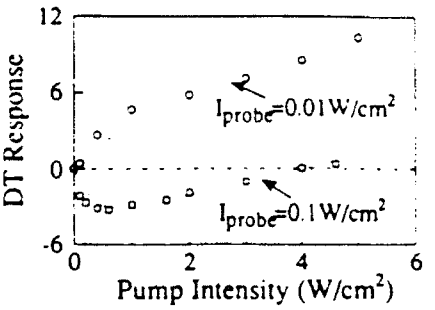

FIG. 2. The intensity dependence of DT spectra as a function of pump intensity for two different probe intensities. Measurements are made for the case of Fig. 1(c) where Ω_1 is set 1.1 meV below Ω_1. The dotted curves show the fitting based on a two component model: an incoherent two photon stepwise excitation dominates at high probe intensity (square) and a single saturation type nonlinear response dominates at low probe intensity (circle) characterized by a smaller saturation intensity than that of a two photon-type nonlinear response.

excitation intensity ($\sim$0.5 W/cm^2), shows the sharp resonance again corresponding to the spectral hole seen in Fig. 1(b). As expected from phase space filling effects, a decrease in absorption is observed in the spectral hole (a positive signal corresponds to a *decrease* in absorption). However, away from the spectral hole, the DT measurement shows an unexpected *increase in absorption*. It is easy to see that the DT response ($\propto \mathrm{Im}\chi^{(3)}$) away from the spectral hole is much larger than expected based on FWM ($\propto |\chi^{(3)}|^2$). Figure 1(d) shows the DT spectrum obtained when the pump frequency Ω_1 is tuned to 1.2 meV above the *hh*1 absorption line center where no spectral hole is expected or observed.[12] This spectrum [Fig. 1(d)] demonstrates that the increase in absorption around *hh*1 is *not related to the spectral hole*. A similar DT spectrum is observed when Ω_1 is tuned above the band edge where free carriers are directly excited. In contrast no signal is obtained when Ω_1 is tuned well below the *hh*1 resonance.

Measurements of the intensity dependence of the FWM signal show that the spectral hole amplitude depends linearly on each of the intensities of the three input beams, indicating that there is minimal contribution from higher order terms in the susceptibility. In the usual approach of estimating the exciton density based on a radiative lifetime of order 1 ns and the input intensity, the exciton density is of order 10^7–10^8 excitons/cm^2/layer. However, even at this low excitation level, the DT signal in Fig. 1(d) is not linear in the pump intensity. In fact, the response also *depends on the probe intensity*. Figure 2 shows the unusual intensity dependence of the DT response as a function of pump intensity for two different probe intensities. Measurements are made for the case of Fig. 1(c) where Ω_2 is set 1.1 meV below Ω_1.

We further characterize the nonlinear response by measuring the relaxation time in the region showing increased absorption. Independent measurements using amplitude modulation DT spectroscopy[13] and FWM by tuning δ[7] show a decay time of order 1–10 μs in contrast to the 0.5–1 ns excitonic recombination rate obtained in this sample by time-resolved luminescence and FWM at the hole burning resonance. While the slow time scale suggests that the nonlinear response could arise due to photorefractive or thermal effects, the first possibility is eliminated since we have determined that there is no energy transfer between beams as would be expected in the presence of two beam coupling. Thermal effects are also eliminated for two reasons: (1) The DT signal strength does not decrease when the sample is immersed in liquid helium as would be expected since in liquid helium, the induced temperature gradient is dramatically reduced; (2) more importantly, the absence of any dependence of the grating decay on the grating spacing sets the upper limit of the diffusion coefficient at 3×10^{-4} cm^2/s. If the nonlinear response were due to thermal effects, then this measurement would correspond to a thermal conductivity at least 4 orders or magnitude below that of GaAs. Hence, we conclude the excitation is electronic in nature and note that the long lifetime results in an estimated excitation density four orders of magnitude higher than that expected based on a 0.5–1.0 ns exciton lifetime.

In discussing these results we first note that many-body effects such as exciton-exciton interactions, band-gap renormalization, and screening can produce a shift or a broadening of the resonance, leading to regions of increased absorption. However, these features resemble the first or second derivative of the resonance, clearly not in agreement with the measurement. Hence, while the current theory has been highly successful in interpreting experimental results obtained on short time scales at high excitation density,[1,10] the results show that the theory does not describe the leading terms in the low intensity cw nonlinear response measured by differential transmission. We would like to stress that identical behavior has been observed in the three different samples we investigated. Earlier experimental evidence for this effect was reported in transient

DT measurements using picosecond lasers.[2] At zero time delay, the low-temperature excitonic response showed a decrease in absorption due to bleaching, yet on longer time scales (~100 ps), the DT signal changed sign, showing an increase in absorption.

The nonlinear response outside the spectral hole can be qualitatively explained by a phenomenological model involving an incoherent two photon stepwise excitation along with an ordinary saturating type nonlinear response (not associated with the spectral hole). In a rate equation description for this system [i.e., a simple two level system (2LS) and an independent three level system (3LS)], a probe dependent DT response similar to the data is obtained as shown by the dotted lines in Fig. 2. In this model, the transition rates for both transitions in the 3LS are comparable. When the pump beam is resonant with the transition from level 1 to level 2 and the probe beam is resonant with the transition from level 2 to level 3, the DT signal due to the 3LS would show an increase in absorption if the beam intensities are reasonably low. However, if the 2LS saturation intensity is smaller than saturation intensities for the 3LS, at very low intensities, the DT signal is dominated by the 2LS. Hence, decreased absorption is observed as shown in Fig. 2. As the probe intensity increases, the relative importance of the 3LS will increase due to the small saturation intensity for the 2LS, resulting in increased absorption in the DT response. Finally, when the pump beam intensity is very high such that both transitions in the 3LS are saturated, the stepwise two-photon transition will be overwhelmed by the saturation effect and an overall decrease in absorption will be observed as shown in Fig. 2.

The relaxation measurements also provide some additional insight into the microscopic origin of the observed nonlinear response in the QW. In particular, even though the nonlinear response is clearly associated with the *hh*1 exciton, the long lifetime of the excitation is not consistent with the presence of ordinary excitons, nor is the negligibly small diffusion coefficient. To explain these effects, we propose that in the presence of disorder, optical excitation produces electron-hole pairs which are localized in separate but closely correlated positions. If we assume that the electron and hole wave functions are localized on a scale length of order 100 Å and then also assume the lifetime is simply related to the wave function overlap, we can estimate that the separation distance is of order 200 Å. Furthermore, using the excitation intensity at the minimum value of the lower DT curve (saturation point of the DT spectrum), we can estimate the resulting *e-h* density to be of order 6×10^{11} *e-h*/cm^2/layer (using 0.5 W/cm^2, taking 50% of the energy distributed over the first 10 layers, and an effective excitation lifetime of 5 μs. This would correspond to an average distance between *e-h* pairs on the order of 140 Å, the same order of magnitude as the *e-h* separation estimated based on the *e-h* pair lifetime. This number could be interpreted as the average distance between *localization* sites. While it is difficult to relate this to interface morphology, it is comparable to that reported by chemical mapping.[4] The stepwise two photon transition discussed in the above 3LS model may correspond to excitations of two closely correlated *e-h* pairs. The unexpected low saturation intensities for the 3LS and 2LS are due to the long lifetime of these systems and the finite number of localization sites (recall that the saturation intensity is $\simeq\hbar\omega N_T/\alpha_0\tau$ where α_0 is the absorption coefficient and N_T is the density of the localization sites).

Our model also provides an explanation for the discrepancy between the FWM and the DT spectra. As is well known, the FWM signal strength is proportional to the contrast ratio of the excitation grating produced by $\mathbf{E}_1^*\cdot\mathbf{E}_2'$. The contrast ratio is reduced if the input beams saturate the system. At the beam intensities used in the measurement ($I_1, I_1' \sim 0.5$ W/cm^2, $I_2 \sim 0.1$ W/cm^2), the density of excitation (associated with spectral hole) is well below the saturation level, however the excitation in the increased absorption region is partially saturated, causing a grating flattening and resulting in a reduced FWM response.

In summary, we have shown that the low intensity nonlinear optical response in GaAs multiple QW is greatly affected by the presence of disorder. The measurements show that the existing theoretical work is inadequate to explain the low intensity nonlinear response in these systems. Finally, the long life time may need to be taken into account in potential device applications.

This work was supported by the Air Force Office of Scientific Research. The authors wish to acknowledge their appreciation to Professor P. K. Bhattacharya for supplying samples.

[1] See, for example, S. Schmitt-Rink, D. S. Chemla, and D. A. B. Miller, Adv. Phys. **38**, 89 (1989).
[2] J. Hegarty and M. D. Sturge, J. Opt. Soc. Am. B **2**, 1143 (1985).
[3] C. Weisbuch, R. Dingle, A. A. Gossard, and W. Wiegmann, Solid State Commun. **38**, 709 (1981).
[4] See, for example, A. Ourmazd, D. W. Taylor, J. Cunningham, and C. W. Tu, Phys. Rev. Lett. **62**, 933 (1989).
[5] C. A. Warwick, W. Y. Jan, A. Ourmazd, and T. D. Harris, Appl. Phys. Lett. **56**, 2666 (1990); D. Gammon, B. V. Shanabrook, and D. S. Katzer, Phys. Rev. Lett. **67**, 1547 (1991).
[6] T. Takagahara, J. Lumin. **44**, 347 (1989).
[7] H. Wang, M. Jiang, and D. G. Steel, Phys. Rev. Lett. **65**, 1255 (1990).
[8] D. G. Steel and J. T. Remillard, Phys. Rev. A **36**, 4330 (1987).
[9] H. Wang and D. G. Steel, Phys. Rev. A **43**, 3823 (1991).
[10] D. A. B. Miller, D. S. Chemla, D. J. Eilenberger, P. W. Smith, A. C. Gossard, and W. T. Tsang, Appl. Phys. Lett. **41**, 679 (1982); W. H. Knox, R. L. Fork, M. C. Downer, D. A. B. Miller, D. S. Chemla, C. V. Shank, A. C. Gossard, and W. Wiegmann, Phys. Rev. Lett. **54**, 1306 (1985); N. Peyghambarian, H. M. Gibbs, J. L. Jewell, A. Antonetti, A. Migus, D. Hulin, and A. Mysyrowicz, Phys. Rev. Lett. **53**, 2433 (1984). See also papers cited in Ref. 1.
[11] The scan in Fig. 1(b) covers a larger spectral region than the data in Ref. 7. However, additional structure is seen at energies away from the spectral hole in Fig. 1(b) compared to Ref. 7 because the value of δ was set to in these data to enable the detection of slower components. In Ref. 7, δ was set to 100 kHz to ensure that only the simple excitonic component was detected.
[12] H. Wang and D. G. Steel, Appl. Phys. A **53**, 514 (1991).
[13] In these measurements, the amplitude or phase shift on the lock-in amplifier is measured as a function of the modulation frequency and can then be easily related to the relaxation time.

Amplitude-squeezed light from quantum-well lasers

M. J. Freeman, H. Wang, and D. G. Steel

Randall Laboratory of Physics, The University of Michigan, Ann Arbor, Michigan 48109

R. Craig and D. R. Scifres

Spectra Diode Laboratories, San Jose, California 95134

Received October 7, 1992

High-impedance pump noise suppression was used to generate amplitude squeezing in an index-guided quantum-well laser. Light exhibiting photon-number noise 1.4 dB below the shot-noise limit was observed, and the corresponding polarization properties were examined. Close-coupled laser-detector measurements made with an unsaturated detector revealed 2.9 dB of squeezing.

Amplitude-squeezed light, which is characterized by photon-number noise below the shot-noise limit (SNL), is of fundamental interest in optical physics and is potentially useful for precision measurements[1] and optical communication.[2] Although it has been known that the photon-number fluctuations of an ideal laser operating far above threshold stem from pump noise and vacuum field fluctuations,[3] it has been appreciated only recently that the laser does not necessarily feature the full shot noise.[4-6] By eliminating pump noise, the output of the laser can, in principle, have an arbitrary amount of amplitude squeezing within the cavity bandwidth.[4,5] Several methods for suppressing pump noise, and thus attaining this type of amplitude squeezing, have been proposed.[4-6] Of these, constant-current operation of a semiconductor diode laser is of particular interest because electrical current pump noise can be easily suppressed to >15 dB below the SNL[7] and because the high quantum efficiency of the diode laser allows the sub-Poissonian electron pump statistics to be transferred to photon statistics.[5] To date, the largest level of amplitude squeezing has been achieved in transverse junction stripe semiconductor lasers. Measurements that close coupled a transverse junction stripe laser to a detector demonstrated a photocurrent fluctuation 8.3 dB below the SNL.[8] With balanced detection, photocurrent fluctuations 1.3 dB below the SNL were obtained.[9]

We report measurements of photon-number fluctuations in an index-guided quantum-well laser. The laser (Spectra Diode Laboratories SDL-5410-C) differs considerably from the transverse junction design used nearly exclusively in earlier research.[7-9] In a collimated geometry, it exhibited photon-number fluctuations 1.4 dB below the SNL when driven by a constant current. The balanced detection scheme used in these measurements also allowed the polarization fluctuations of the laser to be investigated, whereas close coupling the laser to a detector improved the amplitude squeezing to 2.9 dB.

For the first set of experiments, the laser and a collimating lens are placed inside a cryostat, along with a drive circuit consisting of a series resistor ($R = 680\ \Omega$) and a bypass capacitor ($C = 0.1\ \mu F$). The noise properties of the output are measured by balanced detection with a delay line.[9] Equal division of the laser power is obtained with a half-wave plate and a polarization beam splitter (PBS). The resulting two beams are then focused onto Hamamatsu (Model S1722-01) p-i-n photodiodes (quantum efficiency 85%). The ac photocurrents are amplified, one is delayed, and then their difference is obtained with a 180° hybrid junction. This setup yields a common mode suppression >25 dB from 10 to 200 MHz. The delay line allows the sum ($I_1 + I_2$) current, which reflects the laser noise level, and difference ($I_1 - I_2$) current, which gives the shot-noise level, to be simultaneously monitored on a spectrum analyzer.[9,10] The signal alternates between the two as a function of frequency owing to the frequency-dependent phase shift introduced by the delay line.

A typical run exhibiting 1.4 dB of squeezing is shown in Fig. 1 (trace c) for a bias level $I/I_{th} = 19$. The observed ($I_1 - I_2$) noise level agrees well with the shot-noise level established independently with a red-filtered white-light source (trace b) and with a light-emitting diode. These data were taken with the laser at 15 K, where the emission wavelength was 810 nm, the threshold current was 0.9 mA, and the differential quantum efficiency was 78%. The differential laser current-to-detector current transfer ratio was 0.51 above threshold, and thus the overall detection efficiency was 65%. Correcting for this detection efficiency, the 1.4 dB of observed squeezing corresponds to 2.4 dB of squeezing at the laser output facet.

A significant increase in the difference current noise level appeared when a polarizer (extinction ratio $>10^4$:1) located between the laser and the detection setup was removed (trace a of Fig. 1). Previous amplitude-squeezing experiments with similar balanced detection schemes were not sensitive to this type of noise because an optical isolator was used.[7,9] The extra noise results from the use of a PBS and initially appears surprising because the polarization

0146-9592/93/050379-03$5.00/0

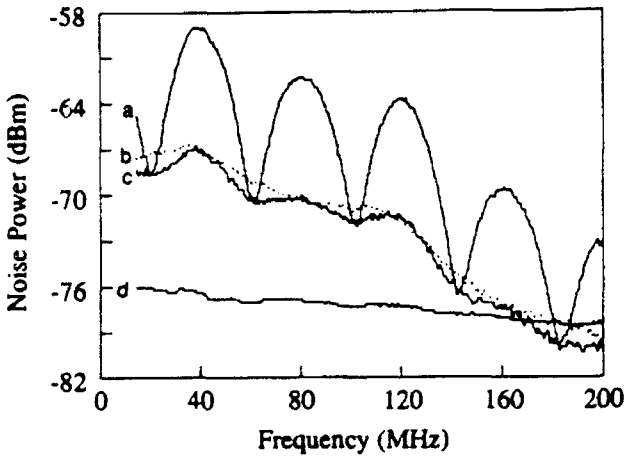

Fig. 1. Balanced mixer amplitude-fluctuation spectra for the laser (traces a and c) and for a red-filtered white-light source (trace b). All three were taken with a total dc photodetector current of 8.00 mA. The amplifier thermal noise (trace d) was subtracted in traces a, b, and c and is given for reference.

extinction ratio of the laser was >400. However, the PBS mixes the initially orthogonally polarized fields generated by the laser, leading to the increased noise.

The mixing can be described quantum mechanically by a unitary transformation relating the input and output photon annihilation operators[11]:

$$\begin{bmatrix} \hat{b}_\perp \\ \hat{b}_\parallel \end{bmatrix} = \begin{bmatrix} \cos(\theta) & \sin(\theta) \\ -\sin(\theta) & \cos(\theta) \end{bmatrix} \begin{bmatrix} \hat{a}_\perp \\ \hat{a}_\parallel \end{bmatrix},$$

$\hat{a}_\perp$ and $\hat{a}_\parallel$ are operators for the orthogonal polarization components of the lasing mode, $\hat{b}_\perp$ and $\hat{b}_\parallel$ are, respectively, operators for the orthogonally polarized transmitted and reflected modes of the PBS, and θ is the angle between the polarization directions of $\hat{a}_\perp$ and $\hat{b}_\perp$. Assigning $\hat{a}_\perp$ to the primary polarization direction of the laser leaves little power for the $\hat{a}_\parallel$ mode. However, this mode leads to the observed extra noise in trace a, as can be seen by calculating the variance of $(I_1 + I_2)$ and $(I_1 - I_2)$ for the case of balanced ($\theta = 45°$) detection:

$$[\Delta(\hat{M}_\perp + \hat{M}_\parallel)]^2 = (\Delta\hat{N}_\perp)^2 + (\Delta\hat{N}_\parallel)^2, \quad (1)$$

$$[\Delta(\hat{M}_\perp - \hat{M}_\parallel)]^2 = \langle\hat{N}_\perp\rangle + \langle\hat{N}_\parallel\rangle + 2\langle\hat{N}_\perp\rangle\langle\hat{N}_\parallel\rangle - 2|\langle\hat{a}_\perp^\dagger\hat{a}_\parallel\rangle|^2 + 2\,\mathrm{Re}[(\Delta\hat{a}_\perp^\dagger\hat{a}_\parallel)^2], \quad (2)$$

where $\hat{N} = \hat{a}^\dagger\hat{a}$ and $\hat{M} = \hat{b}^\dagger\hat{b}$. Equation (1) describes the data in Fig. 1 (trace a) at frequencies leading to $(I_1 + I_2)$. It indicates that the measured amplitude noise in this case corresponds to the simple sum of the noise power contributions of the independent input modes. The agreement between traces a and c at these sum frequencies (recalling that a polarizer was used to eliminate the contribution of the nonlasing polarization in trace c) indicates that the nonlasing mode did not make a detectable contribution to the sum-frequency amplitude noise found in trace a, as expected based on its low power level.

At frequencies where $(I_1 - I_2)$ is displayed, the situation is more complex. Each of the first two terms in Eq. (2) represents the average photon number of one of the two laser polarizations, and their sum gives the SNL. However, the remaining terms are not negligible. The third term is a cross term given by twice the product of each input mode's average photon number, and the last two terms depend on the coherence properties of the two modes.

If both laser modes ($\hat{a}_\perp$ and $\hat{a}_\parallel$) are in coherent states of the electric field, or if either mode has zero photons, the last three terms cancel, giving the shot-noise level. This is clearly not the case for the experiment described, because trace a displays 8 dB of extra noise at the subtracted frequencies, and the sum frequencies indicate a sub-Poissonian primary mode. Similar difference-frequency noise behavior has been observed in split photodetector balanced detection,[12] where it was attributed to stochastic position noise due to regeneratively amplified spontaneous emission into nonlasing modes. Regeneratively amplified spontaneous emission into the nonlasing polarization probably leads to the 8 dB of extra noise observed here also. The statistical properties of this mode become easily observable in this setup because of their interference with the lasing mode.

Given the differential quantum efficiency of our laser, at least 6.6 dB of squeezing at the laser output facet is theoretically expected far above threshold.[5,8,13] The discrepancy between this value and the largest observed squeezing (2.4 dB at the output facet) is probably due to a combination of multimode operation and weak optical feedback into the laser. Measurements of the laser output spectrum indicate a strong correlation between power in modes other than the primary lasing mode and increased photon-number noise, eventually leading to a loss of squeezing at high pump levels ($I/I_{th} > 35$). Optical feedback may also play a role, although replacing the polarizer with an optical isolator (isolation dB) did not increase the observed squeezing.

A second set of experiments was performed, which consisted of close coupling the laser to a single detector. Because this configuration relies on direct detection, the shot-noise level must be calibrated independently. This raises a concern because differing conditions between calibration and laser noise measurement, such as spot size, could alter detector saturation, making interpretation of the experimental results difficult. For example, increased saturation due to a laser spot size much smaller than that of the calibration source would lead to a lower displayed noise power and thus could be mistaken for amplitude squeezing.

Several steps were taken to avoid errors due to detector saturation. The detector (Hamamatsu Model S1722-01) was chosen for its large area (13.2 mm^2) and excellent saturation characteristics.[14] These saturation characteristics were determined experimentally under conditions similar to those for the close-coupled laser. One such experiment used a red-filtered white-light source, focused to a 1.0-mm^2 spot, to generate the shot-noise level at several dc detector current levels (dc detector current was linear with input power to within 0.2% up to 30 mA). The

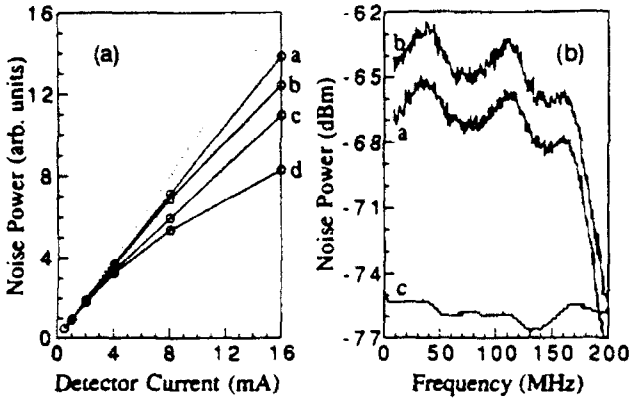

Fig. 2. (a) Red-filtered white-light source was used to study the frequency-dependent saturation characteristic of the detector. The frequencies shown are 10 MHz (trace a), 50 MHz (trace b), 100 MHz (trace c), and 150 MHz (trace d). The dotted line represents the response of an ideal detector. (b) Demonstration of the amplitude squeezing obtained on close coupling the diode laser and detector. Trace a shows the laser noise spectra, trace b shows the shot-noise level corresponding to trace a, and trace c shows the amplifier thermal noise level, which was subtracted from traces a and b.

results are shown in Fig. 2(a). The data indicate that detector saturation is minimal at low frequencies (<50 MHz) out to beyond 8.00 mA.

To ensure that differences between calibration source and laser-beam spot size did not affect the level of this saturation, several laser-to-detector distances (and corresponding spot sizes) were used in the experiments described below. The measured laser noise level remained constant ±6% over a factor of 5 change in spot size and was not directly correlated with spot size. This result, coupled with the fact that the largest laser spot size (0.9 mm^2) was comparable with the calibration spot size (1.0 mm^2), shows that intensity-dependent detector saturation had little effect on the results of these experiments.[14] The insensitivity of this detector to spot size also extended to larger areas (data taken with red light and light-emitting diode spot sizes of up to 10 mm^2 were nearly identical to the 1.0-mm^2 data).

To minimize possible errors, the detector and its associated amplifiers were kept at room temperature while the laser was cooled to 10 K. Here the threshold current was 0.78 mA, and the differential laser current-to-detector current transfer ratio above threshold was 0.67. The results of one experiment for a bias level of $I/I_{th} = 16$ (detector current 8.00 mA) are shown in Fig. 2(b). The amount of squeezing obtained low frequencies (where the effects of saturation are smallest) fell between 2.4 and 2.9 dB as the distance between the laser and detector was varied from 1.5 mm (0.17-mm^2 spot size) to 3.5 mm (0.92-mm^2 spot size) and did not increase at higher bias levels. Owing to a lack of direct correlation with distance, this slight variation in squeezing is believed to be due to weak optical feedback, which depended on the exact orientation of the laser and detector. When corrected for a detection efficiency of 85%, 2.9 dB of squeezing corresponds to 3.7 dB at the output facet of the laser, which is still less than the theoretically expected value of 6.6 dB.

Other lasers of the same type gave similar levels of squeezing, although the temperature at which maximum squeezing was observed varied from laser to laser. Simultaneous monitoring of the laser mode (by collecting light from the back facet and analyzing it with a monochromator) and amplitude fluctuations revealed that longitudinal-mode characteristics were responsible for this temperature dependence. The best squeezing was obtained with a dominant primary mode, indicating that cross-gain saturation did not result in complete negative correlation between the modes.[15] As the side-mode power (relative to the main mode) and the number of side modes increased, so did the amplitude noise. Unfortunately, at high pump levels (typically $I/I_{th} > 25$) this always occurred, which is probably why the full theoretical level of squeezing could not be attained and raises the possibility that mode stabilization may enhance the observed squeezing.

We acknowledge helpful discussions with H. J. Kimble. This research is supported by the U.S. Air Force Office of Scientific Research and is based on research supported under a National Science Foundation Graduate Fellowship.

References

1. H. P. Yuen, Phys. Rev. Lett. **56,** 2176 (1986).
2. Y. Yamamoto and H. A. Haus, Rev. Mod. Phys. **58,** 1001 (1986).
3. M. Sargent III, M. O. Scully, and W. E. Lamb, Jr., *Laser Physics* (Addison-Wesley, Reading, Mass., 1974).
4. Y. M. Golubev and I. V. Sokolov, Sov. Phys. JETP **60,** 234 (1984).
5. Y. Yamamoto, S. Machida, and O. Nilsson, Phys. Rev. A **34,** 4025 (1986); see also Y. Yamamoto and S. Machida, Phys. Rev. A **35,** 5114 (1987).
6. H. Ritsch, P. Zoller, C. W. Gardiner, and D. F. Walls, Phys. Rev. A **44,** 3361 (1991).
7. W. H. Richardson and R. M. Shelby, Phys. Rev. Lett. **64,** 400 (1990).
8. W. H. Richardson, S. Machida, and Y. Yamamoto, Phys. Rev. Lett. **66,** 2867 (1991).
9. S. Machida and Y. Yamamoto, Opt. Lett. **14,** 1045 (1989).
10. H. P. Yuen and V. W. S. Chan, Opt. Lett. **8,** 177 (1983).
11. S. Prasad, M. O. Scully, and W. Martienssen, Opt. Commun. **62,** 139 (1987).
12. M. D. Levenson, W. H. Richardson, and S. H. Perlmutter, Opt. Lett. **14,** 779 (1989).
13. Y. Yamamoto and H. A. Haus, Phys. Rev. A **45,** 6596 (1992).
14. The saturation characteristics of NDL-2208, EG&G C30957E, and Melles Griot 13DSI003 silicon photodiodes were also investigated and were found to be unsatisfactory at the intensity levels imposed by the close-coupled laser. The onset of saturation in these devices was much more abrupt, and the sensitivity to spot-size variations was greater than that of the Hamamatsu detectors.
15. S. Inoue, H. Ohzu, S. Machida, and Y. Yamamoto, Phys. Rev. A **46,** 2757 (1992).